Additivity or Cooperativity: Which Model Can Predict the Influence of Simultaneous Incorporation of Two or More Functionalities in a Ligand Molecule?

Nader N. Nasief , David Hangauer

PII: S0223-5234(14)01098-8

DOI: 10.1016/j.ejmech.2014.11.056

Reference: EJMECH 7549

To appear in: *European Journal of Medicinal Chemistry*

Received Date: 10 July 2014

Revised Date: 10 October 2014

Accepted Date: 27 November 2014

Please cite this article as: N.N Nasief, D. Hangauer, Additivity or Cooperativity: Which Model Can Predict the Influence of Simultaneous Incorporation of Two or More Functionalities in a Ligand Molecule?, *European Journal of Medicinal Chemistry* (2014), doi: 10.1016/j.ejmech.2014.11.056.

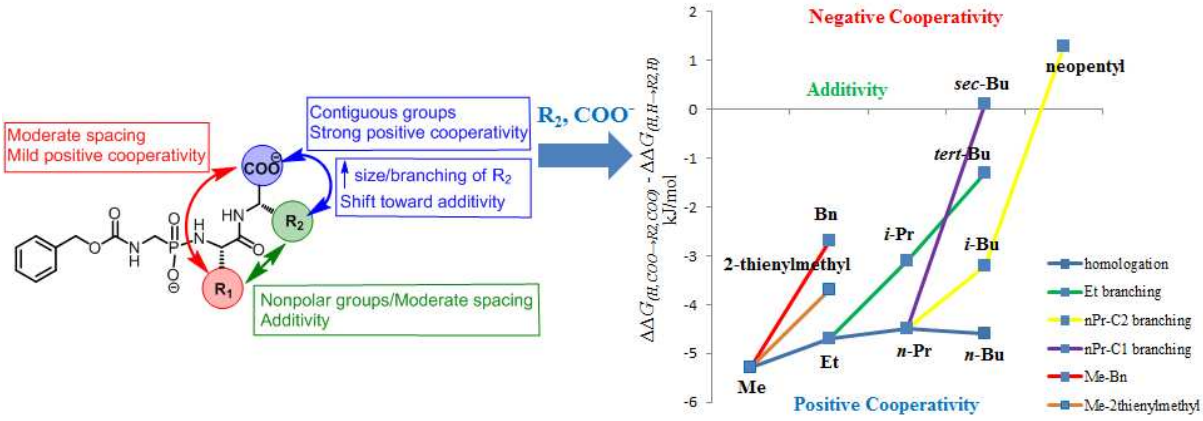

Additivity or Cooperativity: Which Model Can Predict the Influence of Simultaneous Incorporation of Two or More Functionalities in a Ligand Molecule?

Nader N Nasief * and David Hangauer *

Department of Chemistry, University at Buffalo, The State University of New York, Buffalo, New York 14260

KEYWORDS: Drug design, Lead optimization, Structure-activity relationship, Protein-ligand binding, Molecular recognition, Thermolysin

ABSTRACT:

Predicting how binding affinity responds to ligand structural modifications in structure-activity relationship studies (SAR) is a major challenge in medicinal chemistry. This is particularly true when two or more of these modifications are carried out simultaneously. In this study, we present binding affinity data from several series of thermolysin inhibitors in which simultaneous structural modifications were investigated to determine whether they are cooperative or additive. Data revealed that, while additivity is at work in some cases, cooperativity is more commonly demonstrated. Cooperativity and additivity were then correlated with ligand descriptors, such as the spacing and the topological features of the modified groups, in a manner that may provide guidance as to when each model should be utilized. Cooperativity was particularly associated with contiguous groups and small unbranched hydrophobic side chain. Additivity, on the other hand, was associated with moderately distant hydrophobic group combinations and side chain branching. Such correlations can improve the predictability of SAR studies and can provide a starting point for additional investigations that may lead to further significant enhancements in the current scoring functions.

* Correspondences should be addressed to D H at hangauer@buffalo.edu or N N N at nnnasief@yahoo.com.

1. Introduction:

Lead optimization involves cycles of structural modifications which aim at improving the lead's binding affinity or enhancing its pharmacokinetic properties. A typical structural modification might be the replacement of an H or a functional group with another. It is not uncommon for a medicinal chemist to perform more than one structural modification at a time in order to reduce the number of compounds to be synthesized. For example, the structural modifications A→X and B→Y could be carried out individually (two compounds are synthesized) and then combined in a third compound after evaluating whether these structural modifications move the process towards the desired goal. Alternatively, a medicinal chemist may opt to synthesize the third compound after evaluating only one or neither of these modifications (i.e. one or two compounds are synthesized). It should be noted that each of these choices could be misleading in one way or another. For instance, suppose the structural modifications A→X and B→Y are carried out, and one of them is found to be disadvantageous. The medicinal chemist might be discouraged from synthesizing the third compound that has both modifications, even though this third compound, if synthesized and evaluated, might display what has previously been termed "positive cooperativity" between the two modifications [1-3] and—as a consequence—might be good. On the other hand, skipping the evaluation of the individual modifications carries the risk of missing good modifications if the third compound is not good because the two modifications are negatively cooperative (i.e. the individual modifications are good, while the combination is bad). It is therefore crucial for medicinal chemists to be capable of accurately predicting not only the impact of the individual structural modifications on the binding affinity (or the pharmacokinetic property that is desired to be improved), but also the correct model that is to be employed when two, or even more, structural modifications are combined in a ligand.

<Insert Figure 1>

Now, how can we identify cooperativity or additivity between two structural modifications in a ligand? A typical analysis that has been commonly used to study cooperative phenomena is the double mutant cycle analysis [4-8]. This analysis has been used to determine whether ligand structural modifications are cooperative or additive with regard to their binding affinity/free energy [1-2, 9]. To illustrate how this analysis works in general terms, consider Figure 1. In this

figure, the relationship between the structural modifications H→X and H'→Y is evaluated by comparing the binding free energy change (the differential binding energy)[10] occurring when both groups exist in the ligand ($\Delta\Delta G_{(H,H'\rightarrow X,Y)}$) with the sum of the binding free energy changes occurring when each group exists individually ($\Delta\Delta G_{(H,H'\rightarrow X,H')} + \Delta\Delta G_{(H,H'\rightarrow H,Y)}$). There are three possible outcomes: (1) $\Delta\Delta G_{(H,H'\rightarrow X,Y)} = \Delta\Delta G_{(H,H'\rightarrow X,H')} + \Delta\Delta G_{(H,H'\rightarrow H,Y)}$; (2) $\Delta\Delta G_{(H,H'\rightarrow X,Y)} < \Delta\Delta G_{(H,H'\rightarrow X,H')} + \Delta\Delta G_{(H,H'\rightarrow H,Y)}$; and (3) $\Delta\Delta G_{(H,H'\rightarrow X,Y)} > \Delta\Delta G_{(H,H'\rightarrow X,H')} + \Delta\Delta G_{(H,H'\rightarrow H,Y)}$. In the first case H→X and H'→Y demonstrate additivity, while in both the second and the third cases H→X and H'→Y are cooperative (The second is a case of positive cooperativity, and the third is a case of negative cooperativity). Alternatively, one can compare either the differential binding free energy associated with the replacement of the ligand H with group X in the presence ($\Delta\Delta G_{(H,Y\rightarrow X,Y)}$) and absence ($\Delta\Delta G_{(H,H'\rightarrow X,H')}$) of group Y, or the differential binding energy caused by the H'→Y replacement in the presence ($\Delta\Delta G_{(X,H'\rightarrow X,Y)}$) and absence ($\Delta\Delta G_{(H,H'\rightarrow H,Y)}$) of group X. If, for example, $\Delta\Delta G_{(H,Y\rightarrow X,Y)}$ and $\Delta\Delta G_{(H,H'\rightarrow X,H')}$ are equal, H→X and H'→Y are deemed additive. On the other hand, a more negative and a more positive $\Delta\Delta G_{(H,Y\rightarrow X,Y)}$ values indicate positive and negative cooperativities, respectively. Cooperativity may therefore be defined as a variation in $\Delta\Delta G_{(H\rightarrow X)}$ which occurs when a second group Y is incorporated in the ligand molecule.

1.1. Additivity/Cooperativity and the Partitioning of the Differential Binding Energy

Figure 2 illustrates a "three-dimensional" Born-Haber cycle which can be used to partition the binding of two ligands LH and LX to a biological target P [11-12]. These two ligands differ only in that ligand LX has the functional group X replacing an H in ligand LH. The differential binding energy caused by this functional group replacement is therefore represented by the free energy difference ($\Delta G_{LX} - \Delta G_{LH}$). Because each of these free energy terms can be partitioned into basic components as illustrated by Eq. 1 which represents the partitioning of ΔG_{LH}, the differential binding energy can be partitioned as well, and this partitioning is illustrated by Eq. 2. This equation describes the partitioning of the differential free energy $\Delta\Delta G_{(H\rightarrow X)}$ into three major components: the differential desolvation of the ligand ($\Delta G_{LX\text{-}desolv} - \Delta G_{LH\text{-}desolv}$), the differential ligand-protein association ($\Delta G_{LX\text{-}assoc} - \Delta G_{LH\text{-}assoc}$), and the differential ligand-protein complex resolvation ($\Delta G_{LX\text{-}resolv} - \Delta G_{LH\text{-}resolv}$). It should be noted that both Eq. 1 and Eq. 2 should include

other terms if conformational or ionization changes occur in either the ligands or the target during the course of binding.

<Insert Figure 2>

$$\Delta G_{LH} = \Delta G_{LH\text{-}desolv} + \Delta G_{P\text{-}desolv} + \Delta G_{LH\text{-}assoc} + \Delta G_{LH\text{-}resolv} \quad \textbf{(Eq. 1)}$$

$$\Delta\Delta G_{(H\rightarrow X)} = \Delta G_{LX} - \Delta G_{LH} = (\Delta G_{LX\text{-}desolv} - \Delta G_{LH\text{-}desolv}) + (\Delta G_{LX\text{-}assoc} - \Delta G_{LH\text{-}assoc}) + (\Delta G_{LX\text{-}resolv} - \Delta G_{LH\text{-}resolv}) \quad \textbf{(Eq. 2)}$$

Given that additivity and cooperativity were previously defined in terms of variation in the differential free energy, these phenomena can be explained through the differential free energy partitioning. Additivity, for instance, exists when the differential free energy of a structural modification (e.g. H→X) is the same, no matter whether the initial or the final group of the second modification exists in the ligand (e.g. H' or Y; Figure 1): $\Delta\Delta G_{(H,H'\rightarrow X,H')} = \Delta\Delta G_{(H,Y\rightarrow X,Y)}$. This case could be obtained if (1) none of the differential free energy components illustrated in Eq. 2 changes when the structural modification H→X is carried out in presence of the H' or the Y of the modification H'→Y; or (2) in the presence of Y vs. H', more than one of these free energy components change in opposite directions so that no net change in the differential free energy is produced (e.g. $(\Delta G_{LX\text{-}desolv} - \Delta G_{LH\text{-}desolv})$ and $(\Delta G_{LX\text{-}assoc} - \Delta G_{LH\text{-}assoc})$ change in opposite directions but with the same magnitude). On the other hand, cooperativity is obtained when the differential binding free energy of the modification H→X differs based on the existence of the initial or the final group of the second modification in the ligand ($\Delta\Delta G_{(H,H'\rightarrow X,H')} \neq \Delta\Delta G_{(H,Y\rightarrow X,Y)}$). Cooperativity is obtained when one or more of the differential free energy components vary when group Y exists vs. the H' (i.e. Y modulates one or more of the differential free energy components). For example, $(\Delta G_{LX\text{-}desolv} - \Delta G_{LH\text{-}desolv})$ and/or $(\Delta G_{LX\text{-}assoc} - \Delta G_{LH\text{-}assoc})$ might become more negative (more favorable) in presence of group Y. As a consequence, $\Delta\Delta G_{(H,Y\rightarrow X,Y)}$ becomes more favorable and positive cooperativity is produced (more details are given in the supplementary materials). It is important to note that the way the differential free energy is partitioned in Figure 2 is not the only way to partition this quantity; rather, we previously utilized another partitioning scheme that bypasses the gas phase to explain the origin of cooperativity [2].

1.2. Additivity or Cooperativity?

Deviations from the additivity principle occur frequently in SAR studies. For example, Patel et al. analyzed eight nearly complete combinatorial libraries assayed on several different biological responses and showed that only half exhibit clear additive behavior [13]. Furthermore, the importance of the cooperativity (nonadditivity) principle in molecular recognition and ligand binding studies was demonstrated by Muley and co-workers, who showed that hydrophobic interactions and hydrogen bonding reinforce each other in thrombin inhibitors [1]. Cooperativity was then regarded by Bissantz et al. as one of the important factors affecting molecular interactions [14]. Given that both additivity and cooperativity can be obtained experimentally, the major challenge we face is to determine when additivity is a valid assumption and when, on the contrary, a cooperative model would more accurately describe the binding process. In order to address this challenge, extensive studies of the relationships among functional groups in multiple ligand-biological target systems are needed. These studies should focus on (1) correlating additive/cooperative behaviors with the structural features of both the ligand and the biological target; (2) unraveling the interwoven nature of the binding elements and understanding when particular elements become more significant than others; and (3) identifying recurring additivity/cooperativity patterns that can be utilized prospectively to predict the outcomes of SAR studies.

1.3. Designing a Study to Explore the Additivity/Cooperativity in Thermolysin Inhibitors

The study presented in the current contribution was intended to be an initial endeavor to address the aforementioned challenge. The phosphonamidate-thermolysin system, which was the subject of some of our recent studies, [2, 15-16] was deemed an appropriate ligand-protein system for this study. We, therefore, aimed at identifying patterns of additivity and/or cooperativity in series of phosphonamidate ligands with respect to their binding to thermolysin (TLN). TLN is a thermostable bacterial zinc-metalloprotease that is obtained from *Bacillus thermoproteolyticus* [17-19]. It shares common active site structural features with other zinc-metalloproteases such as carboxypeptidase A [20] and angiotension-converting enzyme (ACE) [21]. One of these common structural features is the presence of zinc ion which facilitates the substrate peptide bond cleavage via coordinating the C=O group. Other important features of the TLN active site are the S1' pocket, which is a deep hydrophobic pocket that largely determines

substrate specificity, [22] and the S2' pocket, which is a shallow, flat, solvent-exposed pocket. The phosphonamidate inhibitors chosen for this study coordinate with the zinc ion via the PO_2^- moiety (Figure 3). They also form several H-bonds with various residues in the active site. These H-bonds include a charge-assisted H-bond formed between the inhibitor terminal COO^- group and the Asn112 $–C(=O)NH_2$ group (Figure 3). In addition, these inhibitors can have hydrophobic side chains which bind both the S1' and the S2' pockets (e.g. R_1 and R_2 groups).

The study presented herein was designed to investigate the additive or cooperative relationship between (1) the ligand terminal COO^- group and the R_1 hydrophobic side chain; (2) the ligand terminal COO^- group and the R_2 hydrophobic side chain; and (3) the ligand two major hydrophobic side chains R_1 and R_2. It is worth mentioning that, with regard to the second group pair (i.e. the COO^- and the R_2 side chain), positive cooperativity has already been demonstrated between the COO^- and the Me side chain [2]. The design of the current study furthermore involved evaluating the correlations between the experimentally observed cooperative/additive patterns and some of the structural features of the ligand and the protein. For example, questions like the following were investigated: is the relationship between a polar group and a hydrophobic side chain (the COO^- and R_1 or R_2) different from the relationship between two hydrophobic side chains (R_1 and R_2), in terms of the cooperative/additive behavior? Is the cooperative/additive behavior distance-dependent (the COO^- and R_2 vs. the COO^- and R_1)? Is this behavior dependent on the nature of the protein pocket (S1' vs. S2')? Is this behavior dependent on hydrophobic side chain descriptors such as the size, the degree of branching, and the aliphaticity/aromaticity of the hydrophobic side chain? Figure 3 illustrates the group pairs that were studied and indicates some of the characteristics that were correlated with the observed cooperative/additive behaviors.

<Insert Figure 3>

The first studied group pair was the (R_1, COO^-) pair. In order to study this pair, two series of inhibitors were designed (Scheme 1: Series I and II). In both series, the hydrophobic side chain was grown from Me to Et, *n*-Pr, and *i*-Bu. One of these series, however, lacks the COO^- group (i.e. Series I). The absence of the COO^- group in this series made it possible to evaluate how the COO^- group influences the contributions of different R_1 side chains to the binding affinity, and thus double mutant cycles similar to the ones shown in Figure 1 could be constructed. Second, in order to study the (R_2, COO^-) group pair, two series, which differ only in the presence or absence

of the COO^- group, were investigated (Series III and IV, Scheme 1). Initially, the R_2 side chain in both series was grown from H to Me, Et, *n*-Pr, and *n*-Bu. Later on, the scope of studying this pair was expanded to include branched and aromatic side chains. Furthermore, the influence of truncating the R_1 side chain from *i*-Bu to Me on the cooperative/additive behavior of this group pair was explored by testing two additional series having a varied R_2 side chain and a Me as the R_1 side chain, without and with the COO^- (Series V and VI, Scheme 1). Finally, the (R_1, R_2) pair was studied by comparing the data of series V, which has a Me side chain as R_1, with the data of some ligands from series III (series III-R, Scheme 1). This comparison involved varying the hydrophobicity of R_1 and R_2 individually and simultaneously. For example, the R_2 side chain was varied from Me to Et, *i*-Bu, and Bn, while the R_1 side chain was either Me (series V) or *i*-Bu (series III-R).

Details about the double mutant cycles that evaluate the cooperative/additive relationships in the group pairs being studied herein are given later. In the next section, the synthesis of the ligands that belong to these group pairs will be discussed in detail.

<Insert Scheme 1>

2. Results and Discussions

2.1. Chemistry [23]:

The synthesis of the intermediate **4** is illustrated in Scheme 2. Commercially available benzylcarbamate was heated in an aqueous basic formaldehyde solution to give benzyl *N*-(hydroxymethyl) carbamate **1** [24]. The terminal hydroxyl group of intermediate **1** was acetylated using acetic anhydride to give benzyl *N*-(acetoxymethyl) carbamate **2**. Intermediate **2** was converted to dimethyl *N*-benzyloxycarbonyl aminomethylphosphonate **3** by refluxing with trimethyphosphite. Intermediate **4** was obtained by the hydrolysis of one of the two methyl phosphonate esters in **3** using 10% NaOH solution.

<Insert Scheme 2>

The synthesis of ligands **1-38** is shown in Scheme 3. First, the commercially available Boc-protected amino acids were coupled to the hydrochloride salts of various amines or amino acid esters to give the intermediates **IA1-38**. Either EDCI/HOBt or PyBop in anhydrous DMF were

used effectively to achieve the coupling in presence of diisopropylethylamine. The intermediates **IB1-38** were then obtained as hydrochloride salts upon the removal of the Boc groups from **IA1-38**. In order to remove the Boc groups, either 3 M HCl/MeOH solution was used, or HCl gas was bubbled into an ethyl acetate solution of the Boc-protected intermediate to avoid transesterification with MeOH.

<Insert Scheme 3>

Finally, intermediate **4** was coupled to each of the intermediates **IB1-38** in anhydrous dichloromethane using PyBop as the coupling reagent to give **IC1-38**. Compounds **IC1-38** were then hydrolyzed using lithium hydroxide to give the final compounds **1-38** either as dilithium salts (when the carboxylate group is present) or monolithium salts (when the carboxylate group is absent). All the final compounds were purified by reverse-phase HPLC to at least 95% purity. The substitution patterns of the synthesized ligands and their intermediates are illustrated in Table 1.

<Insert Table 1>

2.2. Biochemical assay:

The inhibition constants (K_i) for compounds **1-38** were determined in a standard TLN biochemical assay using 2-furanacryloyl-Gly-Leu-NH_2 as a substrate [25]. The assay was carried out in a high salt concentration which improves the enzyme activity as well as the substrate binding to the enzyme. More details about the assay conditions are given in the experimental section. The K_i and the corresponding free energy of binding values for the TLN inhibitors **1-38** are provided in Table 2.

<Insert Table 2>

2.3. The relationship between the hydrophobic side chain R_1 and the terminal COO^- group

<Insert Figure 4>

In order to investigate the relationship between the R_1 side chain and the COO^- group, the differential binding free energies of the Me→R_1 modifications in absence of the COO^- group were compared to the differential binding energies of the same modifications in presence of the COO^-. This comparison is illustrated in the double mutant cycle shown in Figure 4. In this

double mutant cycle, ligand **1** is mutated to **2**, **3**, or **4**, and the differential binding energy in absence of the COO^- ($\Delta\Delta G_{(Me,H\rightarrow R1,H)}$) is obtained when the binding free energy of **1** is subtracted from that of either **2**, **3**, or **4**. This double mutant cycle also involves the mutation of ligand **5** to **6**, **7**, or **8**, which yields values for ($\Delta\Delta G_{(Me,COO\rightarrow R1,COO)}$). These values are obtained by subtracting the free energy of **5** from that of **6**, **7**, or **8**. The values of the differential free energies in both the absence and the presence of the COO^- are given in Table 3. This table also includes values for ($\Delta\Delta G_{(Me,COO\rightarrow R1,COO)} - \Delta\Delta G_{(Me,H\rightarrow R1,H)}$), which is the term that indicates positive cooperativity if negative, negative cooperativity if positive, and additivity if 0. As shown in Table 3, the replacement of Me with Et is not influenced by the presence of the COO^- (i.e. additive). As the side chain is grown, mild cooperativity starts to show up. For example, the Me→*n*-Pr and the Me→*i*-Bu replacements are little more contributive to the binding free energy in presence of the COO^- (by 2.1 kJ/mol in the former and 1.8 kJ/mol in the latter case: about 2X additional improvement in Ki compared to what would be anticipated based on the additivity principle).

<Insert Table 3>

With regard to the mild cooperativity observed in the data of the group pair (R_1, COO^-), several points should be noted.

<Insert Figure 5>

(1) It is not likely that the COO^- would influence the differential desolvation (i.e. $\Delta G_{LR1\text{-}desolv} - \Delta G_{LMe\text{-}desolv}$: Eq. 2) of ligands in which the Me is grown to a larger side chain. For the differential desolvation to be dependent on the presence of the COO^-, the water molecules hydrating the R_1 side chain (i.e. in the unbound state) should reorganize differently when the Me is grown to a larger side chain in presence vs. in absence of the COO^-. This might require the COO^- to be in direct contact with the hydration layer of the R_1 side chain, but, most likely, this is not the case. For example, Figure 5a reveals that the R_1 side chain and the COO^- group might be positioned on opposite sides of the molecule, and therefore the required direct contact between the COO^- and the R_1 hydration layer might not be achievable. It should be noted that the conformation shown in the figure is the bioactive conformation, which is not necessarily the same as the global minimum of the unbound ligand (the conformation that needs to be investigated when ligand desolvation is considered). However, the hydrophobic collapse between the two hydrophobic side chains R_1 and R_2 in the bioactive conformation indicates that the spatial arrangement of the

R_1, R_2, and the COO^- in this conformation is favorable in terms of free energy, and might therefore be the same, or at least very close to the spatial arrangement of these groups in the global minimum of the unbound ligand. Conclusions drawn from the bioactive conformation regarding these groups might therefore be extrapolated to the unbound ligand.

(2) The differential resolvation (i.e. $\Delta G_{LR1\text{-}resolv} - \Delta G_{LMe\text{-}resolv}$: Eq. 2) of ligands in which the Me is grown to a larger side chain is not likely influenced by the presence of the COO^-. In fact, this differential resolvation term might be equivalent to zero both in presence and absence of the COO^-. For this term to exist, the complex of a ligand with a Me side chain should be resolvated differently from the complex of a ligand with a larger side chain. Given that both the Me and the larger side chains are buried in the deep S1' pocket (Figure 5b), the only way to achieve this different resolvation is if the complex of the ligand with Me side chain traps water molecule(s) in the unoccupied space of the S1' pocket. This is however unlikely because of the large entropic penalty of trapping such water molecule(s). Even if waters were trapped in the S1' pocket of the complex of a ligand with a Me side chain (and therefore $\Delta G_{LR1\text{-}resolv} - \Delta G_{LMe\text{-}resolv} \neq 0$), this water, being isolated to a great extent, would not be anticipated to sense the presence of the COO^-, and therefore the differential resolvation term would not be influenced by the COO^- group.

(3) If the COO^- alters neither the differential desolvation nor the differential resolvation terms, the mild cooperativity observed in Table 3 might be attributed to variation in the differential association term (i.e. $\Delta G_{LR1\text{-}assoc} - \Delta G_{LMe\text{-}assoc}$: Eq. 2) caused by the COO^- group. The most apparent cause for such variation is the mutual reinforcement of the direct interactions of the COO^- and R_1 groups with the protein (a H-bond with Asn112 in case of the COO^-, and dispersion interactions in case of the R_1 side chain; $\Delta G_{LR1\text{-}assoc}$ shifts to the negative when the COO^- is present, see supplementary materials section 1.1). It was previously mentioned that Muley and coworkers described this kind of cooperative behavior in thrombin inhibitors [1]. The cooperativity described by them, however, accounted for about an order of magnitude of activity enhancement (i.e. strong cooperativity). It is important to note, however, that the functional group pair studied by Muley et al., unlike the (R_1, COO^-) pair, involves groups that are in close proximity to each other. This might therefore suggest that the distance between the functional groups involved in this type of cooperativity correlates with how much benefit can be obtained

from the cooperative enhancement of non-covalent interactions (i.e. short and moderate distances yield strong and mild cooperativity, respectively).

2.4. The relationship between the hydrophobic side chain R_2 and the terminal COO^- group

<Insert Figure 6>

<Insert Figure 7>

In order to investigate the relationship between the R_2 side chain and the COO^- group, the differential binding free energies of the $H \rightarrow R_2$ modifications in absence and presence of the COO^- group were compared. This comparison is illustrated by the double mutant cycle in Figure 6. In this double mutant cycle, ligand **9** is mutated to **10-19**, or **4**; and the differential binding energy in absence of the COO^- ($\Delta\Delta G_{(H,H\rightarrow R2,H)}$) is obtained when the binding free energy of **9** is subtracted from that of any of ligands **10-19**, and **4**. This double mutant cycle also involves the mutation of ligand **20** to **21-30**, or **8**, which yields values for ($\Delta\Delta G_{(H,COO\rightarrow R2,COO)}$). A "$\Delta\Delta G_{(H,COO\rightarrow R2,COO)}$" value is obtained by subtracting the free energy of **20** from that of any of ligands **21-30**, and **8**. The values of the differential free energies in both the absence and the presence of the COO^- are given in Table 4. This table also includes values for ($\Delta\Delta G_{(H,COO\rightarrow R2,COO)} - \Delta\Delta G_{(H,H\rightarrow R2,H)}$).

<Insert Table 4>

The data presented in Table 4 reveal a complex cooperativity/additivity pattern between R_2 and the COO^-. This complex pattern is graphically illustrated in Figure 7 through plotting the quantity "$\Delta\Delta G_{(H,COO\rightarrow R2,COO)} - \Delta\Delta G_{(H,H\rightarrow R2,H)}$" against the R_2 side chain modifications. Both Table 4 and Figure 7 show that positive cooperativity is at maximum when the R_2 side chain is Me. This positive cooperativity, then, slightly diminishes when the R_2 side chain is grown from Me to Et, *n*-Pr and *n*-Bu (i.e. homologation: the blue line in Figure 7). The branching of the R_2 side chain reduces the positive cooperativity as well, but to a larger extent. For example, when the Et side chain is branched to *i*-Pr and *tert*-Bu, positive cooperativity decreases from -4.7 kJ/mol to -3.1 and -1.3 kJ/mol, respectively. A larger decrease in positive cooperativity was observed upon the branching of the *n*-Pr side chain to *sec*-Bu (-4.5 kJ/mol→ -0.1 kJ/mol: -0.1 kJ/mol indicates additivity), or to *i*-Bu and neopentyl (-4.5 kJ/mol→ -3.2 and 1.3 kJ/mol, respectively). In case of the neopentyl, "$\Delta\Delta G_{(H,COO\rightarrow R2,COO)} - \Delta\Delta G_{(H,H\rightarrow R2,H)}$" value, in fact,

shows that some negative cooperativity is at work (i.e. indicated by the positive sign of the 1.3 kJ/mol). Positive cooperativity also diminishes when an aromatic moiety is introduced in the R_2 side chain. For example, when the Me is replaced with either Bn or 2-thienylmethyl side chain, positive cooperativity decreases from -5.3 kJ/mol to either -2.7 kJ/mol in case of the Bn or -3.7 kJ/mol in case of the 2-thienylmethyl side chain.

The data presented for series III and IV; therefore, indicate that there is a correlation between the cooperativity/additivity pattern and the characteristics of the hydrophobic side chain being investigated. Size, degree of branching, and aromaticity are some of these characteristics which can be correlated with the cooperative behavior. For example, small and linear hydrophobic side chains, like the Me, Et, and *n*-Bu are more synergistic with a nearby COO^- than a bulky, branched, or aromatic side chains. It is worth mentioning that positive cooperativity, when manifested in contiguous groups (i.e. R_2 and the COO^-), is more prominent than in moderately distant ones (i.e. R_1 and the COO^-). This confirms our earlier conclusion that the distance between the correlated functional groups/side chains plays an important role in determining the magnitude of cooperativity. Also, unlike the (R_1, COO^-) pair, the close proximity of the COO^- and the R_2 side chain likely causes the COO^- to strongly influence the structural and the thermodynamic features of the water molecules hydrating the R_2, both in the unbound and the complexed states. For example, water may reorganize differently when R_2 is modified in presence vs. absence of the COO^- group. This effect has been previously shown to be the most likely cause for the dependency of the thermodynamic signature associated with the modification of the R_2 side chain on the COO^- group [16]. Furthermore, the influence of the COO^- on the water reorganization that is associated with replacing the H with Me (**9→10** and **20→21**) in the complexed state was demonstrated by X-ray crystallography and was correlated with the positive cooperativity between the Me and the COO^- (water mediated cooperativity) [2]. This correlation was suggested based on the analysis of the crystallographic data using the previously referenced partitioning scheme, which bypasses the gas phase. Now, can this correlation be made if the crystallographic data are analyzed using the partitioning scheme in Figure 2 which includes a gas phase state?

<Insert Figure 8>

Simply put, this partitioning scheme can be equivalently used, and this is how. First, because we need to examine the water networks of ligand-protein complexes, our focus should be on the final step of the Born-Haber cycle in Figure 2 (the resolvation of the ligand-protein complex). Second, we need to demonstrate that, when the COO^- exists, the differential resolvation term ($\Delta G_{LMe\text{-}resolv} - \Delta G_{LH\text{-}resolv}$) varies in a manner that produces the observed cooperativity. To do this, Figure 8 that demonstrates the ligand-protein complex resolvation of **9** and **10** in comparison with **20** and **21** can be consulted. This figure reveals that, in the presence of the COO^-, the H-bond network of the LH-TLN resolvation shell is broken (e.g., ligand **20** vs ligand **9**). This can be translated into a less enthalpically and more entropically favorable resolvation, or a $\Delta H_{LH\text{-}resolv}$ and a $-T\Delta S_{LH\text{-}resolv}$ that are shifted in the presence of the COO^- toward the positive and the negative, respectively. On the other hand, the presence of the COO^- supports the resolvation network of the LMe-TLN complex. For instance, in case of ligand **21**, the water network is characterized by the presence of additional crystallographic waters that participate into a more developed H-bond network. The resolvation of LMe-TLN is therefore more enthalpically and less entropically favorable, and the presence of the COO^- shifts $\Delta H_{LMe\text{-}resolv}$ and $-T\Delta S_{LMe\text{-}resolv}$ toward the negative and the positive, respectively. Taken together, a $\Delta H_{LMe\text{-}resolv}$ shifted toward the negative and a $\Delta H_{LH\text{-}resolv}$ shifted toward the positive yield a ($\Delta H_{LMe\text{-}resolv} - \Delta H_{LH\text{-}resolv}$) shifted toward the negative; and a $-T\Delta S_{LMe\text{-}resolv}$ shifted toward the positive and a $-T\Delta S_{LH\text{-}resolv}$ shifted toward the negative yield a ($-T\Delta S_{LMe\text{-}resolv} - (-T\Delta S_{LH\text{-}resolv})$) shifted toward the positive (SI; Enthalpy: sections 1.2 # 3; Entropy: section 1.3 # 6). These shifts indeed explain the experimentally observed enthalpic synergism and entropic antagonism [2]. The difficult question, however, is whether the negative shift in the differential resolvation enthalpy can overcome the positive shift in the differential resolvation entropy to produce a net negative shift in differential resolvation energy (and, in turn, a positive cooperativity between the Me and the COO^-). Most likely, this is the case. Previously, we have shown that, for the phosphonamidate-TLN system, the differential free energy correlates well with the differential enthalpy [16]. The observed enthalpic synergism in the case of the (Me, COO^-) pair is therefore anticipated to be accompanied by a net free energy synergism. Now that we pointed out that the most likely cause for the observed cooperativity is the differential resolvation, could there be any other source for this cooperativity?

Consider the ligand-protein association step. In this step, the additional Me group in LMe contributes some additional dispersion interactions with the protein. The favorable impact of these dispersion interactions on the differential enthalpy of association is not anticipated to change, whether the COO^- group exists or not (i.e. ($\Delta H_{LMe\text{-}assoc} - \Delta H_{LH\text{-}assoc}$) for ligands **21** and **20** is the same as for **10** and **9**). Therefore, it is not likely for cooperativity between the Me and the COO^- to be due to ligand-protein direct interaction. This hypothesis, however, is currently under investigations using QM calculations. The other important consequence for the ligand-protein association is the restriction of the ligand's mobility upon binding. For example, the ligand's translational and rotational degrees of freedom are converted into vibrational degrees of freedom, causing a significant loss in entropy ($-T\Delta S_{L\text{-}assoc} > 0$). Additionally, torsional degrees of freedom are restricted and consequently contribute to the entropic loss. Can this factor be responsible for cooperativity?

In ref 2 we have pointed out that such factor is not responsible for the entropic negative cooperativity. Using Born-Haber analysis (Figures 2 and 8), we can reach the same conclusion. For instance, the number of the torsional degrees of freedom being restricted upon ligand binding is the same in ligands **21** and **20**. On the other hand, ligand **10**, relative to ligand **9**, has an additional rotatable bond that gets restricted upon binding (Figure 8). $-T\Delta S_{LMe\text{-}assoc}$, in case of the **10** and **9** ligand pair, is therefore significantly more positive (unfavorable) than $-T\Delta S_{LH\text{-}assoc}$; and consequently, the differential entropy ($-T\Delta S_{LMe\text{-}assoc} - (-T\Delta S_{LH\text{-}assoc})$) is shifted to the positive when the COO^- is absent. A positive shift in ($-T\Delta S_{LMe\text{-}assoc} - (-T\Delta S_{LH\text{-}assoc})$) when the COO^- is absent is by default a negative shift in this quantity when the COO^- is present, and this, in turn, is translated into a negative shift in $-T\Delta\Delta S_{(H\rightarrow Me)}$ (SI, section 1.3). This proposed negative shift in $-T\Delta\Delta S_{(H\rightarrow Me)}$ was not observed experimentally [2]; consequently, the entropic signature of the ligand-protein association is not the factor responsible for the entropic negative cooperativity. With regard to the free energy, however, the proposed negative shift in $-T\Delta\Delta S_{(H\rightarrow Me)}$ can and indeed did display itself as a negative shift in $\Delta\Delta G_{(H\rightarrow Me)}$ (i.e. a positive cooperativity; Note: $\Delta\Delta G_{(H\rightarrow Me)} = \Delta\Delta H_{(H\rightarrow Me)} + (-T\Delta\Delta S_{(H\rightarrow Me)})$, supplementary materials, Eq. S2). We only do not know to what extent this factor participates in the free energy cooperativity, but we can make a reasonable suggestion that aligns with what was learned about the binding thermodynamics in this ligand-protein system. Based on our findings in ref 16, it can be hypothesized that 27% of the enthalpic cooperativity that is originated from variability in the solvation-resolvation patterns

of the ligand and/or the ligand-protein complex is demonstrated as free energy cooperativity. This portion would be equivalent to 27% × 7.2 kJ/mol = 1.94 kJ/mol, or about 60% of the cooperativity observed in the isothermal titration calorimetry (ITC) data [16] (Note: the biochemical assay data presented in the current study and the ITC free energy data are not identical but are correlated well, supplementary materials, section 2). What about the other 40%? Most likely, this 40% comes from the restriction of the additional rotatable bond in ligand **10** and the entropic consequence of this bond restriction.

2.5. The influence of size reduction of the R_1 side chain on the relationship between R_2 and the COO^-

In order to investigate the influence of reducing the size of the R_1 side chain (from *i*-Bu to Me) on the relationship between the R_2 side chain and the COO^- group, the differential binding free energies of each H→R_2 modification in series V was compared with that of the same H→R_2 modification in series VI. This is illustrated by the double mutant cycle in Figure 9. In this double mutant cycle, ligand **31** is mutated to **32**, **33**, **1**, or **34**; and the differential binding energy ($\Delta\Delta G_{(H,H\rightarrow R2,H)}$) is obtained when the binding free energy of **31** is subtracted from that of any of ligands **32**, **33**, **1**, and **34**. Similarly, the mutation of ligand **35** to **36**, **37**, **5**, or **38** yields values for ($\Delta\Delta G_{(H,COO\rightarrow R2,COO)}$) via subtracting the free energy of **35** from that of any of ligands **36**, **37**, **5**, and **38**. The values of these differential free energies are given in Table 5. This table also includes the values of ($\Delta\Delta G_{(H,COO\rightarrow R2,COO)} - \Delta\Delta G_{(H,H\rightarrow R2,H)}$).

<Insert Figure 9>

The data presented in Table 5 reveal that, in most cases, the cooperativity between the R_2 side chain and the COO^- is not significantly influenced by the reduction in the size of the R_1 side chain. For example, when R_1 = Me, the modification of the R_2 side chain from H to Me yields a -5.2 kJ/mol positive cooperativity, which is almost the same amount produced when R_1 = *i*-Bu (Table 4). The same trend is observed when R_2 is modified from H to Et or *i*-Bu (within experimental error).

<Insert Table 5>

When the H is replaced by Bn, however, a reduction in the positive cooperativity is observed when the R_1 side chain is Me (i.e. -0.9 kJ/mol vs. -2.7 kJ/mol). It could therefore be concluded

that a large R_1 hydrophobic side chain might augment the positive cooperativity between the R_2 side chain and the COO^-, but only when the R_2 side chain is modified into a bulky (and probably aromatic) group. Because only one case of such influence is presented herein, and the difference in the cooperativity indicator (i.e. $\Delta\Delta G_{(H,COO\rightarrow R2,COO)}$ - $\Delta\Delta G_{(H,H\rightarrow R2,H)}$) is not very pronounced (only 1.8 kJ/mol), this deviation from the main conclusion drawn from these series (i.e. that R_1 does not influence the cooperativity between the R_2 and the COO^-) should be viewed with caution. More data that can test this hypothesis further might therefore be needed. Figure 10 graphically depicts the cooperative behavior in series V and VI (R_1 = Me), in relation to the same R_2 modifications done in series III and IV (R_1 = *i*-Bu).

<Insert Figure 10>

2.6. The relationship between the hydrophobic side chains R_1 and R_2

The relationship between the hydrophobic side chains R_1 and R_2 were investigated using series V and some of series III ligands (series III-R). The double mutant cycle in Figure 11 reveals how these series were used in this investigation. Specifically, the H→R_2 replacements (H→Me/Et/*i*-Bu/Bn) were carried out while R_1 = Me (small, less hydrophobic side chain), and while R_1 = *i*-Bu (large, more hydrophobic side chain). The differential free energy values for the H→R_2 replacement while R_1 = Me were then compared with the differential free energies of these replacement while R_2 = *i*-Bu (i.e. $\Delta\Delta G_{(H,Me\rightarrow R2,Me)}$ vs. $\Delta\Delta G_{(H,i\text{-}Bu\rightarrow R2,i\text{-}Bu)}$), and the values of $\Delta\Delta G_{(H,i\text{-}Bu\rightarrow R2,i\text{-}Bu)} - \Delta\Delta G_{(H,Me\rightarrow R2,Me)}$ were calculated and listed in Table 6. These data demonstrate uncoupling between the R_1 and the R_2 side chain (i.e. they behave in an additive manner). For example, there is no significant difference between any $\Delta\Delta G_{(H,Me\rightarrow R2,Me)}$ and its corresponding $\Delta\Delta G_{(H,i\text{-}Bu\rightarrow R2,i\text{-}Bu)}$. In other words, the term $\Delta\Delta G_{(H,i\text{-}Bu\rightarrow R2,i\text{-}Bu)}$ - $\Delta\Delta G_{(H,Me\rightarrow R2,Me)}$ is always close to zero.

<Insert Figure 11>

<Insert Table 6>

3. Conclusions

The study presented herein reveals that the relationships among the ligand functional groups/side chains can be complex. For example, in some instances, mild positive cooperativity

is demonstrated. This is shown in the relationship between the R_1 side chains and the terminal COO^- group of the TLN phosphonamidate inhibitors. In other instances, strong positive cooperativity is at work. This is clearly demonstrated in the relationship between most of the R_2 side chains and the terminal COO^-. In some of the more branched R_2 side chains, however, additivity or even negative cooperativity exists. The cooperative/additive behavior of this particular ligand group pair (R_2, COO^-) did not show sufficient evidence for being influenced by the change in the R_1 side chain (Me vs. *i*-Bu). Additionally, investigating the relationship between the side chains R_1 and R_2 demonstrates that these two side chains are independent, and they show additive behavior. It follows that the first conclusion which can be drawn from this study is that ligand functional groups can be additive, synergistic, or antagonistic. Given that the cooperativity indicator described and utilized in this study is more likely to deviate from zero, cooperativity, including both synergism and antagonism, is anticipated to be the more common experimental finding, and this is what was observed in this study. One, however, should not assume that one type of behavior will be always observed as is commonly assumed with traditional scoring functions that completely ignore cooperativity. Also, the additivity principle should not be completely dismissed; rather, we should attempt to determine the molecular basis of each type of behavior, and in turn predict how the system would behave in each setting.

The second conclusion that can be drawn from this study is that the cooperative/additive behavior of a ligand functional group pair may be correlated with the properties of the involved groups. For example, a polar group and a hydrophobic side chain are likely to be synergistic (e.g. the COO^- and the R_1 or R_2 side chain). The magnitude of this synergism is however influenced by the distance between the group pair, and by the size or the degree of branching of the hydrophobic moiety (e.g., a more branched R_2 causes the synergism to be diminished). For example, strong synergism, which amounts to 5.0 kJ/mol, can be observed when the two groups are adjacent (the COO^- and the R_2 side chain, which are separated by 2 single bonds), while synergism accounts only for about 2.0 kJ/mol when the two groups are moderately distant (the COO^- and the R_1, which are separated by 5 single, rotatable bonds). Synergism diminishes when the side chain is branched (e.g., R_2 side chain), most likely due to a reduction in the stability of organized water arrangements that hydrates the hydrophobic side chain in either the unbound, the complexed state, or both [16]. On the other hand, hydrophobic-hydrophobic side chains might

show additivity when they are moderately distant (e.g. R_1 and R_2 side chains, which are separated by 5 single bonds).

It is important to note that the correlations made in the current study between the additivity/cooperativity patterns and the structural/physicochemical characteristics of the ligand functional groups represent a starting point for proposing SAR and QSAR models that incorporate such patterns. The end result will be a substantial improvement in our ability to predict the outcomes of lead optimizations with regard to the binding affinity. For example, a preliminary algorithm, which provides guidance as to whether medicinal chemists would encounter cooperativity or additivity in the course of simultaneous incorporation of two or more functionalities in a ligand molecule, can be constructed based upon this study (Scheme 4). Additional studies involving other ligand-protein model systems could result in further refinements to this algorithm. An improvement in our ability to predict cooperativity vs. additivity is also much needed in order to develop novel, more accurate scoring functions. A notable recent advancement in this field was the development of ScorpionScore, an empirical scoring function that goes beyond the additive treatment of non-covalent ligand-protein interactions (i.e. it incorporates the cooperativity principle) [27]. The current and subsequent related studies, which will be reported in due course, are likely to be very contributive to such endeavors.

<Insert Scheme 4>

4. Experimental Section

4.1. Biochemical assay: The inhibition constants of the thermolysin phosphonamidate inhibitors **1-38** were determined photometrically at 345 nm using 2-furanacryloyl-Gly-Leu-NH_2 as a substrate [25]. The assay was carried out on a Cary 100/300 UV/VIS spectrophotometer at 25.0 ± 0.2 ºC. A 0.05 M Tris buffer containing 0.02 M $CaCl_2$, 2.5 M NaBr [10], and 1.25% DMF, was used in all measurements. Buffer pH was adjusted to 7.3 ± 0.05 at room temperature prior to use. The concentration of the enzyme stock solution was determined by UV absorbance at 280nm ($\varepsilon 1\% = 17.65\ cm^{-1}$) [28]. The concentrations of the stock solutions of the substrate and the inhibitors were determined from accurately weighed samples. The enzyme concentration in all the final assay solutions was approximately 8 nM, the substrate concentration in the final assay

solutions was 0.8 M, and the inhibitors' concentrations were in the range of $0.5K_i$ – $10K_i$ for each inhibitor. The inhibition constant (K_i) for the inhibitor was taken to be the average of at least three K_i determinations, each of which was calculated from the experimentally determined IC_{50} using Cheng-Prusoff equation [29] (K_m= 3.9± 0.6 mM). The IC_{50} values were determined from υ_0/υ_i vs. [I] plots [10, 30] for all of the inhibitors with inhibition constants above 30 nM ($\upsilon_0/\upsilon_i = [I]/IC_{50} + 1$), or Henderson plots [31] for inhibitors with inhibition constants below this. At least six different inhibitor concentrations [I] were used to construct each plot.

4.2. Chemistry

4.2.1. General methods: Reagents were obtained from commercial suppliers and used without further purification. Anhydrous solvents were purchased as sealed bottles from Aldrich and were maintained under an argon atmosphere. Tetrahydrofuran (THF) was distilled from a sodium/benzophenone still and used immediately. Dichloromethane (DCM) was distilled from a calcium hydride still and used immediately. Solvent removal was performed on a rotary evaporator equipped with a 20-60° C water bath and a self-contained aspirator. Thin-layer chromatography (TLC) was performed on Analtech (Newark, DE) 200 micron Silica Gel F coated on polyethylene sheets. Visualization was accomplished with 254 nm UV light or iodine staining. The silica gel used in the flash chromatography was 40-75 μm flash grade purchased from Sorbent Technologies (Atlanta, GA). All amino acids used are L unless otherwise noted. Proton, phosphorus and carbon nuclear magnetic resonance was performed in deuterated solvents purchased from Cambridge Isotope Laboratories, Inc (Andover, MD) on one of the following instruments: Varian Gemini 300 MHz, Varian Inova 400 MHz, or Varian Inova 500 MHz. ^{1}H NMR data is reported in the following format: chemical shift (ppm values in relation to TMS or appropriate solvent peak), multiplicity (s = singlet, d = doublet, t = triplet, q = quartet, dd = doublet of doublet, dt = doublet of triplet, dq = doublet of quartet, m = multiplet, brs = broad singlet), coupling constant(s), and integration. Whenever fractions of chemically equivalent protons appear at widely-spaced chemical shifts, like when the compound exists in multiple conformations, the chemical shifts are reported; followed by the multiplicity(ies) preceded by the number of peaks (e.g. 2 s, 2 d, etc.), the coupling constant(s), and the sum of the integrations of these peaks. Low resolution ESI mass spectrometry was performed on a Thermo Finnigan LCQ Advantage instrument using 60% methanol in water with 1% acetic acid or 60% acetonitrile in

water with 0.1% trifluoroacetic acid as the mobile phase. Preparative and semi-preparative HPLC instrumentation included a Milton Roy gm4000 gradient programmer, Milton Roy Constametric I and III pumps, a Rheodyne 7125 injector with a 5.00 mL sample loop, and a Knauer Variable Wavelength Detector set at either 218 nm or 254 nm with a preparative flow cell. The HPLC column used was a Phenomenex LUNA C18(2), 5 μm, 100A pore, 21 mm X 250 mm with Security Guard cartridge used with a flow rate of 8 mL/min. All final compounds were at least 95% pure by HPLC analysis. The HPLC analysis of the final compounds involved the use of acetonitrile/water as a mobile phase in a gradient elution method (10→90% acetonitrile over 14 min). Given below are the detailed synthesis and the characterization of the final compounds and their intermediates that were not previously reported. The detailed synthesis and characterization of the other compounds are previously reported [16].

4.2.2. Synthesis of benzyl *N*-(hydroxymethyl)-carbamate (1)

Benzyl carbamate (6.0 g, 40 mmol) was added to a solution of 37% formalin (4.4 g, 56 mmol) and sodium carbonate (2.2 g, 20 mmol) in 65 mL water. The mixture was heated until all the solids were dissolved, then cooled to room temperature and stirred overnight. The precipitated solid was then filtered, dried, and redissolved in dichloromethane. The solution was dried using anhydrous magnesium sulfate and the solvent was removed under vacuum to give the product as a white solid which was used in the next step without further purification (5.4 g, 74%) ^{1}H NMR ($CDCl_3$) δ 4.10 (s, 1H), 4.71 (d, J = 6.5 Hz, 2H), 5.13 (s, 2H), 6.07 (s, 1H), 7.36 (s, 5H); m/z (LCMS, ESI): calc. for $[M + H]^+$ 182.1; found 182.2

4.2.3. Synthesis of benzyl *N*-(acetoxymethyl)-carbamate (2)

Compound **1** (3.6 g, 20 mmol) was dissolved in 25 mL anhydrous THF and was added slowly to an ice-cooled stirred solution of 23 mL acetic anhydride and 6.5 mL anhydrous pyridine under Argon. The mixture was stirred at r.t. for 2 h, then the solution was diluted with 150 mL ethyl acetate and washed with 1 M HCl (3X 150 mL) and brine (2X 150 mL). The organic layer was dried with anhydrous magnesium sulfate and the volatile materials were removed under vacuum to give an oily residue which was purified with flash chromatography (3.0 g, 67%) of the pure product. ^{1}H NMR ($CDCl_3$) δ 2.08 (s, 3H), 5.16 (s, 2H), 5.23 (d, J = 7.5 Hz, 2H), 6.08 (s, 1H), 7.38 (s, 5H); m/z (LCMS, ESI): calc. for $[M + Na]^+$ 246.1; found 246.0

4.2.4. Synthesis of dimethyl *N*-(benzyloxycarbonyl)-aminomethylphosphonate (3)

A mixture of compound **2** (2.9 g, 13 mmol) and trimethylphosphite (4.6 mL, 39 mmol) was refluxed for 3 h. The volatile materials were removed by distillation at 60^{o} C under reduced pressure to give the product as an oily residue which was used in the next step without further purification (3.4 g, 97%) ^{1}H NMR ($CDCl_3$) δ 3.62 (dd, J = 6.5 Hz, J_{H-P} = 11.0 Hz, 2H), 3.72 (d, J_{H-P} = 11.0 Hz, 6H), 5.09 (s, 2H), 5.83 (s, 1H), 7.25-7.40 (m, 5H), ^{31}P NMR ($CDCl_3$) δ 25.32; m/z (LCMS, ESI): calc. for $[M + Na]^+$ 296.1; found 296.1

4.2.5. Synthesis of methyl *N*-(benzyloxycarbonyl)-aminomethylphosphonate (4)

Compound **3** (3.3 g, 12 mmol) was shook vigorously with 10% NaOH (14.5 mL, 3 equiv.) until it was completely dissolved. The mixture was stirred at room temperature for 2 h then diluted with water, extracted with ethyl acetate (2X 30 mL), and acidified to pH 1 with 2 M HCl. The aqueous solution was extracted with dichloromethane (2X 100 mL) and ethyl acetate (2X 50 mL). The dichloromethane layers were combined, washed with brine (2X 50 mL), and dried using anhydrous magnesium sulfate. The ethyl acetate layers were also combined, washed with brine (2X 25 mL), and dried with anhydrous magnesium sulfate. The two organic layers were then combined and the volatile solvents were removed under high vacuum to give the product as a pure white solid (2.3 g, 73%). ^{1}H NMR ($CDCl_3$) δ 3.64 (d, J_{H-P} = 11.0 Hz, 2H), 3.71 (d, J_{H-P} = 11.0 Hz, 3H), 5.12 (s, 2H), 5.7 (brs, 1H), 7.28-7.42 (m, 5H), 11.8 (brs, 1H), ^{31}P NMR ($CDCl_3$) δ 24.12; m/z (LCMS, ESI): calc. for $[M + Na]^+$ 282.1; found 282.1

4.2.6. General procedure for amide coupling: To a cooled solution of Boc-L-leucine (1.0 equiv.), the amine/α-aminoester HCl (1.2-1.5 equiv.), and PyBop 1.2 equiv. (or EDCI.HCl 1.2 equiv. and HOBt 1.2 equiv.) in anhydrous DMF was added diisopropylethylamine (3.3-4.0 equiv.) gradually. The reaction mixture was stirred at room temperature for 5 h to overnight, diluted with ethyl acetate (50 mL for every 5 mL DMF), then extracted with 1 M HCl (3X), saturated sodium bicarbonate (3X), and brine (2X). The organic layer was then dried with anhydrous sodium sulfate and the solvent was evaporated under vacuum to give the products which were purified by flash chromatography whenever needed.

4.2.6.1. (*S*)-2-(*tert*-butoxycarbonylamino)-*N*-isopentylpropanamide (IA1)

Following the general procedure for amide coupling, Boc-L-alanine (473 mg, 2.5 mmol) was reacted with isoamylamine (262 mg, 3.0 mmol) in anhydrous DMF (10 mL), using PyBop as a coupling reagent (1.56 g, 3.0 mmol) and diisopropylethylamine (1.07 g, 8.25 mmol) as a base. 419 mg of compound **IA1** was obtained after purification with flash chromatography (65%). ^{1}H NMR (DMSO-d_6) δ 0.85 (d, J = 6.4 Hz, 6H), 1.14 (d, J = 6.8 Hz, 3H), 1.29 (m, 2H), 1.37 (s, 9H), 1.55 (m, 1H), 3.06 (m, 2H), 3.90 (m, 1H), 6.81 (d, J = 8.5 Hz, 1H), 7.66 (t, 1H); m/z (LCMS, ESI): calc. for $[M + H]^+$ 259.2; found 259.1

4.2.6.2. (*S*)-2-(*tert*-butoxycarbonylamino)-*N*-isopentylbutanamide (IA2)

Following the general procedure for amide coupling, Boc-L-α-aminobutyric acid (508 mg, 2.5 mmol) was reacted with isoamylamine (262 mg, 3.0 mmol) in anhydrous DMF (10 mL), using PyBop as a coupling reagent (1.56 g, 3.0 mmol) and diisopropylethylamine as a base (1.07 g, 8.25 mmol). 483 mg of compound **IA2** was obtained after purification with flash chromatography (71%). ^{1}H NMR (DMSO-d_6) 0.82 (t, J = 7.0 Hz, 3H), δ 0.85 (d, J = 6.5 Hz, 6H), 1.28 (q, J = 7.5 Hz, 2H), 1.38 (s, 9H), 1.47 (m, 2H), 1.55 (m, 1H), 3.06 (m, 2H), 3.78 (m, 1H), 6.72 (d, J = 8.0 Hz, 1H), 7.73 (t, J = 6.3 Hz, 1H); m/z (LCMS, ESI): calc. for $[M + H]^+$ 273.2; found 273.2

4.2.6.3. (*S*)-2-(*tert*-butoxycarbonylamino)-*N*-isopentylpentanamide (IA3)

Following the general procedure for amide coupling, Boc-L-norvaline (543 mg, 2.5 mmol) was reacted with isoamylamine (262 mg, 3.0 mmol) in anhydrous DMF (10 mL) using PyBop as a coupling reagent (1.56 g, 3.0 mmol) and diisopropylethylamine (1.07 g, 8.25 mmol). 493 mg of compound **IA3** was obtained after purification with flash chromatography (69%). ^{1}H NMR (DMSO-d_6) δ 0.79 (m, 9H), 1.29 (m, 4H), 1.30 (s, 9H), 1.44 (m, 3H), 2.99 (m, 2H), 3.77 (m, 1H), 6.65 (d, J = 6.4 Hz, 1H), 7.64 (t, 1H); m/z (LCMS, ESI): calc. for $[M + Na]^+$ 309.2; found 309.1

4.2.6.4. ((*S*)-2-(*tert*-butoxycarbonylamino)propanoyl)-L-leucine methyl ester (IA5)

Following the general procedure for amide coupling, Boc-L-alanine (473 mg, 2.5 mmol) was reacted with L-leucine methyl ester hydrochloride (545 mg, 3.0 mmol) in anhydrous DMF (10

mL), using PyBop as a coupling reagent (1.56 g, 3.0 mmol) and diisopropylethylamine (1.07 g, 8.25 mmol) as a base. 569 mg of compound **IA5** was obtained after purification with flash chromatography (72%). ^{1}H NMR (DMSO-d_6) δ 0.84 (d, J = 6.5 Hz, 3H), 0.90 (d, J = 6.5 Hz, 3H), 1.17 (d, J = 7.0 Hz, 3H), 1.38 (s, 9H), 1.45-1.70 (m, 3H), 3.62 (s, 3H), 3.98 (m, 1H), 4.30 (m, 1H), 6.88 (d, J = 8.5 Hz, 1H), 8.07 (d, J = 7.5 Hz, 1H); m/z (LCMS, ESI): calc. for $[M + Na]^+$ 339.2; found 339.1

4.2.6.5. ((*S*)-2-(*tert*-butoxycarbonylamino)butanoyl)-L-leucine methyl ester (IA6)

Following the general procedure for amide coupling, Boc-L-α-aminobutyric acid (508 mg, 2.5 mmol) was reacted with L-leucine methyl ester hydrochloride (545 mg, 3.0 mmol) in anhydrous DMF (10 mL), using PyBop as a coupling reagent (1.56 g, 3.0 mmol) and diisopropylethylamine (1.07 g, 8.25 mmol) as a base. 644 mg of compound **IA6** was obtained after purification with flash chromatography (78%). ^{1}H NMR (DMSO-d_6) δ 0.85 (m, 6H), 0.9 (d, J = 6.5 Hz, 3H), 1.38 (s, 9H), 1.45-1.70 (m, 5H), 3.62 (s, 3H), 3.87 (m, 1H), 4.31 (m, 1H), 6.76 (d, J = 8.5 Hz, 1H), 8.22 (d, J = 7.5 Hz, 1H); m/z (LCMS, ESI): calc. for $[M + H]^+$ 331.2; found 331.2

4.2.6.6. ((*S*)-2-(*tert*-butoxycarbonylamino)pentanoyl)-L-leucine methyl ester (IA7)

Following the general procedure for amide coupling, Boc-L-norvaline (543 mg, 2.5 mmol) was reacted with L-leucine methyl ester hydrochloride (545 mg, 3.0 mmol) in anhydrous DMF (10 mL), using PyBop as a coupling reagent (1.56 g, 3.0 mmol) and diisopropylethylamine (1.07 g, 8.25 mmol) as a base. 645 mg of compound **IA7** was obtained after purification with flash chromatography (75%). ^{1}H NMR (DMSO-d_6) δ 0.83 (m, 9H), 1.29 (m, 2H), 1.35 (s, 9H), 1.38-1.68 (m, 5H), 3.59 (s, 3H), 3.90 (m, 1H), 4.17 (m, 1H), 6.75 (d, J = 8.4 Hz, 1H), 8.07 (d, J = 8.0 Hz, 1H); m/z (LCMS, ESI): calc. for $[M + Na]^+$ 367.2; found 367.1

4.2.6.7. (*S*)-2-(*tert*-butoxycarbonylamino)-*N*-ethylpropanamide (IA32)

Following the general procedure for amide coupling, Boc-L-alanine (473 mg, 2.5 mmol) was reacted with ethylamine hydrochloride (306 mg, 3.7 mmol) in anhydrous DMF (12 mL), using EDCI.HCl (573 mg, 3.0 mmol) and HOBt (405 mg, 3.0 mmol) as coupling reagents and diisopropylethylamine (1.29 g, 10.0 mmol) as a base. 437 mg of compound **IA32** was obtained and used without further purification (67%). ^{1}H NMR (DMSO-d_6) δ 1.00 (t, J = 7.5 Hz, 3H),

1.15 (d, J = 6.5 Hz, 3H), 1.38 (s, 9H), 3.05 (m, 2H), 3.90 (m, 1H), 6.82 (d, J = 7.5 Hz, 1H), 7.74 (t, 1H); m/z (LCMS, ESI): calc. for $[M + Na]^+$ 239.2; found 239.0

4.2.6.8. (*S*)-2-(*tert*-butoxycarbonylamino)-*N*-propylpropanamide (IA33)

Following the general procedure for amide coupling, Boc-L-alanine (473 mg, 2.5 mmol) was reacted with propylamine hydrochloride (287 mg, 3.0 mmol) in anhydrous DMF (10 mL), using EDCI.HCl (573 mg, 3.0 mmol) and HOBt (405 mg, 3.0 mmol) as coupling reagents and diisopropylethylamine (1.07 g, 8.25 mmol) as a base. 403 mg of compound **IA33** was obtained and used without further purification (70%). ^{1}H NMR (DMSO-d_6) δ 0.83 (t, 3H), 1.15 (d, J = 7.5 Hz, 3H), 1.38 (s, 9H), 1.40 (m, 2H), 3.00 (m, 2H), 3.92 (m, 1H), 6.83 (d, J = 8.5 Hz, 1H), 7.71 (t, 1H); m/z (LCMS, ESI): calc. for $[M + Na]^+$ 253.2; found 253.1

4.2.6.9. (*S*)-2-(*tert*-butoxycarbonylamino)-*N*-(2-phenylethyl)-propanamide (IA34)

Following the general procedure for amide coupling, Boc-L-alanine (473 mg, 2.5 mmol) was reacted with 2-phenylethylamine hydrochloride (473 mg, 3.0 mmol) in anhydrous DMF (10 mL), using EDCI.HCl (573 mg, 3.0 mmol) and HOBt (405 mg, 3.0 mmol) as coupling reagents and diisopropylethylamine (1.07 g, 8.25 mmol) as a base. 504 mg of compound **IA34** was obtained after purification with flash chromatography (69%). ^{1}H NMR (DMSO-d_6) δ 1.12 (d, J = 7.0 Hz, 3H), 1.38 (s, 9H), 2.51 (t, J = 7.5 Hz, 2H), 3.34 (m, 2H), 3.72 (m, 1H), 6.83 (d, J = 8.5 Hz, 1H), 7.16-7.32 (m, 5H), 7.83 (t, J = 5.0 Hz, 1H); m/z (LCMS, ESI): calc. for $[M + Na]^+$ 315.2; found 315.1

4.2.6.10. (*N*-(*tert*-butoxycarbonyl)-L-alaninyl)-glycine ethyl ester (IA35)

Following the general procedure for amide coupling, Boc-L-alanine (473 mg, 2.5 mmol) was reacted with glycine ethyl ester hydrochloride (419 mg, 3.0 mmol) in anhydrous DMF (10 mL), using EDCI.HCl (573 mg, 3.0 mmol) and HOBt (405 mg, 3.0 mmol) as coupling reagents and diisopropylethylamine (1.07 g, 8.25 mmol) as a base. 501 mg of compound **IA35** was obtained after purification with flash chromatography (73%). ^{1}H NMR (DMSO-d_6) δ 1.18 (m, 6H), 1.38 (s, 9H), 3.83 (m, 2H), 4.00 (m, 1H), 4.08 (q, J = 7.0 Hz, 2H), 6.94 (d, J = 7.5 Hz, 1H), 8.18 (t, 1H); m/z (LCMS, ESI): calc. for $[M + Na]^+$ 297.2; found 297.1

4.2.6.11. (*N*-(*tert*-butoxycarbonyl)-L-alaninyl)-L-alanine methyl ester (IA36)

Following the general procedure for amide coupling, Boc-L-alanine (473 mg, 2.5 mmol) was reacted with alanine methyl ester hydrochloride (419 mg, 3.0 mmol) in anhydrous DMF (10 mL), using EDCI.HCl (573 mg, 3.0 mmol) and HOBt (405 mg, 3.0 mmol) as coupling reagents and diisopropylethylamine (1.07 g, 8.25 mmol) as a base. 480 mg of compound **IA36** was obtained after purification with flash chromatography (70%). ^{1}H NMR (DMSO-d_6) δ 1.17 (d, 3H), 1.28 (d, J = 7.5 Hz, 3H), 1.38 (s, 9H), 3.62 (s, 3H), 3.98 (m, 1H), 4.27 (m, 1H), 6.88 (d, J = 8.0 Hz, 1H), 8.18 (d, J = 7.0 Hz, 1H); m/z (LCMS, ESI): calc. for $[M + Na]^+$ 297.2; found 297.1

4.2.6.12. Methyl (*S*)-*N*-(*N*-(*tert*-butoxycarbonyl)-L-alaninyl)-2-aminobutanoate (IA37)

Following the general procedure for amide coupling, Boc-L-alanine (473 mg, 2.5 mmol) was reacted with methyl L-α-aminobutyrate hydrochloride (461 mg, 3.0 mmol: synthesized in-house) in anhydrous DMF (10 mL), using EDCI.HCl (573 mg, 3.0 mmol) and HOBt (405 mg, 3.0 mmol) as coupling reagents and diisopropylethylamine (1.07 g, 8.25 mmol) as a base. 547 mg of compound **IA37** was obtained after purification with flash chromatography (76%); m/z (LCMS, ESI): calc. for $[M + Na]^+$ 311.2; found 311.1

4.2.6.13. (*N*-(*tert*-butoxycarbonyl)-L-alaninyl)-L-phenylalanine methyl ester (IA38)

Following the general procedure for amide coupling, Boc-L-alanine (473 mg, 2.5 mmol) was reacted with phenylalanine methyl ester hydrochloride (647 mg, 3.0 mmol) in anhydrous DMF (10 mL), using EDCI.HCl (573 mg, 3.0 mmol) and HOBt (405 mg, 3.0 mmol) as coupling reagents and diisopropylethylamine (1.07 g, 8.25 mmol) as a base. 683 mg of compound **IA38** was obtained after purification with flash chromatography (78%). ^{1}H NMR (DMSO-d_6) δ 1.12 (d, J = 7.5 Hz, 3H), 1.37 (s, 9H), 2.98 (m, 2H), 3.58 (s, 3H), 3.97 (m, 1H), 4.47 (m, 1H), 6.87 (d, J = 8.5 Hz, 1H), 7.17-7.29 (m, 5H), 8.23 (d, J = 7.5 Hz, 1H); m/z (LCMS, ESI): calc. for $[M + Na]^+$ 373.2; found 373.1

4.2.7. General procedure for Boc deprotection: The Boc-protected compound was dissolved either in 3 M HCl/MeOH or in ethyl acetate. When the compound is dissolved into ethyl acetate, hydrogen chloride gas generated from the reaction of sulfuric acid and sodium chloride was bubbled into the solution at 0 °C. The solution was then stirred for 1.5-3 h at room temperature when HCl/MeOH solution is used or at 0 °C when HCl is bubbled into the solution. The volatile

materials were then removed under vacuum to give the product as hygroscopic solid which was purified with reverse phase HPLC.

4.2.7.1. (*S*)-2-amino-*N*-isopentylpropanamide hydrochloride (IB1)

Following the general procedure for Boc deprotection, compound **IA1** (387 mg, 1.5 mmol) was exposed to 3 M HCl/MeOH (3.0 mL) for 3 h. 276 mg of compound **IB1** was obtained after purification with reverse phase HPLC (95%). ^{1}H NMR (DMSO-d_6) δ 0.84 amd 0.85 (2 x d, J = 6.5 Hz, 6H), 1.30 (q, J = 7.0 Hz, 2H), 1.34 (d, J = 7.0 Hz, 3H), 1.57 (m, 1H), 3.07 (m, 1H), 3.12 (m, 1H), 3.81 (m, 1H), 8.35 (brs, 3H), 8.69 (t, J = 5.5 Hz, 1H); m/z (LCMS, ESI): calc. for $[M + H]^+$ 159.2; found 159.1

4.2.7.2. (*S*)-2-amino-*N*-isopentylbutanamide hydrochloride (IB2)

Following the general procedure for Boc deprotection, compound **IA2** (408 mg, 1.5 mmol) was exposed to 3 M HCl/MeOH (3.0 mL) for 3 h. 302 mg of compound **IB2** was obtained after purification with reverse phase HPLC (97%). ^{1}H NMR (DMSO-d_6) δ 0.86 (m, 9H), 1.30 (m, 2H), 1.56 (m, 1H), 1.72 (m, 2H), 3.05 (m, 1H), 3.18 (m, 1H), 3.65 (t, 1H), 8.20 (brs, 3H), 8.55 (t, J = 5.5 Hz, 1H); m/z (LCMS, ESI): calc. $[M + H]^+$ 173.2; found 173.1

4.2.7.3. (*S*)-2-amino-*N*-isopentylpentanamide hydrochloride (IB3)

Following the general procedure for Boc deprotection, compound **IA3** (429 mg, 1.5 mmol) was exposed to 3 M HCl/MeOH (3.0 mL) for 3 h. 315 mg of compound **IB3** was obtained after purification with reverse phase HPLC (95%). ^{1}H NMR (DMSO-d_6) δ 0.85 (m, 9H), 1.27 (m, 4H), 1.62 (m, 3H), 3.05 (m, 1H), 3.17 (m, 1H), 3.68 (t, 1H), 8.25 (brs, 3H), 8.56 (t, J = 5.5 Hz, 1H); m/z (LCMS, ESI): calc. for $[M + Na]^+$ 209.2; found 209.1

4.2.7.4. ((*S*)-2-aminopropanoyl)-L-leucine methyl ester hydrochloride (IB5)

Following the general procedure for Boc deprotection, compound **IA5** (474 mg, 1.5 mmol) was exposed to 3 M HCl/MeOH (3.0 mL) for 3 h. 370 mg of compound **IB5** was obtained after purification with reverse phase HPLC (98%). ^{1}H NMR (CD_3OD) δ 0.93 (d, J = 6.4 Hz, 3H), 0.96 (d, J = 6.4 Hz, 3H), 1.52 (d, J = 6.8 Hz, 3H), 1.67 (m, 3H), 3.71 (s, 3H), 3.76 (m, 1H), 4.49 (m, 1H); m/z (LCMS, ESI): calc. for $[M + H]^+$ 217.2; found 217.1

4.2.7.5. ((*S*)-2-aminobutanoyl)-L-leucine methyl ester hydrochloride (IB6)

Following the general procedure for Boc deprotection, compound **IA6** (495 mg, 1.5 mmol) was exposed to 3 M HCl/MeOH (3.0 mL) for 3 h. 383 mg of compound **IB6** was obtained after purification with reverse phase HPLC (96%). ^{1}H NMR (DMSO-d_6) δ 0.88 (m, 9H), 1.46-1.86 (m, 5H), 3.61 (s, 3H), 3.76 (t, 1H), 4.30 (m, 1H), 8.26 (brs, 3H), 8.86 (d, J = 7.2 Hz, 1H); m/z (LCMS, ESI): calc. for $[M + H]^+$ 231.2; found 231.2

4.2.7.6. ((*S*)-2-aminopentanoyl))-L-leucine methyl ester hydrochloride (IB7)

Following the general procedure for Boc deprotection, compound **IA7** (516 mg, 1.5 mmol) was exposed to 3 M HCl/MeOH (3.0 mL) for 3 h. 407 mg of compound **IB7** was obtained after purification with reverse phase HPLC (97%). ^{1}H NMR (DMSO-d_6) δ 0.87 (m, 9H), 1.35 (m, 2H), 1.50 (m, 5H), 3.61 (s, 3H), 3.78 (m, 1H), 4.29 (m, 1H), 8.23 (brs, 3H), 8.83 (d, J = 7.2 Hz, 1H); m/z (LCMS, ESI): calc. for $[M + H]^+$ 245.2; found 245.1

4.2.7.7. (*S*)-2-amino-*N*-ethylpropanamide hydrochloride (IB32)

Following the general procedure for Boc deprotection, compound **IA32** (324 mg, 1.5 mmol) was exposed to 3 M HCl/MeOH (3.0 mL) for 3 h. 213 mg of compound **IB32** was obtained after purification with reverse phase HPLC (94%). ^{1}H NMR (DMSO-d_6) δ 1.03 (t, J = 7.4 Hz, 3H), 1.32 (d, J = 6.8 Hz, 3H), 3.10 (m, 2H), 3.75 (q, 1H), 8.23 (brs, 3H), 8.52 (t, J = 5.5 Hz, 1H); m/z (LCMS, ESI): calc. for $[2M + H]^+$ 233.2; found 233.1

4.2.7.8. (*S*)-2-amino-*N*-propylpropanamide hydrochloride (IB33)

Following the general procedure for Boc deprotection, compound **IA33** (345 mg, 1.5 mmol) was exposed to 3 M HCl/MeOH (3.0 mL) for 3 h. 239 mg of compound **IB33** was obtained after purification with reverse phase HPLC (96%). ^{1}H NMR (DMSO-d_6) δ 0.84 (t, J = 7.4 Hz, 3H), 1.33 (d, J = 6.8 Hz, 3H), 1.42 (m, 2H), 3.04 (m, 2H), 3.78 (q, J = 7.2 Hz, 1H), 8.25 (brs, 3H), 8.54 (t, J = 5.5 Hz, 1H); m/z (LCMS, ESI): calc. for $[M + H]^+$ 130.1; found 130.0

4.2.7.9. (*S*)-2-amino-*N*-(2-phenylethyl)-propanamide hydrochloride (IB34)

Following the general procedure for Boc deprotection, compound **IA34** (438 mg, 1.5 mmol) was exposed to 3 M HCl/MeOH (3.0 mL) for 3 h. 331 mg of compound **IB34** was obtained after purification with reverse phase HPLC (97%). ^{1}H NMR (DMSO-d_6) δ 1.27 (d, J = 7.2 Hz, 3H),

2.73 (m, 2H), 3.26 (m, 1H), 3.38 (m, 1H), 3.73 (brs, 1H), 7.16-7.30 (m, 5H), 8.20 (brs, 3H), 8.57 (t, J = 6.0 Hz, 1H); m/z (LCMS, ESI): calc. for $[2M + H]^+$ 385.2; found 385.0

4.2.7.10. L-alaninyl glycine ethyl ester hydrochloride (IB35)

Following the general procedure for Boc deprotection, an ethyl acetate solution of compound **IA35** (411 mg, 1.5 mmol) was exposed to hydrogen chloride gas bubbling for 3 h. 296 mg of compound **IB35** was obtained after purification with reverse phase HPLC (94%). ^{1}H NMR (DMSO-d_6) δ 1.20 (t, J = 7.0 Hz, 3H), 1.38 (d, J = 7.0 Hz, 3H), 3.92 (m, 3H), 4.10 (q, J = 7.0 Hz, 2H), 8.24 (brs, 3H), 8.94 (t, J = 5.8 Hz, 1H); m/z (LCMS, ESI): calc. for $[2M + H]^+$ 349.2; found 349.0

4.2.7.11. L-alaninyl-L-alanine methyl ester hydrochloride (IB36)

Following the general procedure for Boc deprotection, compound **IA36** (411 mg, 1.5 mmol) was exposed to 3 M HCl/MeOH (3.0 mL) for 3 h. 304 mg of compound **IB36** was obtained after purification with reverse phase HPLC (97%). ^{1}H NMR (DMSO-d_6) δ 1.29 and 1.34 (2 d, J = 7.0 Hz, together 6H), 3.62 (s, 3H), 3.82 (q, 1H), 4.22 (m, 1H), 8.20 (brs, 3H), 8.70 (d, J = 7.0 Hz, 1H); m/z (LCMS, ESI): calc. for $[2M + H]^+$ 349.2; found 349.0

4.2.7.12. Methyl (*S*)-*N*-(L-alaninyl)-2-aminobutanoate hydrochloride (IB37)

Following the general procedure for Boc deprotection, compound **IA37** (432 mg, 1.5 mmol) was exposed to 3 M HCl/MeOH (3.0 mL) for 3 h. 318 mg of compound **IB37** was obtained after purification with reverse phase HPLC (95%). m/z (LCMS, ESI): calc. for $[M + H]^+$ 189.1; found 189.0

4.2.7.13. L-alaninyl-L-phenylalanine methyl ester hydrochloride (IB38)

Following the general procedure for Boc deprotection, compound **IA38** (525 mg, 1.5 mmol) was exposed to 3 M HCl/MeOH (3.0 mL) for 3 h. 419 mg of compound **IB38** was obtained after purification with reverse phase HPLC (98%). m/z (LCMS, ESI): calc. for $[M + H]^+$ 251.1; found 251.1

4.2.8. General procedure for the synthesis of compounds 1-3, 5-7, and 31-38: To a cooled solution of compound **4** (1 equiv.), any of compounds **IB1-3**, **IB5-7** or **IB31-38** (1.2-1.5 equiv.), and PyBop (1.2 equiv.) in anhydrous DCM was added diisopropylethylamine (4 equiv.)

gradually. The reaction mixture was stirred at r.t. for 6 h to overnight. The reaction mixture was then diluted with DCM up to 25 mL; extracted with 5% citric acid (2X 12 mL), saturated sodium bicarbonate (2X 12 mL), and brine (2X 10 mL); and dried over anhydrous sodium sulfate. The solvent was then evaporated under reduced pressure and the residue was purified by semi-preparative HPLC to give the intermediate that corresponds to the starting material among **IC1-3**, **IC5-7** or **IC31-38**. This intermediate was then hydrolyzed in the following manner: 0.2 mmol of this intermediate was vigorously shaken at room temperature with 1-2 mL 0.4 M LiOH aqueous solution until all the solid dissolves (acetonitrile was used as a co-solvent whenever needed). The solution was then stirred for 2– 24 h and concentrated under vacuum. The final compound was then separated as a pure lithium or di-lithium salt using semi-preparative reverse phase HPLC.

4.2.8.1. (*S*)-2-((*N*-(benzyloxycarbonyl)-aminomethylphosphonyl)amino)-*N*-isopentyl propanamide lithium (1)

Following the general procedure for the synthesis of compounds **1-3**, **5-7**, and **31-38**, compound **4** (215 mg, 0.83 mmol) was reacted with compound **IB1** (195 mg, 1.0 mmol) in anhydrous DCM (3.0 mL), using PyBop (520 mg, 1.0 mmol) as a coupling reagent and diisopropylethylamine (428 mg, 3.3 mmol) as a base. 162 mg of compound **IC1**, which is the PO-methyl ester version of the desired product, was obtained after purification with reverse phase HPLC (49%). 80 mg of this compound (0.2 mmol) was then exposed to LiOH (1.5 mL of the 0.4 M solution referred to in the general procedure) overnight, and the final product was separated by reverse phase HPLC as a pure white solid (55 mg, 71%). ^{1}H NMR (D_2O) δ 0.72 (d, J = 7.0 Hz, 6H), 1.10 (d, J = 7.0 Hz, 3H), 1.23 (q, J = 6.5 Hz, 2H), 1.41 (m, 1H), 3.07 (m, 4H), 3.52 (m, 1H), 4.99 (s, 2H), 7.29 (m, 5H), ^{13}C NMR (D_2O) δ 21.83, 21.88, 23.10 and 26.61 (4C, $\underline{C}H(\underline{C}H_3)_2$ & $CH\underline{C}H_3$), 38.72 and 39.12 (2C, $\underline{C}H_2\underline{C}H_2$), 40.95 (d, $J_{C\text{-}P}$ = 543 Hz, 1C, $\underline{C}H_2P$), 52.54 (1C, $\underline{C}HCONH$), 68.53 (1C, $Ph\underline{C}H_2O$), 129.16, 129.82, 130.22 and 137.89 (6C, Ph), 159.66 (1C, Cbz $\underline{C}$=O), 179.09 (1C, $\underline{C}$=O), ^{31}P NMR (D_2O) δ 18.03; m/z (HRMS, ESI): calc. for $C_{17}H_{28}O_5N_3NaP$, $[M - Li + H + Na]^+$, 408.1659; found 408.1668

4.2.8.2. (*S*)-2-((*N*-(benzyloxycarbonyl)-aminomethylphosphonyl)amino)-*N*-isopentylbutanamide lithium (2)

Following the general procedure for the synthesis of compounds **1-3**, **5-7**, and **31-38**, compound **4** (215 mg, 0.83 mmol) was reacted with compound **IB2** (209 mg, 1.0 mmol) in anhydrous DCM (3.0 mL), using PyBop (520 mg, 1.0 mmol) as a coupling reagent and diisopropylethylamine (428 mg, 3.3 mmol) as a base. 192 mg of compound **IC2**, which is the PO-methyl ester version of the desired product, was obtained after purification with reverse phase HPLC (56%). 83 mg of this compound (0.2 mmol) was then exposed to LiOH (1.5 mL of the 0.4 M solution referred to in the general procedure; an additional 1.5 mL of acetonitrile was used as a cosolvent) overnight, and the final product was separated by reverse phase HPLC as a pure white solid (66 mg, 82%). ^{1}H NMR (D_2O) δ 0.72 (m, 9H), 1.23 (q, J = 7.2 Hz, 2H), 1.45 (m, 3H), 3.02 (m, 2H), 3.15 (m, 2H), 3.38 (m, 1H), 4.99 (s, 2H), 7.30 (m, 5H), ^{13}C NMR (CD_3OD) δ 10.37, 22.97, 23.01, and 27.08 (4C, $\underline{C}H(\underline{C}H_3)_2$ & $CH_2\underline{C}H_3$), 28.93 (d, $J_{C\text{-}P}$ = 17.6 Hz, 1C, $\underline{C}H_2CH_3$) 38.84 and 39.49 (2C, $\underline{C}H_2\underline{C}H_2$), 41.68 (d, $J_{C\text{-}P}$ = 544 Hz, 1C, $\underline{C}H_2P$), 58.25 (1C, $\underline{C}HCONH$), 67.79 (1C, $Ph\underline{C}H_2O$), 129.03, 129.12, 129.59 and 138.47 (6C, Ph), 158.97 (d, $J_{C\text{-}P}$ = 32.8 Hz, 1C, Cbz $\underline{C}$=O), 177.35 (1C, $\underline{C}$=O), ^{31}P NMR (D_2O) δ 17.87; m/z (HRMS, ESI): calc. for $C_{18}H_{30}O_5N_3LiP$, $[M + H]^+$, 406.2078; found 406.2091

4.2.8.3. (*S*)-2-((*N*-(benzyloxycarbonyl)-aminomethylphosphonyl)amino)-*N*-isopentyl pentanamide lithium (3)

Following the general procedure for the synthesis of compounds **1-3**, **5-7**, and **31-38**, compound **4** (215 mg, 0.83 mmol) was reacted with compound **IB3** (223 mg, 1.0 mmol) in anhydrous DCM (3.0 mL), using PyBop (520 mg, 1.0 mmol) as a coupling reagent and diisopropylethylamine (428 mg, 3.3 mmol) as a base. 184 mg of compound **IC3**, which is the PO-methyl ester version of the desired product, was obtained after purification with reverse phase HPLC (52%). 85 mg of this compound (0.2 mmol) was then exposed to LiOH (1.5 mL of the 0.4 M solution referred to in the general procedure; an additional 1.5 mL of acetonitrile was used as a cosolvent) overnight, and the final product was separated by reverse phase HPLC as a pure white solid (65 mg, 78%). ^{1}H NMR (D_2O) δ 0.73 (m, 9H), 1.15 (m, 2H), 1.22 (q, J = 7.2 Hz, 2H), 1.41 (m, 3H), 3.07 (m, 4H), 3.45 (m, 1H), 5.00 (s, 2H), 7.30 (m, 5H), ^{13}C NMR (CD_3OD) δ 14.45 and 19.94 (2C, $CH_2\underline{C}H_2\underline{C}H_3$), 22.96, 22.99, and 27.08 (3C, $\underline{C}H(\underline{C}H_3)_2$), 29.20 (d, $J_{C\text{-}P}$ = 20.8 Hz, 1C, $\underline{C}H_2CH_2CH_3$) 38.83 and 39.45 (2C, $\underline{C}H_2\underline{C}H_2$), 41.71 (d, $J_{C\text{-}P}$ = 542 Hz, 1C, $\underline{C}H_2P$), 56.95 (1C, $\underline{C}HCONH$), 67.76 (1C, $Ph\underline{C}H_2O$), 128,98, 129.10, 129.58 and 138.46

(6C, Ph), 158.94 (d, J_{C-P} = 32.8 Hz, 1C, Cbz C=O), 177.61 (1C, C=O), ^{31}P NMR (D_2O) δ 17.69; m/z (HRMS, ESI): calc. for $C_{19}H_{32}O_5N_3LiP$, $[M + H]^+$, 420.2234; found 420.2238

4.2.8.4. Di-lithium ((*S*)-2-((*N*-(benzyloxycarbonyl)-aminomethylphosphonyl)amino)propanoyl)-L-leucinate (5)

Following the general procedure for the synthesis of compounds **1-3**, **5-7**, and **31-38**, compound **4** (215 mg, 0.83 mmol) was reacted with compound **IB5** (252 mg, 1.0 mmol) in anhydrous DCM (3.0 mL), using PyBop (520 mg, 1.0 mmol) as a coupling reagent and diisopropylethylamine (428 mg, 3.3 mmol) as a base. 205 mg of compound **IC5**, which is the di-ester version of the desired product, was obtained after purification with reverse phase HPLC (54%). 91 mg of this compound (0.2 mmol) was then exposed to LiOH (2.0 mL of the 0.4 M solution referred to in the general procedure) for 12 h, and the final product was separated by reverse phase HPLC as a pure white solid (54 mg, 62%). ^{1}H NMR (D_2O) δ 0.73 (d, J = 6.0 Hz, 3H), 0.77 (d, J = 6.0 Hz, 3H), 1.13 (d, J = 7.2 Hz, 3H), 1.48 (m, 3H), 3.17 (m, 2H), 4.05 (m, 1H), 5.02 (s, 2H), 7.31 (m, 5H), ^{13}C NMR (CD_3OD) δ 21.60 (d, J_{C-P} = 18.0 Hz, 1C, CH$\underline{C}H_3$), 22.45, 23.97, and 26.31 (3C, $\underline{C}H(\underline{C}H_3)_2$), 41.25 (d, J_{C-P} = 544 Hz, 1C, $\underline{C}H_2P$), 43.58 (1C, $\underline{C}H_2CH(CH_3)_2$), 52.75 and 54.75 (2C, $\underline{C}HCONH$), 67.78 (1C, Ph$\underline{C}H_2O$), 129.02, 129.07, 129.56 and 138.45 (6C, Ph), 159.18 (d, J_{C-P} = 26.8 Hz, 1C, Cbz C=O), 177.43 and 179.95 (2C, 2C=O), ^{31}P NMR (D_2O) δ 18.21; m/z (HRMS, ESI): calc. for $C_{18}H_{27}O_7N_3Li_2P$, $[M + H]^+$, 442.1901; found 442.1914

4.2.8.5. Di-lithium ((*S*)-2-((*N*-(benzyloxycarbonyl)-aminomethylphosphonyl)amino)butanoyl)-L-leucinate (6)

Following the general procedure for the synthesis of compounds **1-3**, **5-7**, and **31-38**, compound **4** (215 mg, 0.83 mmol) was reacted with compound **IB6** (266 mg, 1.0 mmol) in anhydrous DCM (3.0 mL), using PyBop (520 mg, 1.0 mmol) as a coupling reagent and diisopropylethylamine (428 mg, 3.3 mmol) as a base. 238 mg of compound **IC5**, which is the di-ester version of the desired product, was obtained after purification with reverse phase HPLC (61%). 94 mg of this compound (0.2 mmol) was then exposed to LiOH (2.0 mL of the 0.4 M solution referred to in the general procedure; an additional 2.0 mL of acetonitrile was used as a cosolvent) for 18 h, and the final product was separated by reverse phase HPLC as a pure white solid (78 mg, 86%). ^{1}H NMR (D_2O) δ 0.75 (m, 9H), 1.50 (m, 5H), 3.15 (m, 2H), 3.47 (m, 1H),

4.07 (t, J = 4.4 Hz, 1H), 4.99 (s, 2H), 7.30 (m, 5H), ^{13}C NMR (CD_3OD) δ 10.34 (1C, $CH_2\underline{C}H_3$), 22.37, 23.98, and 26.39 (3C, $\underline{C}H(\underline{C}H_3)_2$), 28.85 (d, $J_{C\text{-}P}$ = 20.8 Hz, 1C, $\underline{C}H_2CH_3$), 41.41 (d, $J_{C\text{-}P}$ = 547 Hz, 1C, $\underline{C}H_2P$), 43.59 (1C, $\underline{C}H_2CH(CH_3)_2$), 54.76 and 58.29 (2C, $\underline{C}HCONH$), 67.79 (1C, $Ph\underline{C}H_2O$), 129.03, 129.06, 129.57 and 138.46 (6C, Ph), 159.24 (d, $J_{C\text{-}P}$ = 30.0 Hz, 1C, Cbz $\underline{C}$=O), 176.65 and 179.90 (2C, 2$\underline{C}$=O), ^{31}P NMR (D_2O) δ 18.05; m/z (HRMS, ESI): calc. for $C_{19}H_{29}O_7N_3Li_2P$, $[M + H]^+$, 456.2058; found 456.2071

4.2.8.6. Di-lithium ((*S*)-2-((*N*-(benzyloxycarbonyl)-aminomethylphosphonyl)amino)pentanoyl)-L-leucinate (7)

Following the general procedure for the synthesis of compounds **1-3**, **5-7**, and **31-38**, compound **4** (215 mg, 0.83 mmol) was reacted with compound **IB7** (280 mg, 1.0 mmol) in anhydrous DCM (3.0 mL), using PyBop (520 mg, 1.0 mmol) as a coupling reagent and diisopropylethylamine (428 mg, 3.3 mmol) as a base. 253 mg of compound **IC7**, which is the di-ester version of the desired product, was obtained after purification with reverse phase HPLC (63%). 97 mg of this compound (0.2 mmol) was then exposed to LiOH (2.0 mL of the 0.4 M solution referred to in the general procedure; an additional 2.0 mL of acetonitrile was used as a cosolvent) overnight, and the final product was separated by reverse phase HPLC as a pure white solid (73 mg, 78%). ^{1}H NMR (D_2O) δ 0.75 (m, 9H), 1.17 (m, 2H), 1.48 (m, 5H), 3.15 (m, 2H), 3.52 (m, 1H), 4.07 (t, J = 8.8 Hz, 1H), 5.00 (s, 2H), 7.28 (m, 5H), ^{13}C NMR (CD_3OD) δ 14.54 and 19.97 (2C, $CH_2\underline{C}H_2\underline{C}H_3$), 22.42, 24.01, and 26.36 (3C, $\underline{C}H(\underline{C}H_3)_2$), 38.23 (d, $J_{C\text{-}P}$ = 18.8 Hz, 1C, $\underline{C}H_2CH_2CH_3$), 41.49 (d, $J_{C\text{-}P}$ = 546 Hz, 1C, $\underline{C}H_2P$), 43.61 (1C, $\underline{C}H_2CH(CH_3)_2$), 54.77 and 57.14 (2C, $\underline{C}HCONH$), 67.82 (1C, $Ph\underline{C}H_2O$), 129.04, 129.10, 129.60 and 138.49 (6C, Ph), 159.28 (d, $J_{C\text{-}P}$ = 38.0 Hz, 1C, Cbz $\underline{C}$=O), 176.99 and 179.91 (2C, 2$\underline{C}$=O), ^{31}P NMR (D_2O) δ 17.90; m/z (HRMS, ESI): calc. for $C_{20}H_{32}O_7N_3LiP$, $[M – Li + 2H]^+$, 464.2138; found 464.2139

4.2.8.7. (*S*)-2-((*N*-(benzyloxycarbonyl)-aminomethylphosphonyl)amino)-*N*-methyl propanamide lithium (31)

Following the general procedure for the synthesis of compounds **1-3**, **5-7**, and **31-38**, compound **4** (215 mg, 0.83 mmol) was reacted with compound **IB31** (139 mg, 1.0 mmol) in anhydrous DCM (3.0 mL), using PyBop (520 mg, 1.0 mmol) as a coupling reagent and diisopropylethylamine (428 mg, 3.3 mmol) as a base. 130 mg of compound **IC31**, which is the PO-methyl ester version of the desired product, was obtained after purification with reverse

phase HPLC (46%). 69 mg of this compound (0.2 mmol) was then exposed to LiOH (1.0 mL of the 0.4 M solution referred to in the general procedure) overnight, and the final product was separated by reverse phase HPLC as a pure white solid (47 mg, 71%). ^{1}H NMR (D_2O) δ 1.08 (d, J = 6.5 Hz, 3H), 2.56 (s, 3H), 3.15 (m, 2H), 3.49 (m, 1H), 4.98 (s, 2H), 7.28 (m, 5H), ^{13}C NMR (D_2O) δ 21.52 (d, J_{C-P} = 18.0 Hz, 1C, CH<u>C</u>H_3), 27.24 (1C, <u>C</u>H_3NH), 40.82 (d, J_{C-P} = 537 Hz, 1C, <u>C</u>H_2P), 52.55 (1C, <u>C</u>HCONH), 68.56 (1C, Ph<u>C</u>H_2O), 129.19, 129.82, 130.22 and 137.91 (6C, Ph), 159.70 (1C, Cbz <u>C</u>=O), 179.98 (1C, <u>C</u>=O), ^{31}P NMR (D_2O) δ 18.21; m/z (HRMS, ESI): calc. for $C_{13}H_{19}O_5N_3LiNaP$, $[M + Na]^+$, 358.1115; found 358.1110

4.2.8.8. (*S*)-2-((*N*-(benzyloxycarbonyl)-aminomethylphosphonyl)amino)-*N*-ethylpropanamide lithium (32)

Following the general procedure for the synthesis of compounds **1-3**, **5-7**, and **31-38**, compound **4** (215 mg, 0.83 mmol) was reacted with compound **IB32** (153 mg, 1.0 mmol) in anhydrous DCM (3.0 mL), using PyBop (520 mg, 1.0 mmol) as a coupling reagent and diisopropylethylamine (428 mg, 3.3 mmol) as a base. 150 mg of compound **IC32**, which is the PO-methyl ester version of the desired product, was obtained after purification with reverse phase HPLC (51%). 71 mg of this compound (0.2 mmol) was then exposed to LiOH (1.5 mL of the 0.4 M solution referred to in the general procedure) overnight, and the final product was separated by reverse phase HPLC as a pure white solid (54 mg, 78%). ^{1}H NMR (D_2O) δ 0.96 (t, J = 7.2 Hz, 3H), 1.11 (d, J = 7.2 Hz, 3H), 3.10 (m, 4H), 3.52 (m, 1H), 5.00 (s, 2H), 7.28 (m, 5H), ^{13}C NMR (D_2O) δ 14.69, 21.39, 35.51 (3C, CH<u>C</u>H_3 and <u>C</u>H_3<u>C</u>H_2NH), 40.64 (d, J_{C-P} = 545 Hz, 1C, <u>C</u>H_2P), 52.27 (1C, <u>C</u>HCONH), 68.30 (1C, Ph<u>C</u>H_2O), 128.95, 129.56, 129.92 and 137.61 (6C, Ph), 159.31 (1C, Cbz <u>C</u>=O), 178.83 (1C, <u>C</u>=O), ^{31}P NMR (D_2O) δ 18.14; m/z (LCMS, ESI): calc. for $[M – Li + Na + H]^+$ 366.1; found 366.0

4.2.8.9. (*S*)-2-((*N*-(benzyloxycarbonyl)-aminomethylphosphonyl)amino)-*N*-propyl propanamide lithium (33)

Following the general procedure for the synthesis of compounds **1-3**, **5-7**, and **31-38**, compound **4** (215 mg, 0.83 mmol) was reacted with compound **IB33** (167 mg, 1.0 mmol) in anhydrous DCM (3.0 mL), using PyBop (520 mg, 1.0 mmol) as a coupling reagent and diisopropylethylamine (428 mg, 3.3 mmol) as a base. 151 mg of compound **IC33**, which is the PO-methyl ester version of the desired product, was obtained after purification with reverse

phase HPLC (49%). 74 mg of this compound (0.2 mmol) was then exposed to LiOH (1.5 mL of the 0.4 M solution referred to in the general procedure) overnight, and the final product was separated by reverse phase HPLC as a pure white solid (51 mg, 70%). ^{1}H NMR (D_2O) δ 0.72 (t, J = 7.2 Hz, 3H), 1.11 (d, J = 6.8 Hz, 3H), 1.36 (m, 2H), 2.98 (m, 2H), 3.15 (m, 2H), 3.53 (m, 1H), 4.99 (s, 2H), 7.29 (m, 5H), ^{13}C NMR (CD_3OD) δ 11.88 and 23.77 (2C, $CH_2\underline{C}H_2\underline{C}H_3$), 21.58 (d, $J_{C\text{-}P}$ = 15.2 Hz, 1C, $CH\underline{C}H_3$), 41.51 (d, $J_{C\text{-}P}$ = 538 Hz, 1C, $\underline{C}H_2P$), 42.34 (1C, $\underline{C}H_2NH$), 52.69 (1C, $\underline{C}HCONH$), 67.81 (1C, $Ph\underline{C}H_2O$), 129.06, 129.14, 129.61 and 138.49 (6C, Ph), 159.97 (1C, Cbz $\underline{C}$=O), 178.27 (1C, $\underline{C}$=O), ^{31}P NMR (D_2O) δ 18.10; m/z (HRMS, ESI): calc. for $C_{15}H_{24}O_5N_3NaP$, $[M - Li + Na + H]^+$, 380.1346; found 380.1353

4.2.8.10. (*S*)-2-((*N*-(benzyloxycarbonyl)-aminomethylphosphonyl)amino)-*N*-(2-phenylethyl)- propanamide lithium (34)

Following the general procedure for the synthesis of compounds **1-3**, **5-7**, and **31-38**, compound **4** (215 mg, 0.83 mmol) was reacted with compound **IB34** (229 mg, 1.0 mmol) in anhydrous DCM (3.0 mL), using PyBop (520 mg, 1.0 mmol) as a coupling reagent and diisopropylethylamine (428 mg, 3.3 mmol) as a base. 197 mg of compound **IC34**, which is the PO-methyl ester version of the desired product, was obtained after purification with reverse phase HPLC (55%). 87 mg of this compound (0.2 mmol) was then exposed to LiOH (1.5 mL of the 0.4 M solution referred to in the general procedure; 1.5 mL of acetonitrile was used as a cosolvent) overnight, and the final product was separated by reverse phase HPLC as a pure white solid (68 mg, 81%). ^{1}H NMR (D_2O) δ 1.02 (d, J = 7.2 Hz, 3H), 2.68 (t, J = 6.8 Hz, 2H), 3.05 (m, 2H), 3.28 (m, 2H), 3.46 (m, 1H), 4.97 (m, 2H), 7.10-7.34 (m, 10H), ^{13}C NMR (CD_3OD) δ 21.64 (d, $J_{C\text{-}P}$ = 14.8 Hz, 1C, $CH\underline{C}H_3$), 36.72 (1C, $\underline{C}H_2Ph$), 41.40 (d, $J_{C\text{-}P}$ = 461 Hz, 1C, $\underline{C}H_2P$), 42.19 (1C, $\underline{C}H_2NH$), 52.70 (1C, $\underline{C}HCONH$), 67.81 (1C, $Ph\underline{C}H_2O$), 127.44, 129.05, 129.13, 129.61, 129.62, 129.99, 138.49, and 140.72 (12C, 2Ph), 158.99 (d, $J_{C\text{-}P}$ = 26.8 Hz, 1C, Cbz $\underline{C}$=O), 178.27 (1C, $\underline{C}$=O), ^{31}P NMR (D_2O) δ 18.10; m/z (HRMS, ESI): calc. for $C_{20}H_{26}O_5N_3NaP$, $[M - Li + Na + H]^+$, 442.1502; found 442.1496

4.2.8.11. Di-lithium ((*S*)-2-((*N*-(benzyloxycarbonyl)-aminomethylphosphonyl)amino)propanoyl)-glycinate (35)

Following the general procedure for the synthesis of compounds **1-3**, **5-7**, and **31-38**, compound **4** (215 mg, 0.83 mmol) was reacted with compound **IB35** (211 mg, 1.0 mmol) in

anhydrous DCM (3.0 mL), using PyBop (520 mg, 1.0 mmol) as a coupling reagent and diisopropylethylamine (428 mg, 3.3 mmol) as a base. 179 mg of compound **IC35**, which is the di-ester version of the desired product, was obtained after purification with reverse phase HPLC (52%). 83 mg of this compound (0.2 mmol) was then exposed to LiOH (2.0 mL of the 0.4 M solution referred to in the general procedure) overnight, and the final product was separated by reverse phase HPLC as a pure white solid (63 mg, 82%). ^{1}H NMR (D_2O) δ 1.04 (d, J = 7.2 Hz, 3H), 3.08 (m, 2H), 3.50 (m, 3H), 4.89 (s, 2H), 7.20 (m, 5H), ^{13}C NMR (D_2O) δ 21.13 (d, J_{C-P} = 14.8 Hz, 1C, CH<u>C</u>H$_3$), 41.56 (d, J_{C-P} = 542 Hz, 1C, <u>C</u>H$_2$P), 44.35 (1C, HN<u>C</u>H$_2$NCOO), 52.17 (1C, <u>C</u>HCONH), 68.20 (1C, Ph<u>C</u>H$_2$O), 128.86, 129.47, 129.87, and 137.57 (6C, Ph), 158.28 (d, J_{C-P} = 26.8 Hz, 1C, Cbz <u>C</u>=O), 177.46 and 178.78 (2C, 2<u>C</u>=O), ^{31}P NMR (D_2O) δ 18.43; m/z (LCMS, ESI): calc. for $[M - Li + 2H]^+$ 380.1; found 380.1

4.2.8.12. Di-lithium ((*S*)-2-((*N*-(benzyloxycarbonyl)-aminomethylphosphonyl)amino)propanoyl)-L-alaninate (36)

Following the general procedure for the synthesis of compounds **1-3**, **5-7**, and **31-38**, compound **4** (215 mg, 0.83 mmol) was reacted with compound **IB36** (211 mg, 1.0 mmol) in anhydrous DCM (3.0 mL), using PyBop (520 mg, 1.0 mmol) as a coupling reagent and diisopropylethylamine (428 mg, 3.3 mmol) as a base. 196 mg of compound **IC36**, which is the di-ester version of the desired product, was obtained after purification with reverse phase HPLC (57%). 83 mg of this compound (0.2 mmol) was then exposed to LiOH (2.0 mL of the 0.4 M solution referred to in the general procedure) overnight, and the final product was separated by reverse phase HPLC as a pure white solid (61 mg, 77%). ^{1}H NMR (D_2O) δ 1.12 (d, J = 7.2 Hz, 3H), 1.19 (d, J = 7.2 Hz, 3H), 3.17 (m, 2H), 3.56 (m, 1H), 3.96 (q, J = 7.2 Hz, 1H), 4.99 (s, 2H), 7.30 (m, 5H), ^{31}P NMR (D_2O) δ 18.32; m/z (LCMS, ESI): calc. for $[M - Li + 2H]^+$ 394.1; found 394.0

4.2.8.13. Di-lithium (*2S*)-*N*-((*S*)-2-((*N*-(benzyloxycarbonyl)-aminomethylphosphonyl)amino) propanoyl)-2-aminobutanoate (37)

Following the general procedure for the synthesis of compounds **1-3**, **5-7**, and **31-38**, compound **4** (215 mg, 0.83 mmol) was reacted with compound **IB37** (225 mg, 1.0 mmol) in anhydrous DCM (3.0 mL), using PyBop (520 mg, 1.0 mmol) as a coupling reagent and diisopropylethylamine (428 mg, 3.3 mmol) as a base. 185 mg of compound **IC37**, which is the

di-ester version of the desired product, was obtained after purification with reverse phase HPLC (52%). 86 mg of this compound (0.2 mmol) was then exposed to LiOH (2.0 mL of the 0.4 M solution referred to in the general procedure) overnight, and the final product was separated by reverse phase HPLC as a pure white solid (59 mg, 72%). ^{1}H NMR (D_2O) δ 0.73 (t, J = 7.4 Hz, 3H), 1.13 (d, J = 6.8 Hz, 3H), 1.61 (m, 2H), 3.17 (m, 2H), 3.59 (m, 1H), 3.94 (t, J = 6.2 Hz, 1H), 4.99 (s, 2H), 7.30 (m, 5H), ^{31}P NMR (D_2O) δ 18.28; m/z (LCMS, ESI): calc. for $[M – 2Li + 2H + Na]^+$ 424.1; found 424.0

4.2.8.14. Di-lithium ((*S*)-2-((*N*-(benzyloxycarbonyl)-aminomethylphosphonyl)amino)propanoyl)-L-phenylalaninate (38)

Following the general procedure for the synthesis of compounds **1-3**, **5-7**, and **31-38**, compound **4** (215 mg, 0.83 mmol) was reacted with compound **IB38** (287 mg, 1.0 mmol) in anhydrous DCM (3.0 mL), using PyBop (520 mg, 1.0 mmol) as a coupling reagent and diisopropylethylamine (428 mg, 3.3 mmol) as a base. 254 mg of compound **IC38**, which is the di-ester version of the desired product, was obtained after purification with reverse phase HPLC (61%). 98 mg of this compound (0.2 mmol) was then exposed to LiOH (2.0 mL of the 0.4 M solution referred to in the general procedure; 2.0 mL of acetonitrile was used as a cosolvent) overnight, and the final product was separated by reverse phase HPLC as a pure white solid (70 mg, 74%). ^{1}H NMR (D_2O) δ 0.98 (d, J = 6.8 Hz, 3H), 2.85 (m, 2H), 3.08 (m, 2H), 3.47 (m, 1H), 4.28 (q, J = 4.8 Hz, 1H), 4.98 (s, 2H), 7.05-7.35 (m, 10H), ^{13}C NMR (CD_3OD) δ 21.67 (d, J_{C-P} = 14.4 Hz, 1C, CH<u>C</u>H$_3$), 39.35 (1C, CH<u>C</u>H$_2$Ph) 41.25 (d, J_{C-P} = 544 Hz, 1C, <u>C</u>H$_2$P), 52.80 and 57.08 (2C, 2<u>C</u>HCONH), 67.69 (1C, Ph<u>C</u>H$_2$O), 127.33, 128.98, 129.02, 129.17, 129.52, 130.77, 138.47, and 139.70 (12C, 2Ph), 158.99 (d, J_{C-P} = 26.8 Hz, 1C, Cbz <u>C</u>=O), 177.27 and 178.17 (2C, 2<u>C</u>=O), ^{31}P NMR (D_2O) δ 18.32; m/z (HRMS, ESI): calc. for $C_{21}H_{26}O_7N_3NaP$, $[M – 2Li + 2H + Na]^+$, 486.1401, found 486.1411

ABBREVIATIONS

Bn: benzyl, *i*-Bu: isobutyl, *n*-Bu: normal butyl. *sec*-Bu: secondary butyl, *tert*-Bu: tertiary butyl, Et: ethyl, Eq.: equation, ITC: isothermal titration calorimetry, Me: methyl, *i*-Pr: isopropyl, *n*-Pr: normal propyl, TLN: thermolysin.

REFERENCES:

[1] L. Muley, B. Baum, M. Smolinski, M. Freindorf, A. Heine, G. Klebe, D. Hangauer, J. Med. Chem. 53 (2010) 2126-2135.

[2] N.N. Nasief, H. Tan, J. Kong, D. Hangauer, J. Med. Chem. 55 (2012) 8283-8302.

[3] B. Baum, L. Muley, M. Smolinski, A. Heine, D. Hangauer, G. Klebe, J. Mol. Biol. 397 (2010) 1042–1054.

[4] A. Horovitz, A.R. Fersht, J. Mol. Biol. 214 (1990) 613-617.

[5] A. Horovitz, Fold Des. 1 (1996) R121-R126.

[6] E.D. Cera; Chem. Rev. 98 (1998) 1563-1591.

[7] S.L. Cockroft, C.A. Hunter, Chem. Soc. Rev. 36 (2007) 172-188.

[8] A. Camara-Campos, D. Musumeci, C.A. Hunter, S. Turega, J. Am. Chem. Soc. 131 (2009) 18518-18524.

[9] S.H. Kawai, M.D. Bailey, T. Halmos, P. Forgione, S.R. LaPlante, M. Llinas-Brunet, J. Naud, N. Goudreau, ChemMedChem 3 (2008) 1654 – 1657.

[10] B.P. Morgan, J.M. Scholtz, M.D. Ballinger, I.D. Zipkin, P.A. Bartlett, J. Am. Chem. Soc. 113 (1991) 297-307.

[11] A.H. Daranas, H. Shimizu, S.W. Homans, J. Am. Chem. Soc. 126 (2004) 11870-11876.

[12] S.W. Homans, Top. Curr. Chem. 272 (2007) 51-82.

[13] Y. Patel, V.J. Gillet, T. Howe, J. Pastor, J. Oyarzabal, P. Willett, J. Med. Chem. 51 (2008) 7552-7562.

[14] C. Bissantz, B. Kuhn, M. Stahl, J. Med. Chem. 53 (2010) 5061-5084.

[15] A. Biela, N.N. Nasief, M. Betz, A. Heine, D. Hangauer, G. Klebe, Angew. Chem. Int. Ed. Engl. 52 (2013) 1822-1828.

[16] N.N. Nasief, D. Hangauer, J. Med Chem. 57 (2014) 2315-2333.

[17] S.A. Latt, B. Holmquist, B.L. Vallee, Biochem. Biophys. Res. Commun. 37 (1969) 333-339.

[18] K. Morihara, H. Tsuzuki, Eur. J. Biochem. 15 (1970) 374-380.

[19] D.G. Hangauer, A.F. Monzingo, B.W. Matthews, Biochemistry 23 (1984) 5730-5741.

[20] J.T. Bukrinsky, M.J.Bjerrum, A. Kadziola, Biochemistry 37 (1998) 16555-16564.

[21] R. Natesh, S.L. Schwager, E.D. Sturrock, K.R. Acharya, Nature 421 (2003) 551-554.

[22] K. Morihara, Biochem. Biophys. Res. Commun. 26 (1967) 656-661.

[23] The synthesis of ligands **4**, **8**, and **9-30** was previously reported in ref 2 and 16.

[24] Y. Vo-Quang A.M. Gravey, R. Simonneau, L. Vo-Quang, A.M. Lacoste, F. Le Goffic, Tetrahedron Lett. 28 (1987) 6167-6170.

[25] J. Feder, J.M. Schuck, Biochemistry 9 (1970) 2784-2791.

[26] A. Biela, M. Betz, A. Heine, G. Klebe, ChemMedChem 7 (2012) 1423-1434.

[27] B. Kuhn, J.E. Fuchs, M. Reutlinger, M. Stahl, N.R. Taylor, J. Chem. Info. Model. 51 (2011) 3180-3198.

[28] G. Morgan, J.S. Fruton, Biochemistry, 17 (1978) 3562- 3568.

[29] Y. Cheng, W.H. Prusoff, Biochem. Pharmacol. 22 (1973) 3099–3108.

[30] J. Feder, L. Brougham, B. Wildi, Biochemistry, 13 (1974) 1186- 1189.

[31] P.J.F. Henderson, Biochem. J. 127 (1972) 321- 333.

Figure, Scheme, and Table Captions

Figure 1: A general double mutant cycle showing how cooperativity vs. additivity could be identified by comparing the differential binding energies of the H→X structural modification in presence and absence of group Y (Y vs. H'). Also cooperativity could be identified by comparing the differential binding energies of the H'→Y structural modification in presence and absence of group X (X vs. H).

Figure 2: A "three-dimensional" Born-Haber cycle representing the binding of two ligands LH and LX to a biological target P. These two ligands differ only in that the H of LH is replaced by a functional group X. The pre-association events are simplified to involve only the desolvation of the ligand and the receptor (no conformational or ionization changes). Additional terms would need to be included in Eqs. 1 and 2 if conformational or ionization changes occurred.

Figure 3: Thermolysin phosphonamidate inhibitors: Left: The general scaffold is shown binding in the active site of thermolysin; the important features of the thermolysin active site such as the S1, S1', and S2' hydrophobic pockets as well as the zinc ion are shown. Right: The functional groups and side chains, which were designed to be studied, are indicated. Some of the characteristics that could be correlated with the cooperative/additive behavior are the hydrophobicity/polarity, and the distance between the individual groups in a particular pair.

Figure 4: Double mutant cycle "A" exploring the cooperative/additive relationship in the group pair (R_1, COO^-).

Figure 5: a) the bioactive conformation of ligand **8** extracted from the crystal structure of this ligand with TLN (PDB ID: 4H57). The COO^- group and the R_1 side chain are positioned opposite to each other. Both the R_1 and the R_2 side chain demonstrate a potential hydrophobic collapse. **b)** Part of ligand **8**-TLN complex; the *i*-Bu R_1 side chain of the ligand is shown buried in the deep S1' pocket. If R_1 = Me, the S1' pocket might have enough space to accommodate one or two water molecules. However, trapping these waters might be entropically unfavorable.

Figure 6: Double mutant cycle "B" exploring the cooperative/additive relationship in the group pair (R_2, COO^-).

Figure 7: A plot of $\Delta\Delta G_{(H,COO\rightarrow R2,COO)} - \Delta\Delta G_{(H,H\rightarrow R2,H)}$ (the cooperativity indicator) vs. the structural modifications of the R_2 side chain. The maximum positive cooperativity is attained when the R_2 side chain is Me. This positive cooperativity diminishes slightly when the side chain is homologated, and diminishes largely when the side chain is branched or when an aromatic moiety is introduced. Some side chains like the *sec*-Bu and the neopentyl demonstrate additivity and negative cooperativity, respectively.

Figure 8: **(a)** The association and resolvation steps are for ligands LH and LMe in presence of the COO^- (ligands **20** and **21**). The resolvation of ligand **20**-TLN produces a low quality water network, while the resolvation of **21**-TLN produces a high quality network. **(b)** The association and resolvation of ligands LH and LMe in absence of the COO^- (ligands **9** and **10**). With regard to the quality of the resolvation networks, **9**'s is better than **20**'s (in the presence of the COO^-, $\Delta H_{LH\text{-}resolv}$ shifts to the positive and $-T\Delta S_{LH\text{-}resolv}$ shifts to the negative), but **10**'s is not as good as **21**'s ($\Delta H_{LMe\text{-}resolv}$ shifts to the negative and $-T\Delta S_{LMe\text{-}resolv}$ shifts to the positive). In **b**, ligand **10** has an additional torsional degree of freedom that gets restricted upon protein-ligand association ($-T\Delta S_{LMe\text{-}assoc}$, in absence of the COO^-, is more unfavorable for binding). Crystal structures for **9-**, **10-**, **20-**, and **21**-TLN complexes (PDB IDs: 3T73, 3T8F, 3T8G, and 3T74 [26, 2]) were used to construct this Figure. Protein and ligand atoms are shown in the following colors: C (gray); O (red) and N (blue). Water molecules are shown in red and enlarged whenever unique to a particular water network. Several protein residues and water molecules are omitted for clarity.

Figure 9: Double mutant cycle "C" exploring the cooperative/additive relationship in the group pair (R_2, COO^-) when the R_1 side chain is small (= Me).

Figure 10: A plot of $\Delta\Delta G_{(H,COO\rightarrow R2,COO)} - \Delta\Delta G_{(H,H\rightarrow R2,H)}$ (the cooperativity indicator) vs. the structural modifications of the R_2 side chain. In the blue-lined series, the R_1 side chain is *i*-Bu, while in the red-lined series the R_1 is Me. The influence of varying the size (and the hydrophobicity) of the R_1 side chain on the cooperativity/additivity pattern does not seem to be significant except in the case of the Bn side chain (e.g. the two graph points representing the cooperativity indicators of the Bn group diverge from one series to another).

Figure 11: Double mutant cycle "D" exploring the cooperativity/additivity relationship in the group pair (R_1, R_2).

Scheme 1: The designed TLN inhibitor series. Series I and II were designed to study the cooperative/additive behavior of the (R_1, COO^-) group pair. Series III and IV were designed to study the cooperative/additive behavior of the (R_2, COO^-) group pair. Series V and VI were designed to investigate the influence of truncating the R_1 side chain from *i*-Bu to Me on the cooperative/additive behavior of the same group pair. Series V and III-R (a subseries of III) were compared in order to investigate the cooperative/additive behavior of the (R_1, R_2) group pair. It should be noted that each of series III and V has a common ligand with series I, and each of series IV and VI has a common ligand with series II.

Scheme 2: The synthesis of intermediate 4

Scheme 3: The synthesis of ligands 1-38

Scheme 4: Proposed preliminary algorithm for predicting the outcome of simultaneous incorporation of two functionalities in a ligand molecule with regard to additivity/cooperativity

of the contributions of these functionalities to the binding free energy. Algorithm is based on correlating the data obtained in the current study with the properties of the involved functional groups and their proximity to each other. A "?" signifies that the effect is under investigation.

Table 1: The substitution pattern of IA1-38, IB1-38, IC1-38, and 1-38

Table 2: The K_i and the corresponding ΔG values of the TLN inhibitors 1-38

Table 3: The values of the differential binding free energies of the Me→R_1 replacements in absence and presence of the COO^-, and the values of the cooperativity indicator term

Table 4: The values of the differential binding free energies of the H→R_2 replacements in absence and presence of the COO^-, and the values of the cooperativity indicator term

Table 5: The values of the differential binding free energies of the H→R_2 replacements in absence and presence of the COO^- (R_1 = Me), and the values of the cooperativity indicator term

Table 6: The values of the differential binding free energies of the H→R_2 replacements when R_1 = Me vs. when R_1 = *i*-Bu, and the values of the cooperativity indicator term

Table 1[a]: The substitution patterns of IA1-38, IB1-38, IC1-38, and 1-38

Compounds	R_1	R_2	X`, X
IA1, IB1, IC1, 1	Me	*i*-Bu	H, H
IA2, IB2, IC2, 2	Et	*i*-Bu	H, H
IA3, IB3, IC3, 3	*n*-Pr	*i*-Bu	H, H
IA4, IB4, IC4, 4	*i*-Bu	*i*-Bu	H, H
IA5, IB5, IC5, 5	Me	*i*-Bu	COOMe, COOLi
IA6, IB6, IC6, 6	Et	*i*-Bu	COOMe, COOLi
IA7, IB7, IC7, 7	*n*-Pr	*i*-Bu	COOMe, COOLi
IA8, IB8, IC8, 8	*i*-Bu	*i*-Bu	COOMe, COOLi
IA9, IB9, IC9, 9	*i*-Bu	H	H, H
IA10, IB10, IC10, 10	*i*-Bu	Me	H, H
IA11, IB11, IC11, 11	*i*-Bu	Et	H, H
IA12, IB12, IC12, 12	*i*-Bu	*n*-Pr	H, H
IA13, IB13, IC13, 13	*i*-Bu	*n*-Bu	H, H
IA14, IB14, IC14, 14	*i*-Bu	*i*-Pr	H, H
IA15, IB15, IC15, 15	*i*-Bu	*tert*-Bu	H, H
IA16, IB16, IC16, 16	*i*-Bu	*sec*-Bu	H, H
IA17, IB17, IC17, 17	*i*-Bu	neopentyl	H, H
IA18, IB18, IC18, 18	*i*-Bu	Bn	H, H
IA19, IB19, IC19, 19	*i*-Bu	2-thienylmethyl	H, H
IA20, IB20, IC20, 20	*i*-Bu	H	COOEt, COOLi
IA21, IB21, IC21, 21	*i*-Bu	Me	COOMe, COOLi
IA22, IB22, IC22, 22	*i*-Bu	Et	COOMe, COOLi
IA23, IB23, IC23, 23	*i*-Bu	*n*-Pr	COOMe, COOLi
IA24, IB24, IC24, 24	*i*-Bu	*n*-Bu	COOMe, COOLi
IA25, IB25, IC25, 25	*i*-Bu	*i*-Pr	COOMe, COOLi
IA26, IB26, IC26, 26	*i*-Bu	*tert*-Bu	COOMe, COOLi
IA27, IB27, IC27, 27	*i*-Bu	*sec*-Bu	COOMe, COOLi
IA28, IB28, IC28, 28	*i*-Bu	neopentyl	COOMe, COOLi
IA29, IB29, IC29, 29	*i*-Bu	Bn	COOMe, COOLi
IA30, IB30, IC30, 30	*i*-Bu	2-thienylmethyl	COOMe, COOLi
IA31[*], IB31[#], IC31, 31	Me	H	H, H
IA32, IB32, IC32, 32	Me	Me	H, H
IA33, IB33, IC33, 33	Me	Et	H, H
IA34, IB34, IC34, 34	Me	Bn	H, H
IA35, IB35, IC35, 35	Me	H	COOEt, COOLi
IA36, IB36, IC36, 36	Me	Me	COOMe, COOLi
IA37, IB37, IC37, 37	Me	Et	COOMe, COOLi
IA38, IB38, IC38, 38	Me	Bn	COOMe, COOLi

[a] X` belongs to **IA1-38**, **IB1-38**, and **IC1-38**, while X belongs to **1-38**. [*] **IA-31** was not synthesized due to the commercial availability of **IB-31**. [#] **IB-31** was not synthesized due to its commercial availability.

Table 2: The K_i and the corresponding ΔG values of the TLN inhibitors 1-38

Compound	K_i (μM)	ΔG (kJ/mol)
1	19.5 ± 3.5	-26.9 ± 0.4
2	1.97 ± 0.25	-32.5 ± 0.4
3	0.219 ± 0.037	-38.0 ± 0.5
4	0.069 ± 0.011	-40.9 ± 0.4
5	5.92 ± 0.57	-29.8 ± 0.2
6	0.596 ± 0.125	-35.5 ± 0.5
7	0.029 ± 0.004	-43.0 ± 0.4
8	0.010 ± 0.001	-45.6 ± 0.3
9	0.908 ± 0.165	-34.6 ± 0.4
10	0.291 ± 0.030	-37.3 ± 0.2
11	0.060 ± 0.015	-41.3 ± 0.6
12	0.067 ± 0.017	-41.1 ± 0.7
13	0.059 ± 0.010	-41.3 ± 0.5
14	0.037 ± 0.010	-42.5 ± 0.6
15	0.100 ± 0.019	-40.0 ± 0.5
16	0.026 ± 0.003	-43.8 ± 0.3
17	0.043 ± 0.005	-42.1 ± 0.3
18	0.296 ± 0.058	-37.3 ± 0.5
19	0.189 ± 0.016	-38.4 ± 0.2
20	0.476 ± 0.037	-36.1 ± 0.2
21	0.019 ± 0.001	-44.1 ± 0.1
22	0.0049 ± 0.0002	-47.5 ± 0.1
23	0.0055 ± 0.0009	-47.1 ± 0.4
24	0.0053 ± 0.0011	-47.2 ± 0.3
25	0.0058 ± 0.0012	-47.1 ± 0.5
26	0.031 ± 0.004	-42.8 ± 0.3
27	0.012 ± 0.001	-45.2 ± 0.3
28	0.040 ± 0.004	-42.3 ± 0.3
29	0.054 ± 0.014	-41.5 ± 0.6
30	0.024 ± 0.006	-43.6 ± 0.6
31	185 ± 7	-21.3 ± 0.1
32	56.2 ± 12.9	-24.3 ± 0.6
33	12.4 ± 1.51	-28.0 ± 0.3
34	45.2 ± 10.8	-24.8 ± 0.6
35	189 ± 21.4	-21.2 ± 0.3
36	7.20 ± 2.19	-29.4 ± 0.7
37	1.37 ± 0.32	-33.5 ± 0.6
38	31.1 ± 2.66	-25.6 ± 0.2

Table 3: The values of the differential binding free energies of the Me→R_1 replacements in absence and presence of the COO^-, and the values of the cooperativity indicator term[a]

R_1	$\Delta\Delta G_{(Me,H\rightarrow R1,H)}$ kJ/mol	$\Delta\Delta G_{(Me,COO\rightarrow R1,COO)}$ kJ/mol	$\Delta\Delta G_{(Me,COO\rightarrow R1,COO)} - \Delta\Delta G_{(Me,H\rightarrow R1,H)}$
Et	-5.6	-5.7	-0.1
n-Pr	-11.1	-13.2	-2.1
i-Bu	-14.0	-15.8	-1.8

[a] The cooperativity indicator term is ($\Delta\Delta G_{(Me,COO\rightarrow R1,COO)} - \Delta\Delta G_{(Me,H\rightarrow R1,H)}$), and it has the unit kJ/mol.

Table 4: The values of the differential binding free energies of the H→R_2 replacements in absence and presence of the COO^-, and the values of the cooperativity indicator term

R_2	$\Delta\Delta G_{(H,H\rightarrow R2,H)}$ kJ/mol	$\Delta\Delta G_{(H,COO\rightarrow R2,COO)}$ kJ/mol	$\Delta\Delta G_{(H,COO\rightarrow R2,COO)} - \Delta\Delta G_{(H,H\rightarrow R2,H)}$
Me	-2.7	-8.0	-5.3
Et	-6.7	-11.4	-4.7
n-Pr	-6.5	-11.0	-4.5
n-Bu	-6.7	-11.1	-4.6
i-Pr	-7.9	-11.0	-3.1
tert-Bu	-5.4	-6.7	-1.3
sec-Bu	-9.2	-9.1	0.1
i-Bu	-6.3	-9.5	-3.2
neopentyl	-7.5	-6.2	1.3
Bn	-2.7	-5.4	-2.7
2-thienylmethyl	-3.8	-7.5	-3.7

Table 5: The values of the differential binding free energies of the H→R_2 replacements in absence and presence of the COO^- (R_1 = Me), and the values of the cooperativity indicator term

R_2	$\Delta\Delta G_{(H,H\rightarrow R2,H)}$ kJ/mol	$\Delta\Delta G_{(H,COO\rightarrow R2,COO)}$ kJ/mol	$\Delta\Delta G_{(H,COO\rightarrow R2,COO)} - \Delta\Delta G_{(H,H\rightarrow R2,H)}$
Me	-3.0	-8.2	-5.2
Et	-6.7	-12.3	-5.6
i-Bu	-5.6	-8.6	-3.0
Bn	-3.5	-4.4	-0.9

Table 6: The values of the differential binding free energies of the H→R_2 replacements when R_1 = Me vs. when R_1 = *i*-Bu, and the values of the cooperativity indicator term

R_2	$\Delta\Delta G_{(H,Me\rightarrow R2,Me)}$ kJ/mol	$\Delta\Delta G_{(H,i\text{-}Bu\rightarrow R2,i\text{-}Bu)}$ kJ/mol	$\Delta\Delta G_{(H,i\text{-}Bu\rightarrow R2,i\text{-}Bu)} - \Delta\Delta G_{(H,Me\rightarrow R2,Me)}$
Me	-3.0	-2.7	+0.3
Et	-6.7	-6.7	0.0
i-Bu	-5.6	-6.3	-0.7
Bn	-3.5	-2.7	-0.8

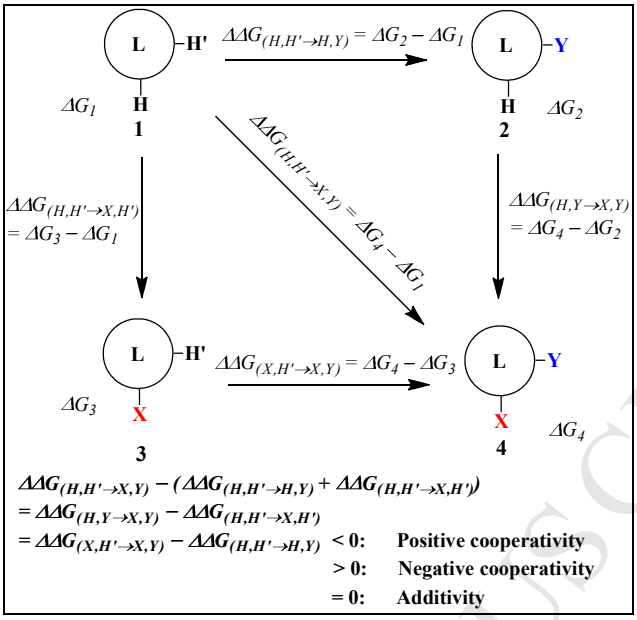

Figure 1: A general double mutant cycle showing how cooperativity vs. additivity could be identified by comparing the differential binding energies of the H→X structural modification in presence and absence of group Y (Y vs. H'). Also cooperativity could be identified by comparing the differential binding energies of the H'→Y structural modification in presence and absence of group X (X vs. H).

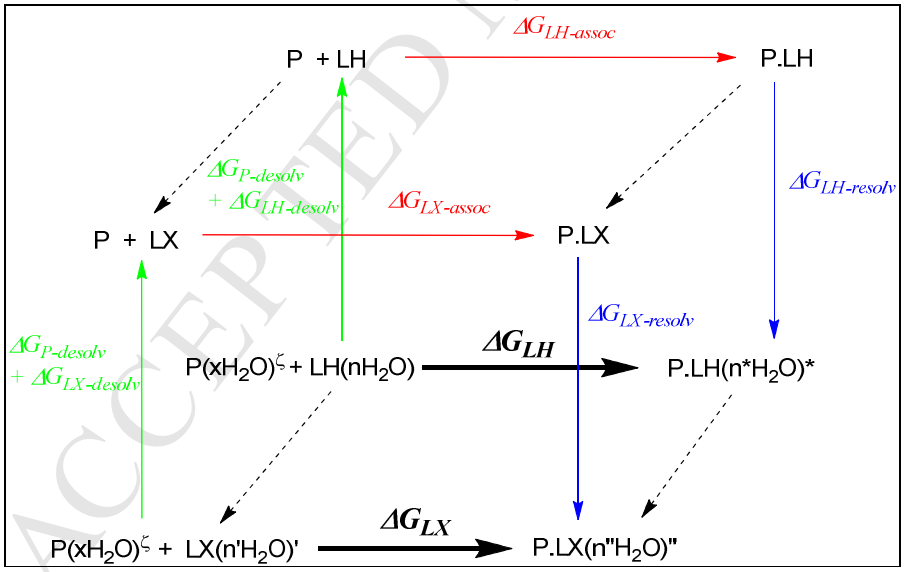

Figure 2: A "three-dimensional" Born-Haber cycle representing the binding of two ligands LH and LX to a biological target P. These two ligands differ only in that the H of LH is replaced by a functional group X. The pre-association events are simplified to involve only the desolvation of the ligand and the receptor (no conformational or ionization changes). Additional terms would need to be included in Eqs. 1 and 2 if conformational or ionization changes occurred.

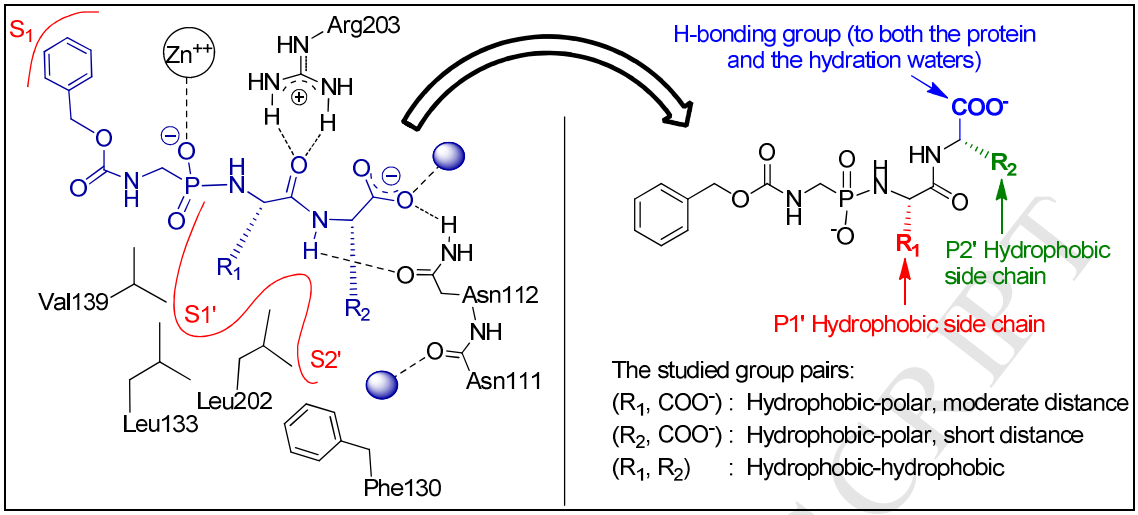

Figure 3: Thermolysin phosphonamidate inhibitors: Left: The general scaffold is shown binding in the active site of thermolysin; the important features of the thermolysin active site such as the S1, S1', and S2' hydrophobic pockets as well as the zinc ion are shown. Right: The functional groups and side chains, which were designed to be studied, are indicated. Some of the characteristics that could be correlated with the cooperative/additive behavior are the hydrophobicity/polarity, and the distance between the individual groups in a particular pair.

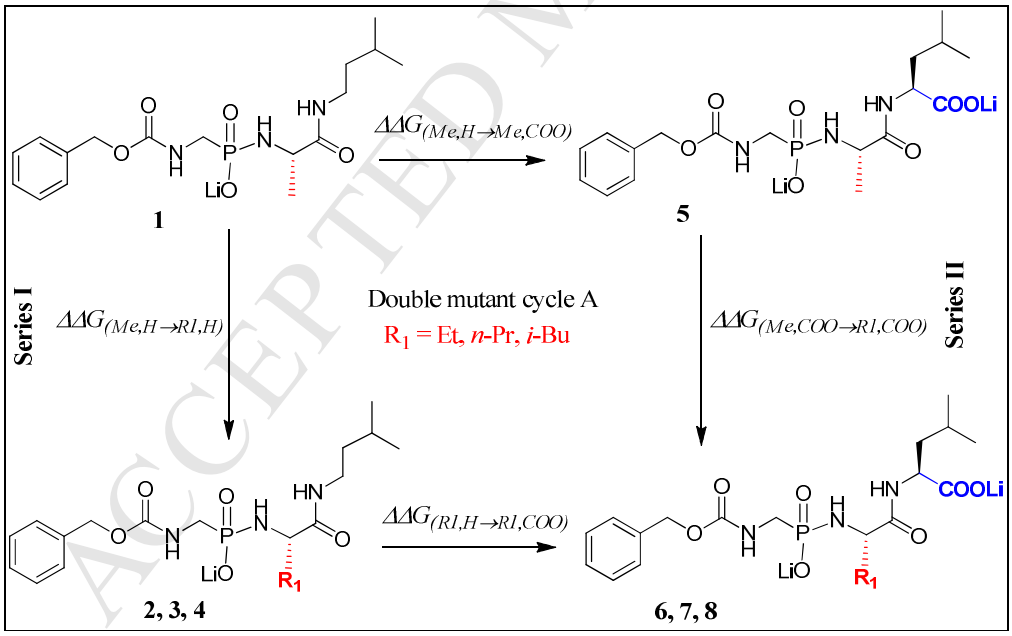

Figure 4: Double mutant cycle "A" exploring the cooperative/additive relationship in the group pair (R_1, COO^-).

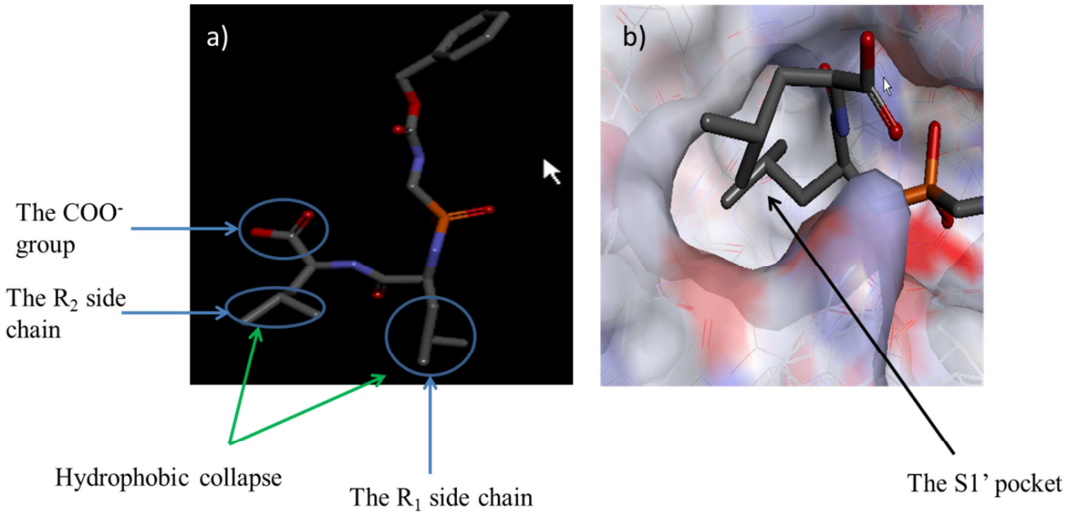

Figure 5: a) the bioactive conformation of ligand **8** extracted from the crystal structure of this ligand with TLN (PDB ID: 4H57). The COO^- group and the R_1 side chain are positioned opposite to each other. Both the R_1 and the R_2 side chain demonstrate a potential hydrophobic collapse. **b)** Part of ligand **8**-TLN complex; the *i*-Bu R_1 side chain of the ligand is shown buried in the deep S1' pocket. If R_1 = Me, the S1' pocket might have enough space to accommodate one or two water molecules. However, trapping these waters might be entropically unfavorable.

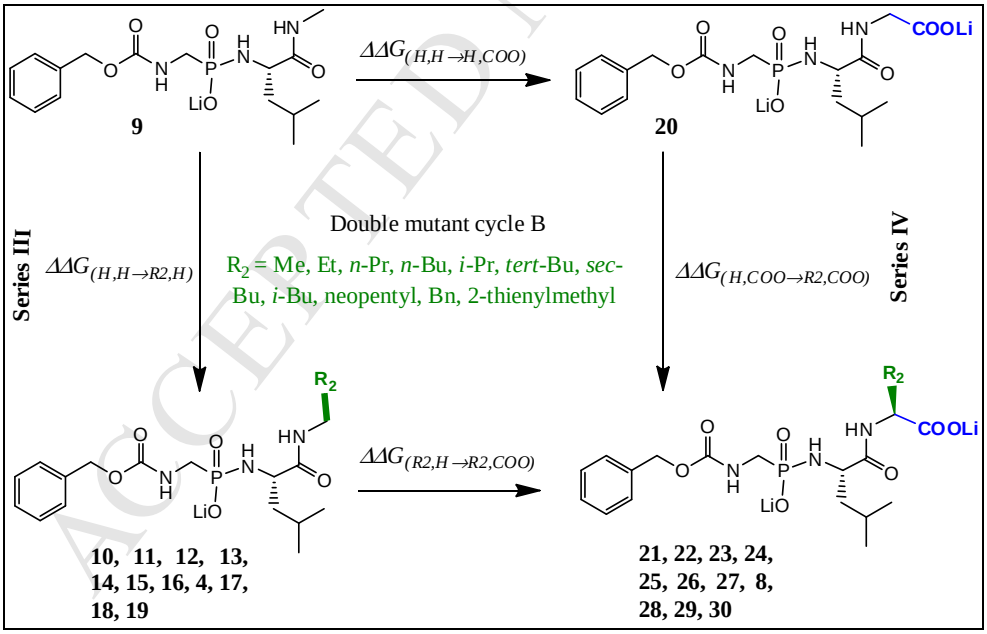

Figure 6: Double mutant cycle "B" exploring the cooperative/additive relationship in the group pair (R_2, COO^-).

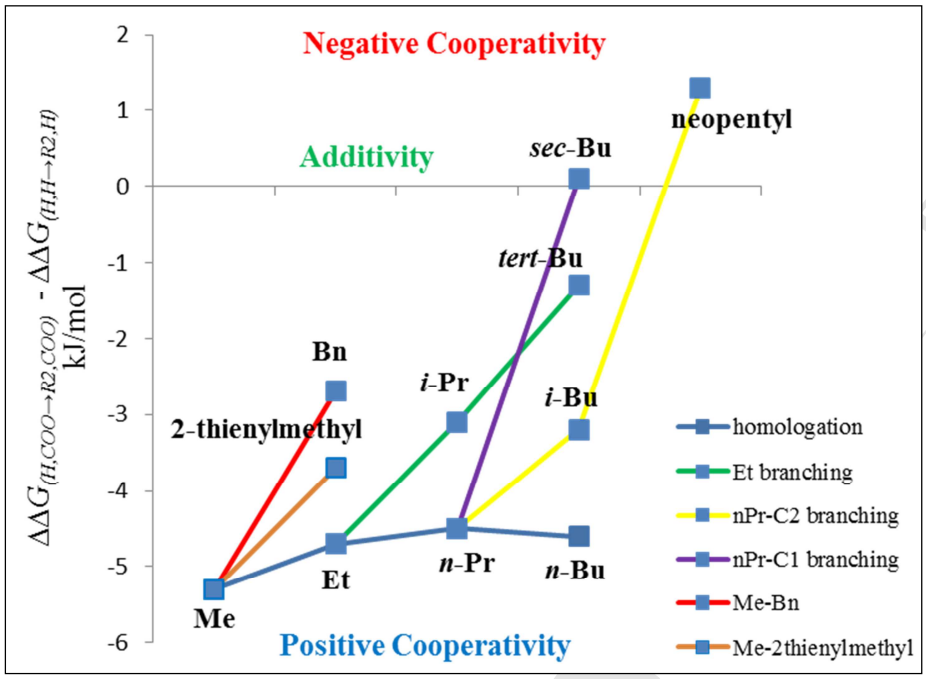

Figure 7: A plot of $\Delta\Delta G_{(H,COO\rightarrow R2,COO)} - \Delta\Delta G_{(H,H\rightarrow R2,H)}$ (the cooperativity indicator) vs. the structural modifications of the R_2 side chain. The maximum positive cooperativity is attained when the R_2 side chain is Me. This positive cooperativity diminishes slightly when the side chain is homologated, and diminishes significantly when the side chain is branched or when an aromatic moiety is introduced. Some side chains like the *sec*-Bu and the neopentyl demonstrate additivity and negative cooperativity, respectively.

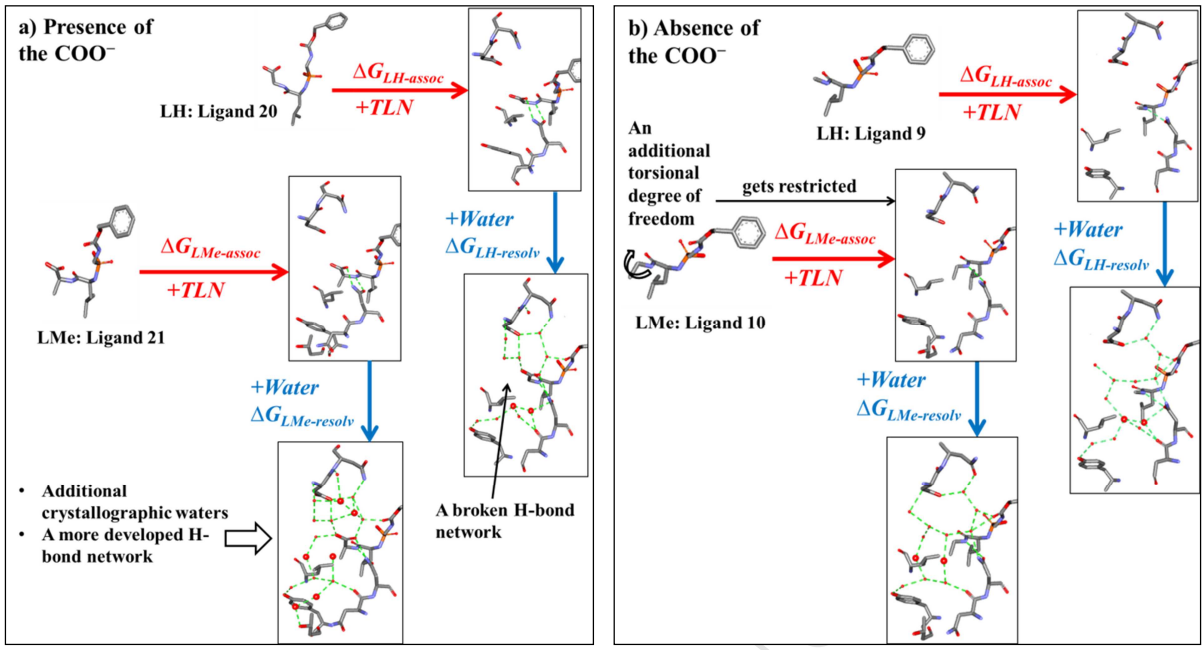

Figure 8: **(a)** The association and resolvation steps are for ligands LH and LMe in presence of the COO^- (ligands **20** and **21**). The resolvation of ligand **20**-TLN produces a low quality water network, while the resolvation of **21**-TLN produces a high quality network. **(b)** The association and resolvation of ligands LH and LMe in absence of the COO^- (ligands **9** and **10**). With regard to the quality of the resolvation networks, **9**'s is better than **20**'s (in the presence of the COO^-, $\Delta H_{LH\text{-}resolv}$ shifts to the positive and $-T\Delta S_{LH\text{-}resolv}$ shifts to the negative), but **10**'s is not as good as **21**'s ($\Delta H_{LMe\text{-}resolv}$ shifts to the negative and $-T\Delta S_{LMe\text{-}resolv}$ shifts to the positive). In **b**, ligand **10** has an additional torsional degree of freedom that gets restricted upon protein-ligand association ($-T\Delta S_{LMe\text{-}assoc}$, in absence of the COO^-, is more unfavorable for binding). Crystal structures for **9**-, **10**-, **20**-, and **21**-TLN complexes (PDB IDs: 3T73, 3T8F, 3T8G, and 3T74 [26, 2]) were used to construct this Figure. Protein and ligand atoms are shown in the following colors: C (gray); O (red) and N (blue). Water molecules are shown in red and enlarged whenever unique to a particular water network. Several protein residues and water molecules are omitted for clarity.

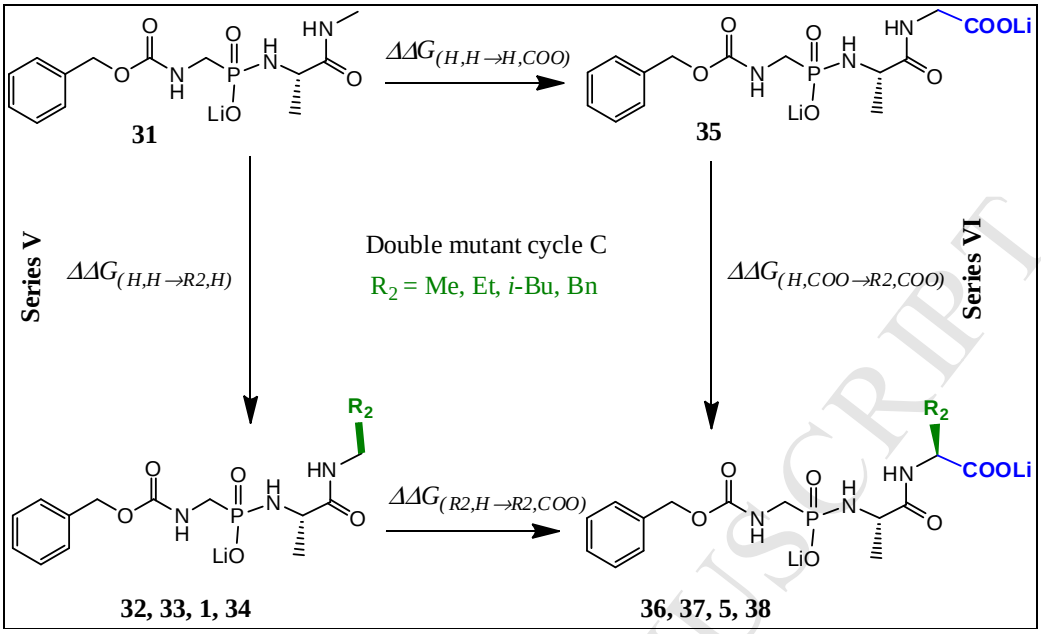

Figure 9: Double mutant cycle "C" exploring the cooperative/additive relationship in the group pair (R_2, COO^-) when the R_1 side chain is small (= Me).

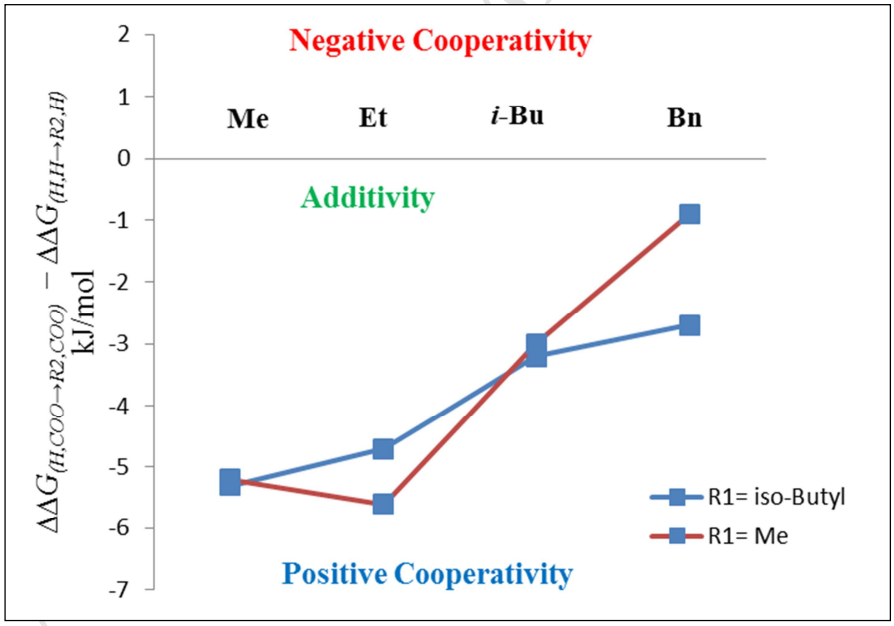

Figure 10: A plot of $\Delta\Delta G_{(H,COO\rightarrow R2,COO)} - \Delta\Delta G_{(H,H\rightarrow R2,H)}$ (the cooperativity indicator) vs. the structural modifications of the R_2 side chain. In the blue-lined series, the R_1 side chain is *i*-Bu, while in the red-lined series the R_1 is Me. The influence of varying the size (and the hydrophobicity) of the R_1 side chain on the cooperativity/additivity pattern does not seem to be significant except in the case of the Bn side chain (e.g. the two graph points representing the cooperativity indicators of the Bn group diverge from one series to another).

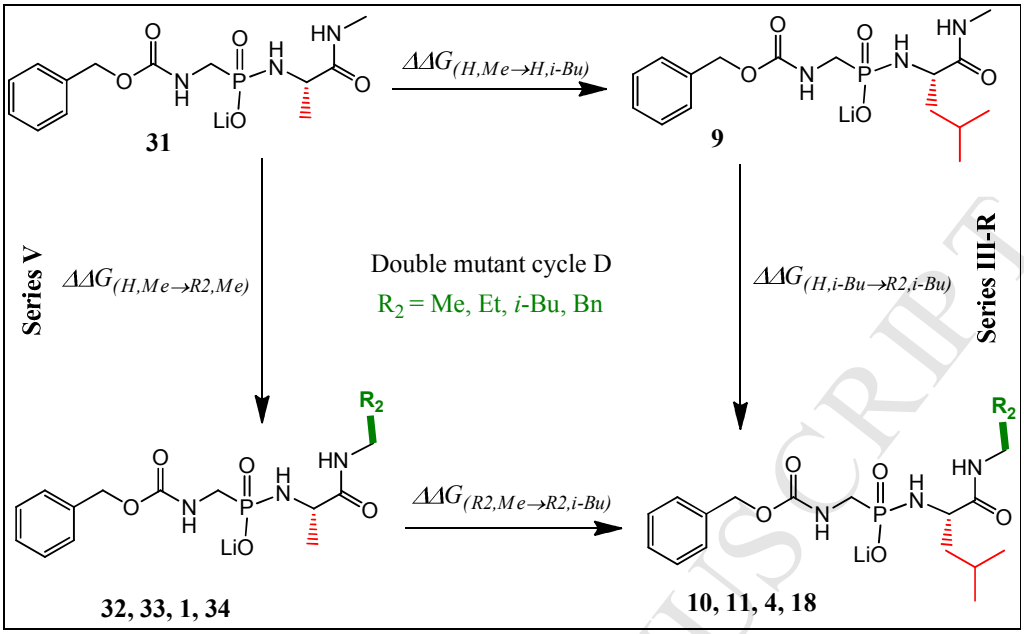

Figure 11: Double mutant cycle "D" exploring the cooperativity/additivity relationship in the group pair (R_1, R_2).

Schemes:

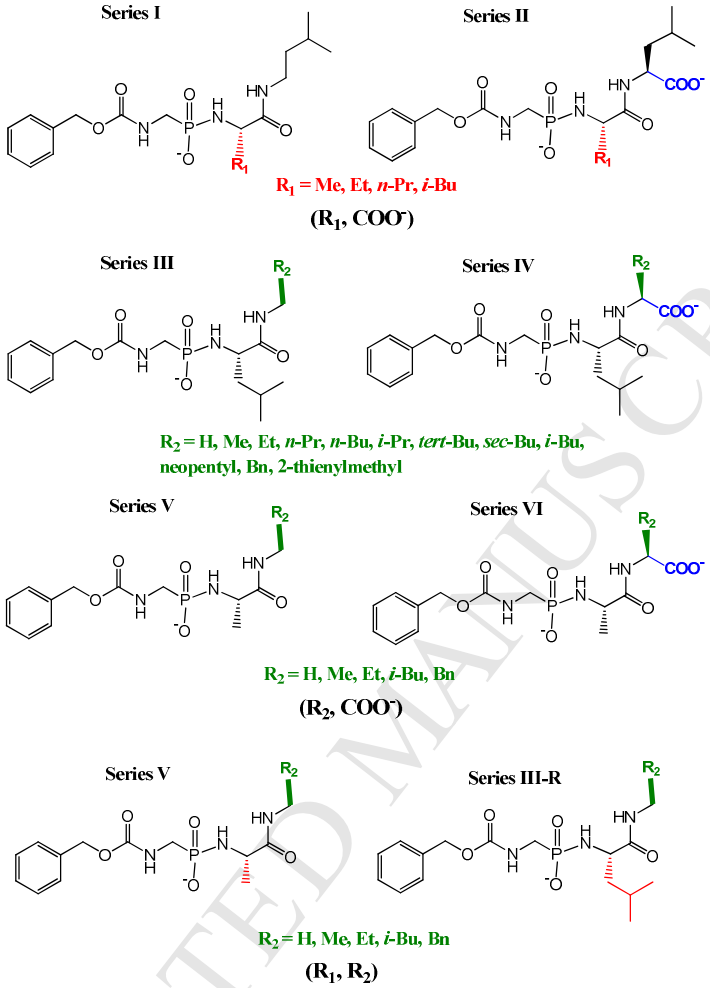

Scheme 1: The designed TLN inhibitor series. Series I and II were designed to study the cooperative/additive behavior of the (R_1, COO^-) group pair. Series III and IV were designed to study the cooperative/additive behavior of the (R_2, COO^-) group pair. Series V and VI were designed to investigate the influence of truncating the R_1 side chain from *i*-Bu to Me on the cooperative/additive behavior of the same group pair. Series V and III-R (a subseries of III) were compared in order to investigate the cooperative/additive behavior of the (R_1, R_2) group pair. It should be noted that each of series III and V has a common ligand with series I, and each of series IV and VI has a common ligand with series II.

Scheme 2: The synthesis of intermediate 4

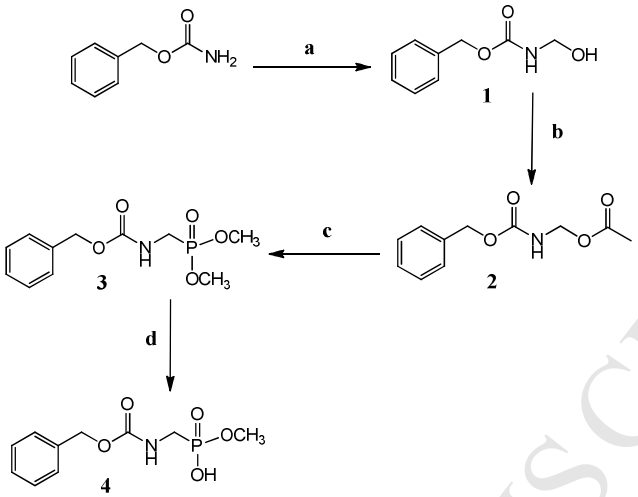

a) 0.5 equiv. Na_2CO_3, 1.5 equiv. 37% HCHO, H_2O, r.t., overnight, 74% **b)** Excess Ac_2O, 6.0 equiv. pyridine, THF, r.t, 2 h, 67% **c)** 3.0-4.0 equiv. $P(OCH_3)_3$, reflux, 3 h, 97% **d)** 6 equiv. 10% NaOH, r.t, 2 h, 73%.

Scheme 3: The synthesis of ligands 1-38

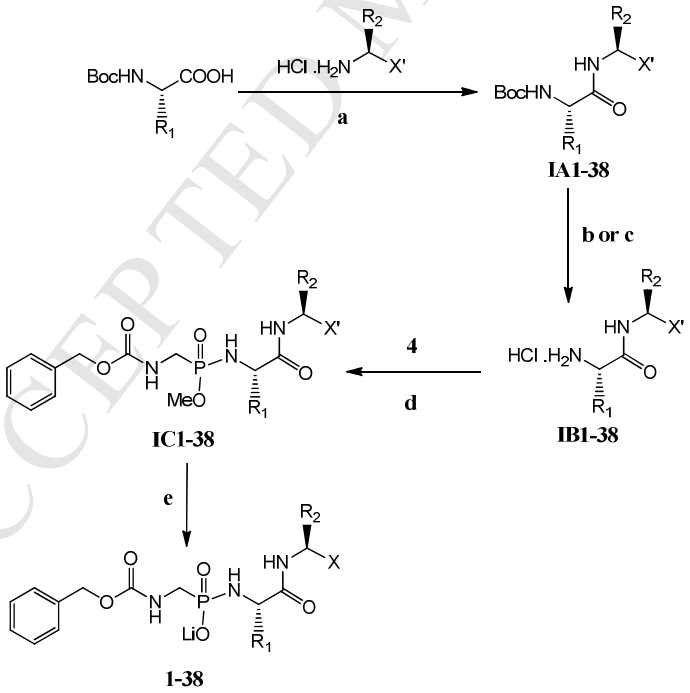

a) 1.2 equiv. PyBop (or 1.2 equiv. EDCI.HCl, 1.2 equiv. HOBt), 3.3-4.0 equiv. DIEA, anhydrous DMF, r.t., 5 h-overnight 65-85% **b)** 3 M HCl/MeOH, r.t, 2-3 h, 93-99% **c)** HCl gas, EtOAc, r.t, 2-3 h, 94-97% **d)** 1.2 equiv. PyBop, 4.0 equiv. DIEA, anhydrous DCM, r.t. 6 h-overnight 45-75% **e)** 2.0-4.0 equiv. LiOH, H_2O/MeCN, r.t. 2 h-overnight, 60-95%.

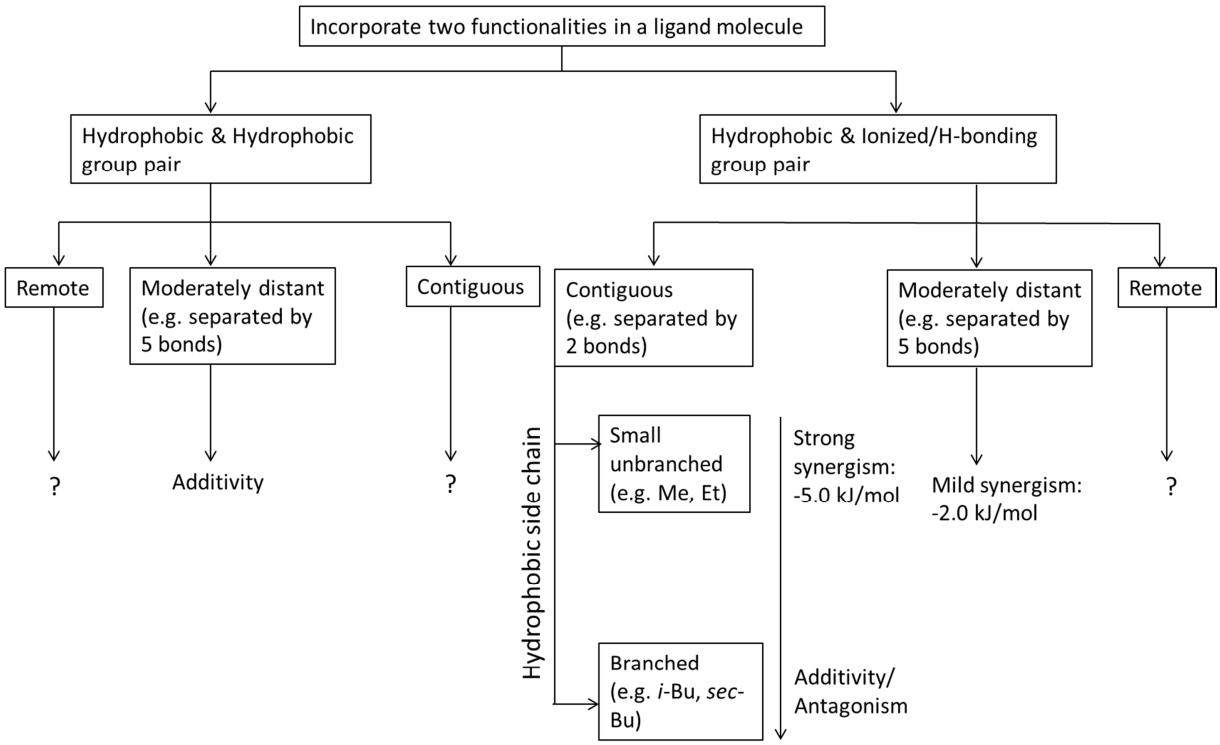

Scheme 4: Proposed preliminary algorithm for predicting the outcome of simultaneous incorporation of two functionalities in a ligand molecule with regard to additivity/cooperativity of the contributions of these functionalities to the binding free energy. Algorithm is based on correlating the data obtained in the current study with the properties of the involved functional groups and their proximity to each other. A "?" signifies that the effect is under investigation.

Highlights

- Functional group cooperativity/additivity was probed in 38 thermolysin inhibitors.
- Cooperativity can account for 10-fold additional improvement in activity.
- Cooperativity correlated with contiguous groups and small-sized side chains.
- Additivity correlated with hydrophobic group combinations and branched side chains.
- A preliminary algorithm for predicting cooperativity vs. additivity was proposed.

Supplementary Materials

Additivity or Cooperativity: Which Model Can Predict the Influence of Simultaneous Incorporation of Two or More Functionalities in a Ligand Molecule?

Nader N Nasief* and David Hangauer*

Department of Chemistry, University at Buffalo, The State University of New York, Buffalo, New York 14260

Table of Contents:

1. Equations for the Differential Thermodynamic Parameters and Rules for Cooperativity

1.1. Binding Free Energy

$$\Delta\Delta G_{(H\rightarrow X)} = \Delta G_{LX} - \Delta G_{LH} = (\Delta G_{LX\text{-}desolv} - \Delta G_{LH\text{-}desolv}) + (\Delta G_{LX\text{-}assoc} - \Delta G_{LH\text{-}assoc}) + (\Delta G_{LX\text{-}resolv} - \Delta G_{LH\text{-}resolv}) \quad \textbf{(Eq. S1)}$$

If $\Delta\Delta G_{(H\rightarrow X)}$ is shifted to the negative in the presence of another group Y→ positive cooperativity (synergism) between X and Y

This occurs when

1. ($\Delta G_{LX\text{-}desolv} - \Delta G_{LH\text{-}desolv}$) value is shifted to the negative in the presence of Y ($\Delta G_{LX\text{-}desolv}$: a negative shift when Y is present or a positive shift when Y is absent; $\Delta G_{LH\text{-}desolv}$: a positive shift when Y is present or a negative shift when Y is absent)
2. ($\Delta G_{LX\text{-}assoc} - \Delta G_{LH\text{-}assoc}$) value is shifted to the negative in the presence of Y ($\Delta G_{LX\text{-}assoc}$: a negative shift when Y is present or a positive shift when Y is absent; $\Delta G_{LH\text{-}assoc}$: a positive shift when Y is present or a negative shift when Y is absent)
3. ($\Delta G_{LX\text{-}resolv} - \Delta G_{LH\text{-}resolv}$) value is shifted to the negative in the presence of Y ($\Delta G_{LX\text{-}resolv}$: a negative shift when Y is present or a positive shift when Y is absent; $\Delta G_{LH\text{-}resolv}$: a positive shift when Y is present or a negative shift when Y is absent).

If $\Delta\Delta G_{(H\rightarrow X)}$ is shifted to the positive in the presence of another group Y→ negative cooperativity (antagonism) between X and Y

This occurs when

4. ($\Delta G_{LX\text{-}desolv} - \Delta G_{LH\text{-}desolv}$) value is shifted to the positive in the presence of Y ($\Delta G_{LX\text{-}desolv}$: a positive shift when Y is present or a negative shift when Y is absent; $\Delta G_{LH\text{-}desolv}$: a negative shift when Y is present or a positive shift when Y is absent)
5. ($\Delta G_{LX\text{-}assoc} - \Delta G_{LH\text{-}assoc}$) value is shifted to the positive in the presence of Y ($\Delta G_{LX\text{-}assoc}$: a positive shift when Y is present or a negative shift when Y is absent; $\Delta G_{LH\text{-}assoc}$: a negative shift when Y is present or a positive shift when Y is absent)
6. ($\Delta G_{LX\text{-}resolv} - \Delta G_{LH\text{-}resolv}$) value is shifted to the positive in the presence of Y ($\Delta G_{LX\text{-}resolv}$: a positive shift when Y is present or a negative shift when Y is absent; $\Delta G_{LH\text{-}resolv}$: a negative shift when Y is present or a positive shift when Y is absent).

$\Delta\Delta G_{(H\rightarrow X)} = \Delta\Delta H_{(H\rightarrow X)} + (-T\Delta\Delta S_{(H\rightarrow X)}))$ **(Eq. S2)**

- If $\Delta\Delta H_{(H\rightarrow X)}/-T\Delta\Delta S_{(H\rightarrow X)}$ is shifted to the negative in the presence of group Y (enthalpic/entropic synergism)→ positive free energy cooperativity between X and Y
- If $\Delta\Delta H_{(H\rightarrow X)}/-T\Delta\Delta S_{(H\rightarrow X)}$ is shifted to the positive in the presence of group Y (enthalpic/entropic antagonism)→ negative free energy cooperativity between X and Y.

1.2. Binding Enthalpy

$\Delta\Delta H_{(H\rightarrow X)} = \Delta H_{LX} - \Delta H_{LH} = (\Delta H_{LX\text{-}desolv} - \Delta H_{LH\text{-}desolv}) + (\Delta H_{LX\text{-}assoc} - \Delta H_{LH\text{-}assoc}) + (\Delta H_{LX\text{-}resolv} - \Delta H_{LH\text{-}resolv})$ **(Eq. S3)**

If $\Delta\Delta H_{(H\rightarrow X)}$ is shifted to the negative in the presence of another group Y→ enthalpic synergism between X and Y

This occurs when

1. $(\Delta H_{LX\text{-}desolv} - \Delta H_{LH\text{-}desolv})$ value is shifted to the negative in the presence of Y ($\Delta H_{LX\text{-}desolv}$: a negative shift when Y is present or a positive shift when Y is absent; $\Delta H_{LH\text{-}desolv}$: a positive shift when Y is present or a negative shift when Y is absent)
2. $(\Delta H_{LX\text{-}assoc} - \Delta H_{LH\text{-}assoc})$ value is shifted to the negative in the presence of Y ($\Delta H_{LX\text{-}assoc}$: a negative shift when Y is present or a positive shift when Y is absent; $\Delta H_{LH\text{-}assoc}$: a positive shift when Y is present or a negative shift when Y is absent)
3. $(\Delta H_{LX\text{-}resolv} - \Delta H_{LH\text{-}resolv})$ value is shifted to the negative in the presence of Y ($\Delta H_{LX\text{-}resolv}$: a negative shift when Y is present or a positive shift when Y is absent; $\Delta H_{LH\text{-}resolv}$: a positive shift when Y is present or a negative shift when Y is absent).

If $\Delta\Delta H_{(H\rightarrow X)}$ is shifted to the positive in the presence of another group Y→ enthalpic antagonism between X and Y

This occurs when

4. $(\Delta H_{LX\text{-}desolv} - \Delta H_{LH\text{-}desolv})$ value is shifted to the positive in the presence of Y ($\Delta H_{LX\text{-}desolv}$: a positive shift when Y is present or a negative shift when Y is absent; $\Delta H_{LH\text{-}desolv}$: a negative shift when Y is present or a positive shift when Y is absent)

5. ($\Delta H_{LX\text{-}assoc} - \Delta H_{LH\text{-}assoc}$) value is shifted to the positive in the presence of Y ($\Delta H_{LX\text{-}assoc}$: a positive shift when Y is present or a negative shift when Y is absent; $\Delta H_{LH\text{-}assoc}$: a negative shift when Y is present or a positive shift when Y is absent)
6. ($\Delta H_{LX\text{-}resolv} - \Delta H_{LH\text{-}resolv}$) value is shifted to the positive in the presence of Y ($\Delta H_{LX\text{-}resolv}$: a positive shift when Y is present or a negative shift when Y is absent; $\Delta H_{LH\text{-}resolv}$: a negative shift when Y is present or a positive shift when Y is absent).

1.3. Binding Entropy

$$-T\Delta\Delta S_{(H\rightarrow X)} = -T\Delta S_{LX} - (-T\Delta S_{LH}) = (-T\Delta S_{LX\text{-}desolv} - (-T\Delta S_{LH\text{-}desolv})) + (-T\Delta S_{LX\text{-}assoc} - (-T\Delta S_{LH\text{-}assoc})) + (-T\Delta S_{LX\text{-}resolv} - (-T\Delta S_{LH\text{-}resolv})) \quad \textbf{(Eq. S4)}$$

If $-T\Delta\Delta S_{(H\rightarrow X)}$ is shifted to the negative in the presence of another group Y→ entropic synergism between X and Y

This occurs when

1. $(-T\Delta S_{LX\text{-}desolv} - (-T\Delta S_{LH\text{-}desolv}))$ value is shifted to the negative in the presence of Y ($-T\Delta S_{LX\text{-}desolv}$: a negative shift when Y is present or a positive shift when Y is absent; $-T\Delta S_{LH\text{-}desolv}$: a positive shift when Y is present or a negative shift when Y is absent)
2. $(-T\Delta S_{LX\text{-}assoc} - (-T\Delta S_{LH\text{-}assoc}))$ value is shifted to the negative in the presence of Y ($-T\Delta S_{LX\text{-}assoc}$: a negative shift when Y is present or a positive shift when Y is absent; $-T\Delta S_{LH\text{-}assoc}$: a positive shift when Y is present or a negative shift when Y is absent)
3. $(-T\Delta S_{LX\text{-}resolv} - (-T\Delta S_{LH\text{-}resolv}))$ value is shifted to the negative in the presence of Y ($-T\Delta S_{LX\text{-}resolv}$: a negative shift when Y is present or a positive shift when Y is absent; $-T\Delta S_{LH\text{-}resolv}$: a positive shift when Y is present or a negative shift when Y is absent).

If $-T\Delta\Delta S_{(H\rightarrow X)}$ is shifted to the positive in the presence of another group Y→ entropic antagonism between X and Y

This occurs when

4. $(-T\Delta S_{LX\text{-}desolv} - (-T\Delta S_{LH\text{-}desolv}))$ value is shifted to the positive in the presence of Y ($-T\Delta S_{LX\text{-}desolv}$: a positive shift when Y is present or a negative shift when Y is absent; $-T\Delta S_{LH\text{-}desolv}$: a negative shift when Y is present or a positive shift when Y is absent)

5. $(-T\Delta S_{LX\text{-}assoc} - (-T\Delta S_{LH\text{-}assoc}))$ value is shifted to the positive in the presence of Y ($-T\Delta S_{LX\text{-}assoc}$: a positive shift when Y is present or a negative shift when Y is absent; $-T\Delta S_{LH\text{-}assoc}$: a negative shift when Y is present or a positive shift when Y is absent)
6. $(-T\Delta S_{LX\text{-}resolv} - (-T\Delta S_{LH\text{-}resolv}))$ value is shifted to the positive in the presence of Y ($-T\Delta S_{LX\text{-}resolv}$: a positive shift when Y is present or a negative shift when Y is absent; $-T\Delta S_{LH\text{-}resolv}$: a negative shift when Y is present or a positive shift when Y is absent).

2. K_d-K_i Correlation

Table S1: The ΔG_{ki} and the ΔG_{kd} data for 24 of the studied ligands as determined by the biochemical assays and the ITC experiments, respectively

Ligand	ΔG_{Ki} (kJ/mol)	ΔG_{Kd}(kJ/mol)
4	-40.9 ± 0.4	-35.0 ± 0.7
8	-45.6 ± 0.3	-38.9 ± 0.9
9	-34.6 ± 0.4	-30.7 ± 0.2
10	-37.3 ± 0.2	-32.4 ± 0.4
11	-41.3 ± 0.6	-36.0 ± 0.6
12	-41.1 ± 0.7	-35.3 ± 0.3
13	-41.3 ± 0.5	-35.3 ± 0.5
14	-42.5 ± 0.6	-35.2 ± 0.8
15	-40.0 ± 0.5	-33.9 ± 0.5
16	-43.8 ± 0.3	-35.8 ± 0.7
17	-42.1 ± 0.3	-35.0 ± 0.5
18	-37.3 ± 0.5	-32.9 ± 0.4
19	-38.4 ± 0.2	-33.1 ± 0.6
20	-36.1 ± 0.2	-33.5 ± 0.2
21	-44.1 ± 0.1	-38.6 ± 0.4
22	-47.5 ± 0.1	-38.9 ± 1.3
23	-47.1 ± 0.4	-39.7 ± 1.2
24	-47.2 ± 0.3	-39.3 ± 1.0
25	-47.1 ± 0.5	-39.3 ± 0.8
26	-42.8 ± 0.3	-36.8 ± 0.2
27	-45.2 ± 0.3	-38.7 ± 0.6
28	-42.3 ± 0.3	-37.2 ± 0.3
29	-41.5 ± 0.6	-36.2 ± 0.4
30	-43.6 ± 0.6	-37.0 ± 0.4

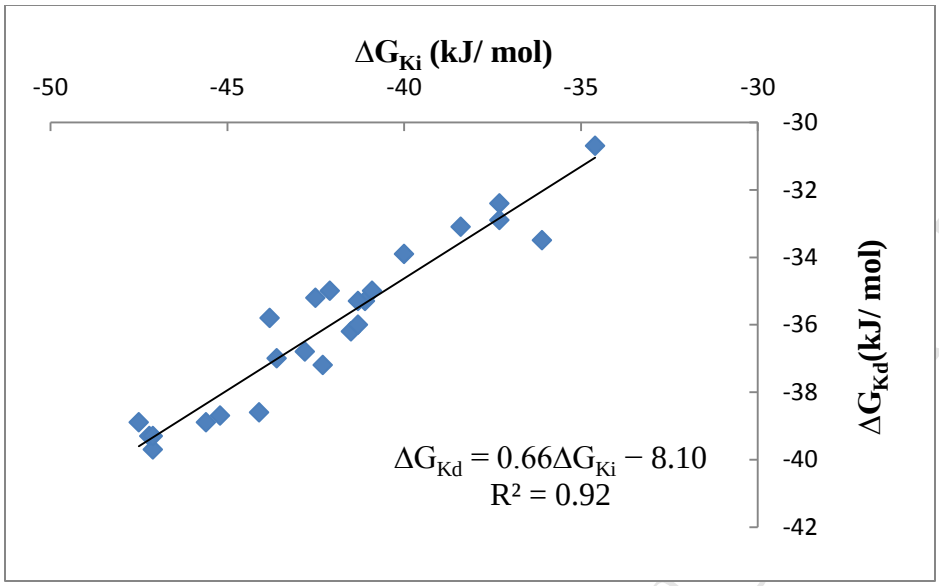

Figure S1: A plot of the ΔG determined by the ITC experiments (ΔG_{Kd}) vs. the ΔG determined by the biochemical assays (ΔG_{Ki}) for 24 of the ligands studied herein. The plot shows a linear relationship between the two sets of data with a slope of 0.66 and an intercept of -8.10 kJ/mol.

Comparing the dissociation constants of the 24 ligands studied in Ref 1 (K_ds obtained from the ITC experiments) with the inhibition constants of these ligands reported in the current study (K_is obtained from the biochemical assays) reveals that the dissociation and the inhibition constants in the studied series of TLN inhibitors are not equal (Table S1). However, plotting the ΔGs obtained from the dissociation constants vs. those obtained from the inhibition constants demonstrates that these binding parameters are correlated in a linear fashion (Figure S1). A potential explanation for this observation is that the biochemical assays were performed in a buffer whose ionic strength is higher than that of the buffer used in the ITC experiments. Ionic strength was previously shown to influence ligand binding[2], and it is possible that, in the case of the phosphonamidate-TLN binding, the binding becomes stronger when the ionic strength is high. Even though this shift can happen, a certain degree of correlation between the two sets of data, like that observed in Figure S1, is anticipated to be maintained. Another possible explanation for the differences observed between the ITC and the biochemical assay data sets is that there is a pH difference of 0.3 units between the two buffers. In order to further investigate which of these two factors is responsible for this observed variability, both the ITC experiments and the biochemical assays need to be performed in exactly the same buffer (this is the subject of

an ongoing research). It should be noted that choosing the buffer that is to be used in ligand binding studies is crucial, because if the data obtained in biochemical assays and/or ITC experiments are to be extrapolated to real biological systems, the buffers used in these experiments need to be as close to the biological medium as possible. This includes having similar ionic strength, pH, etc.

3. References:

(1) Nasief, N. N.; Hangauer, D. Influence of neighboring groups on the thermodynamics of hydrophobic binding: An added complex facet to the hydrophobic effect. *J. Med Chem.* **2014**, 57, 2315-2333.

(2) Shanmugasundaram, V. Part A. Design and synthesis of aminocarboxylate-containing peptide inhibitors of PKA. Part B. Effect of ionic strength, osmolality and organic cosolvents on binding affinities of ligands to PKA. **2000**, pp. 98-120.

4. Representative NMR Spectra

Compound **1** ^{1}H-NMR

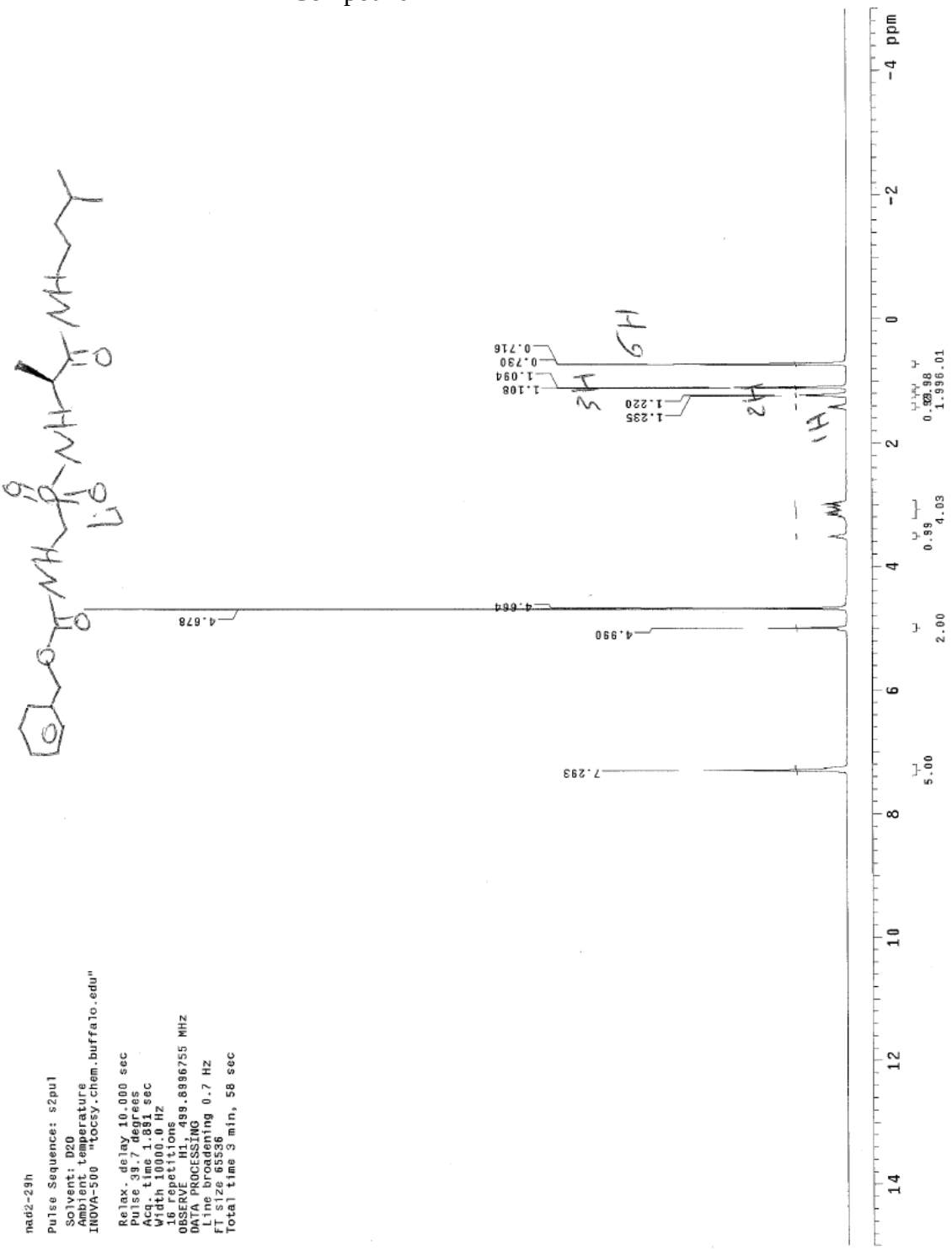

Compound **1** ^{31}P-NMR

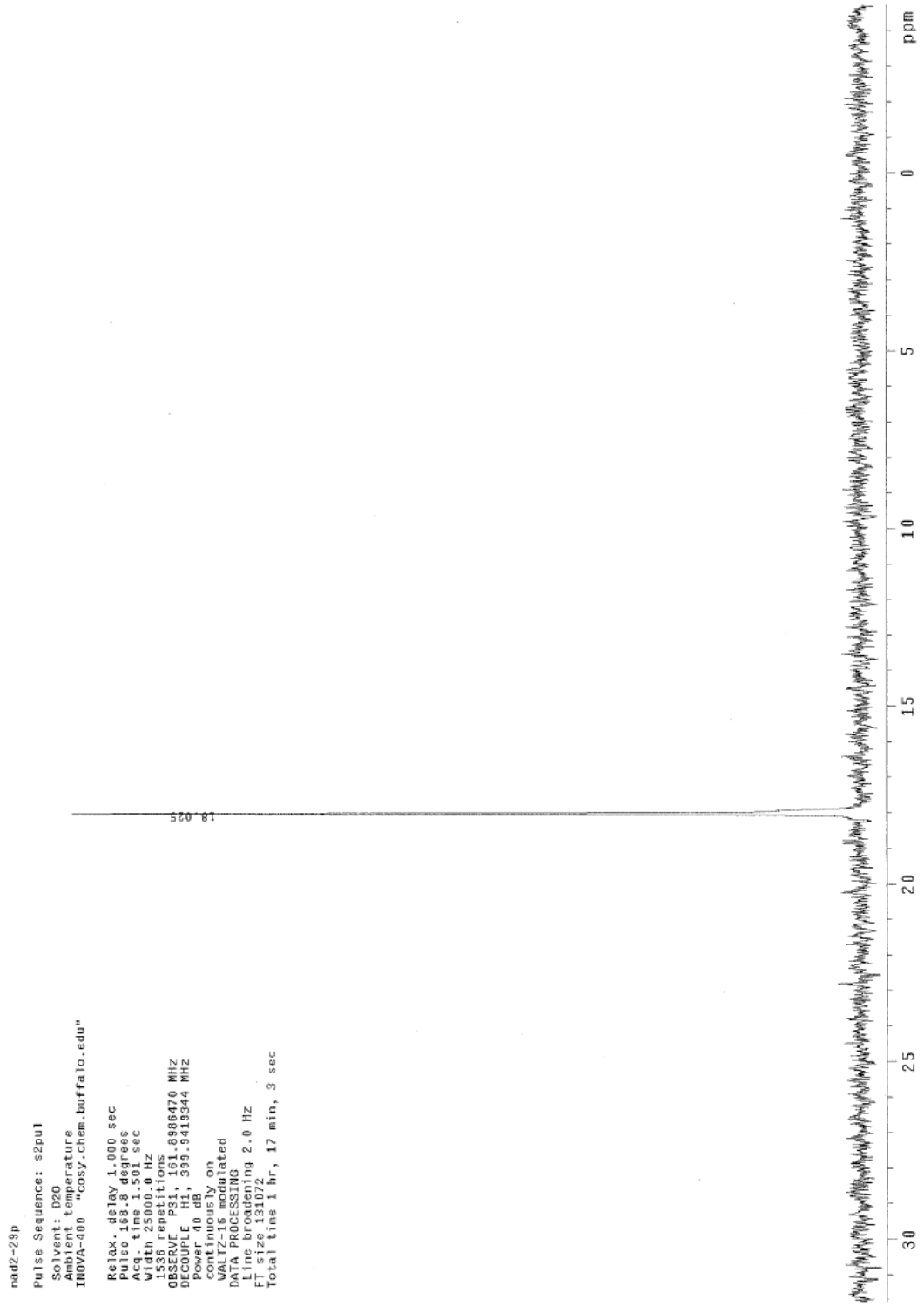

Compound **1** ^{13}C-NMR

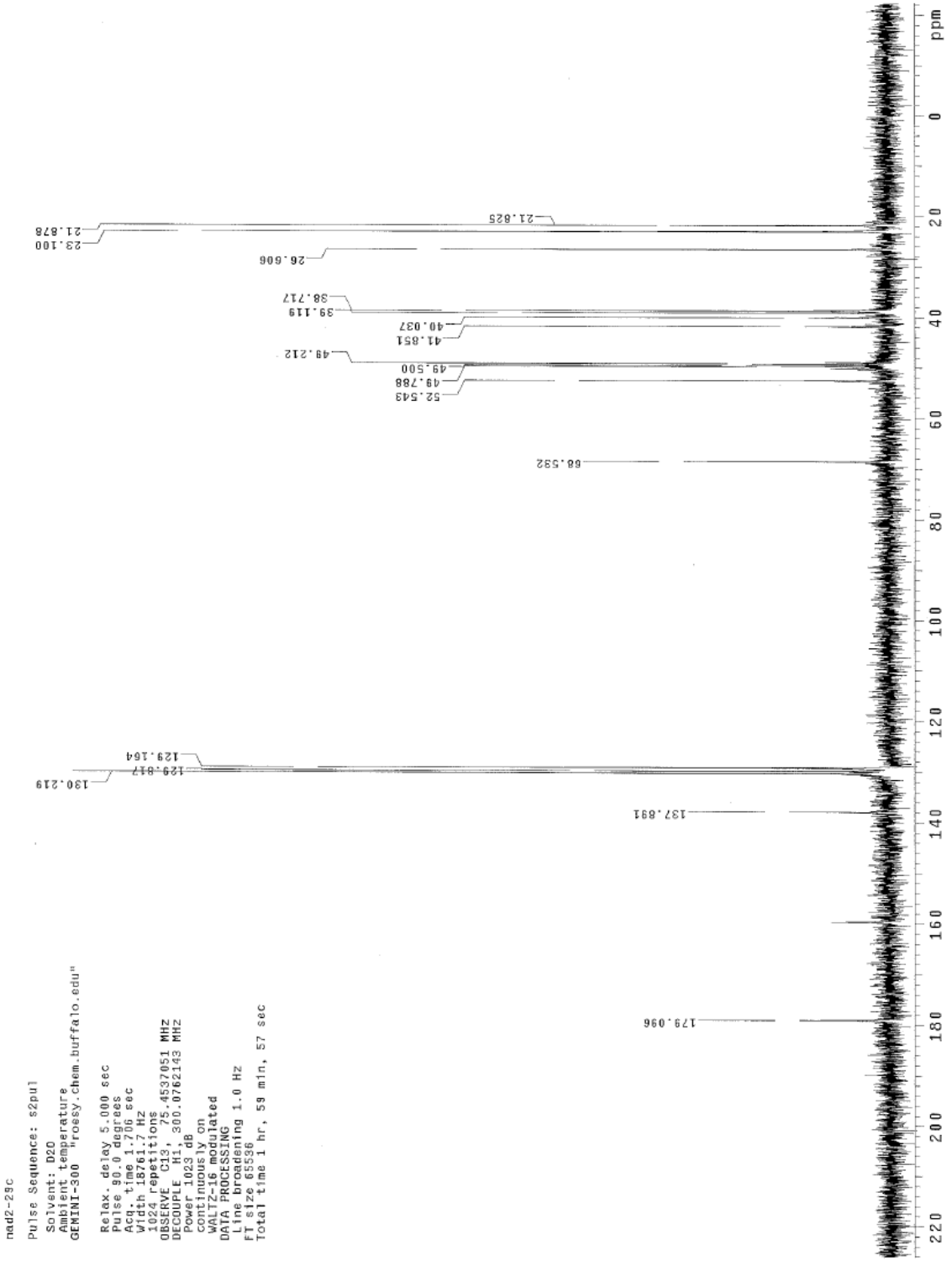

Compound **5** ^{1}H-NMR

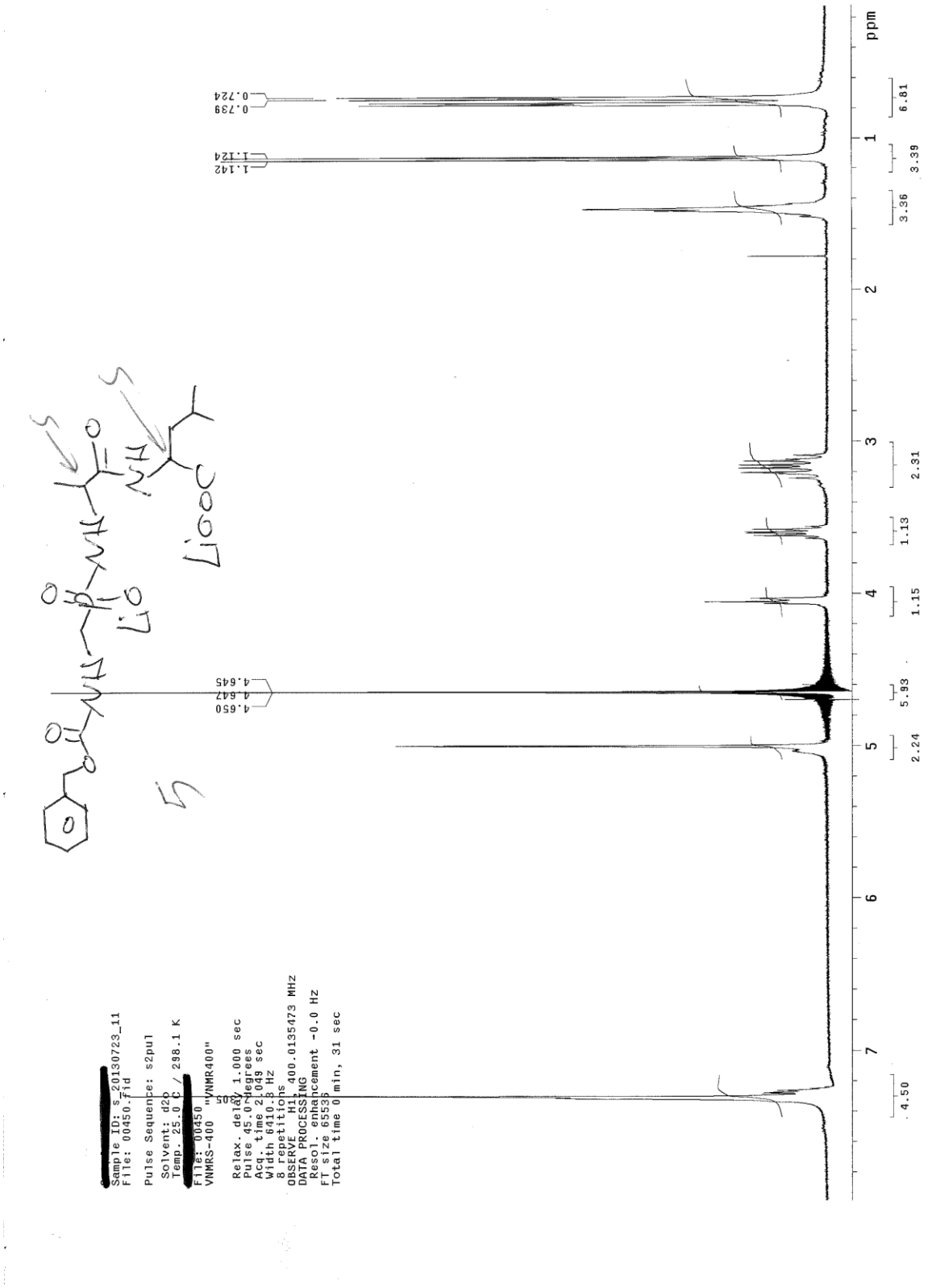

Compound **5** ^{31}P-NMR

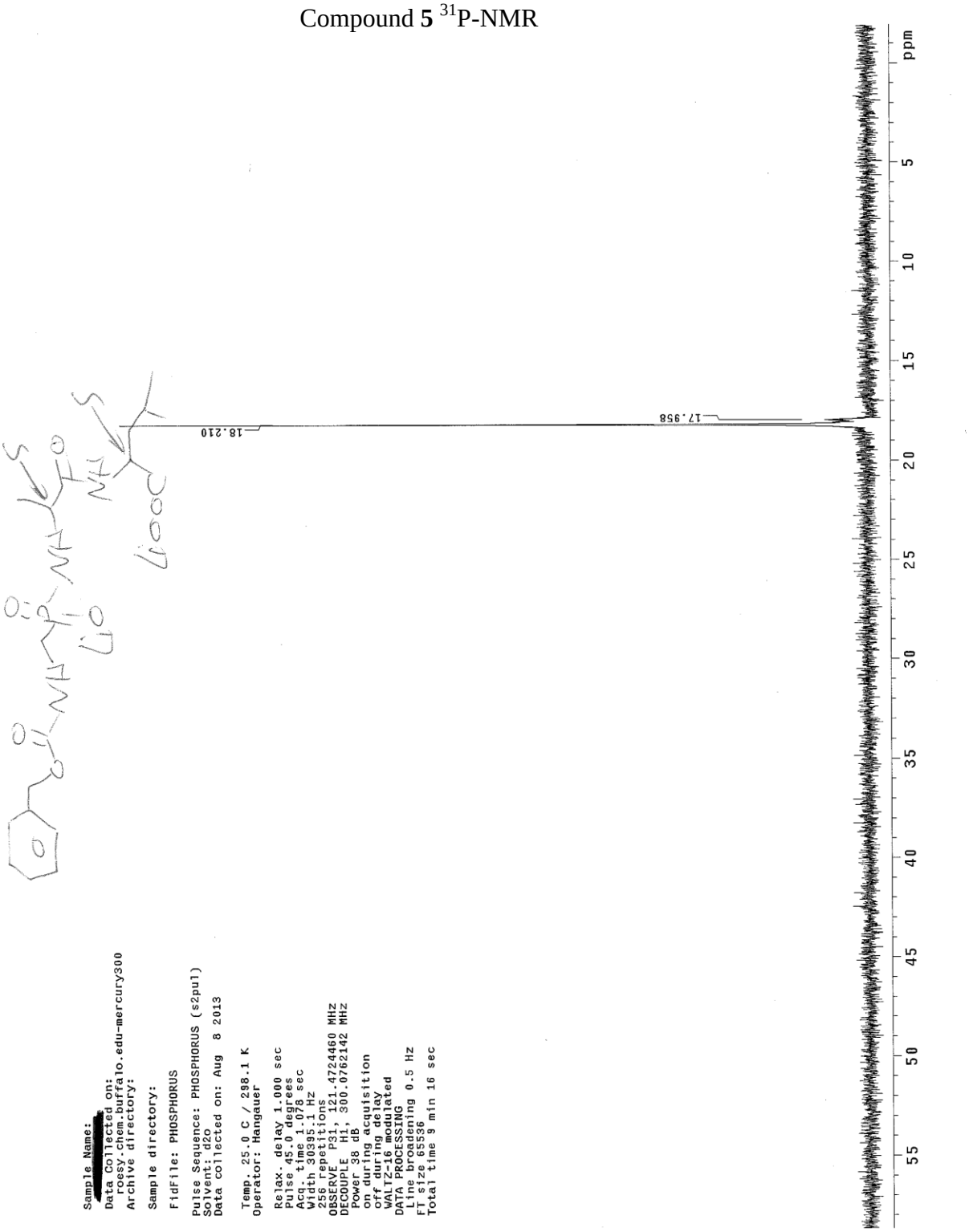

Compound **5** ^{13}C-NMR

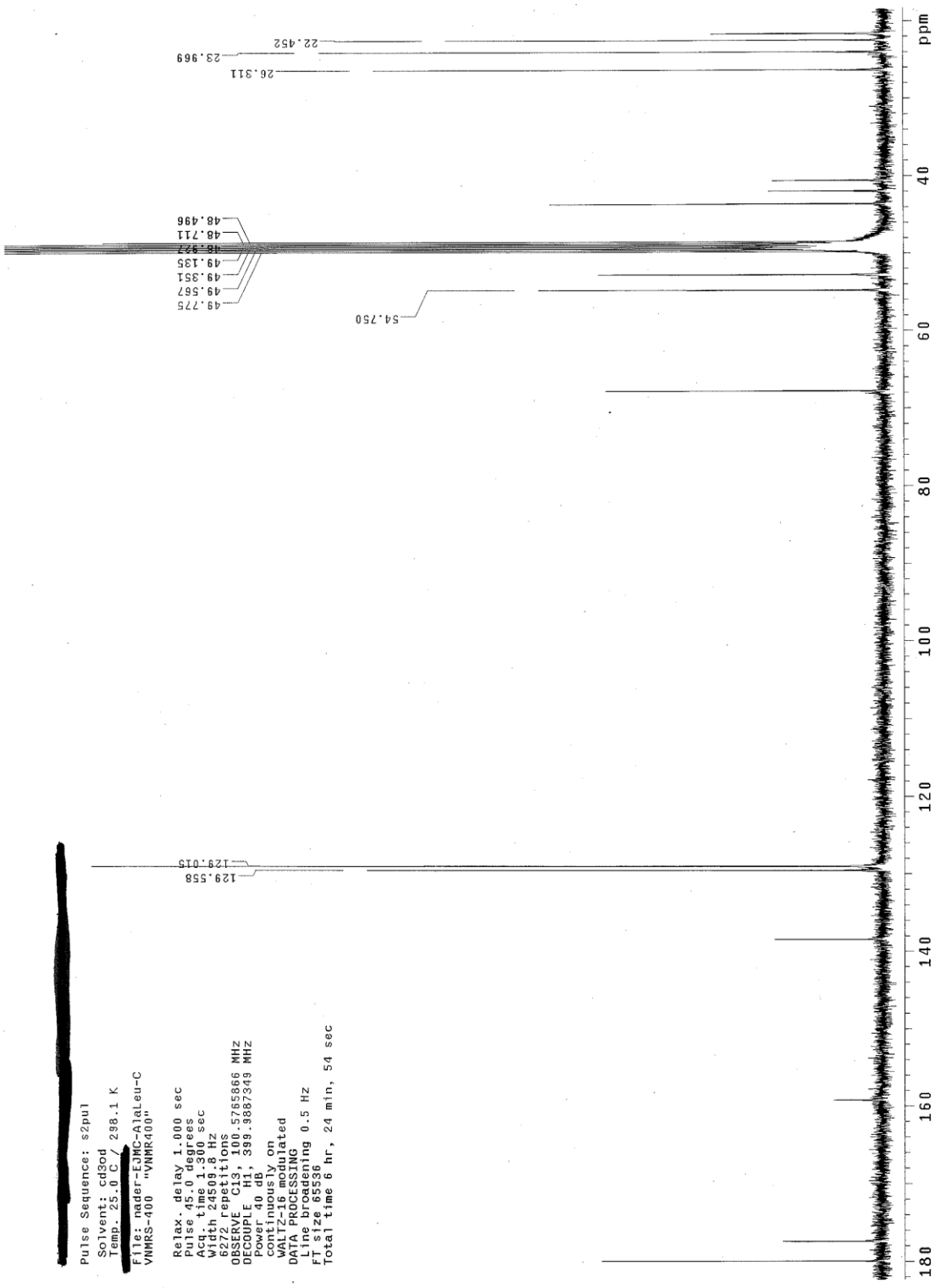

Compound **31** ^{1}H-NMR

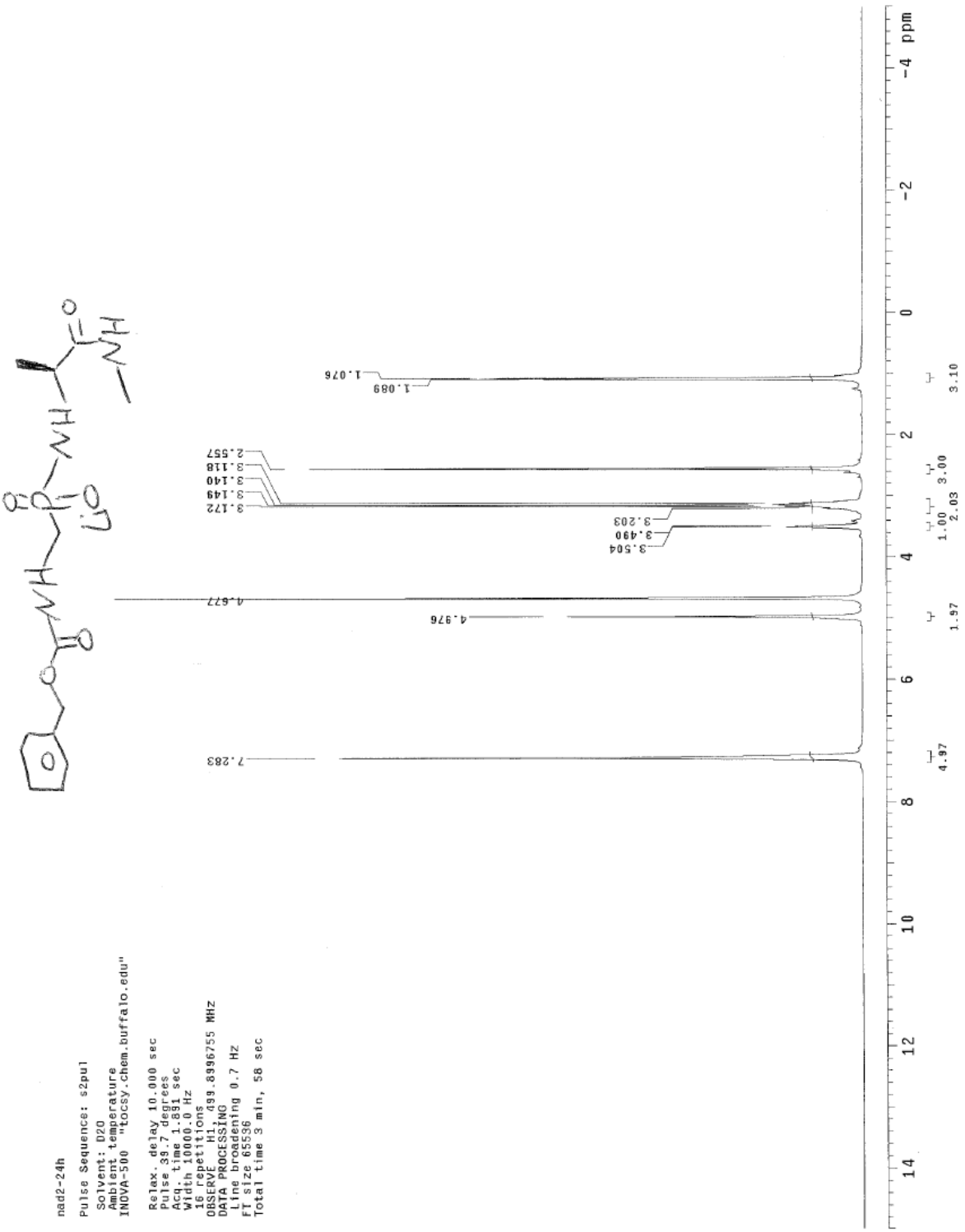

Compound **31** ^{31}P-NMR

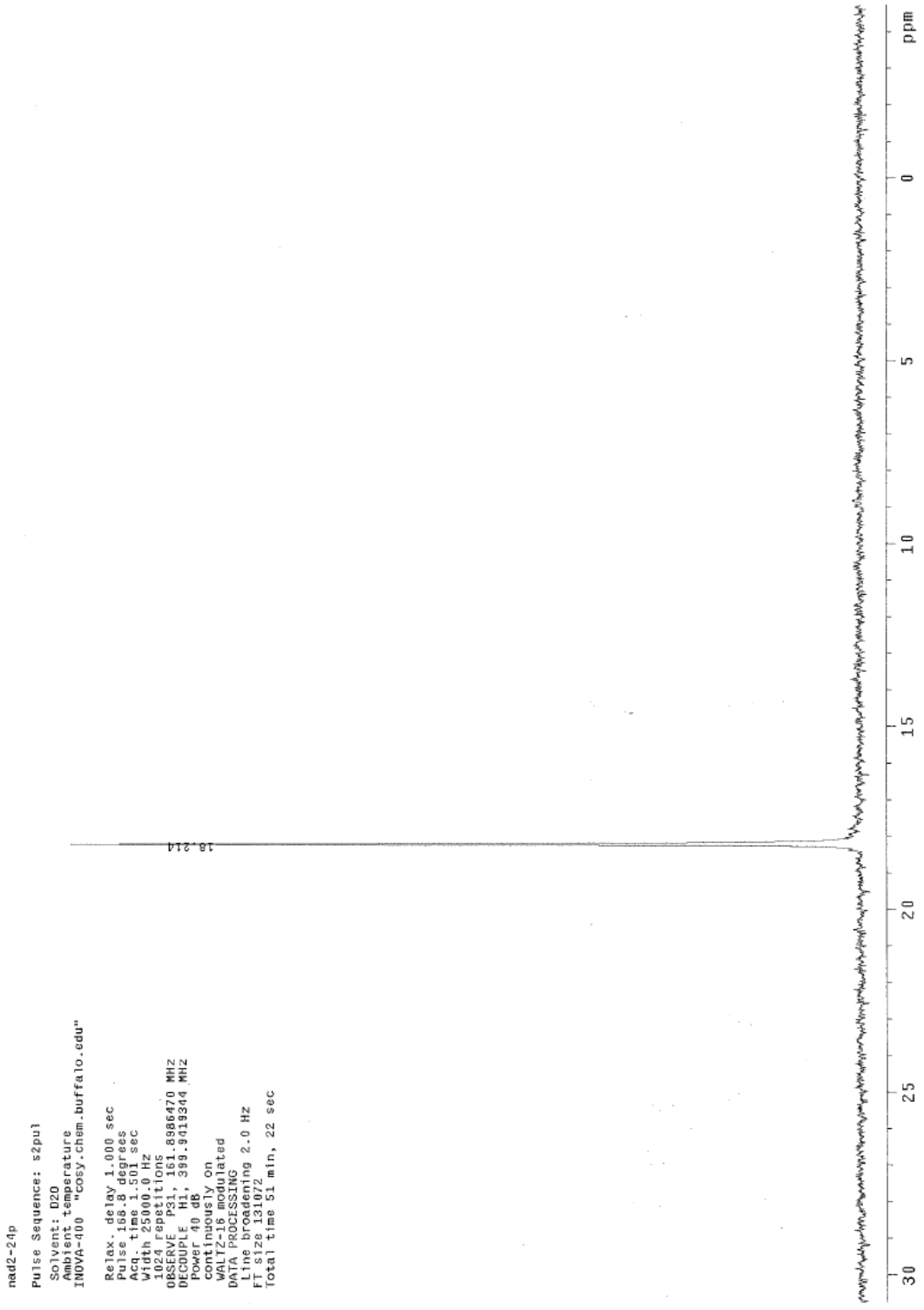

Compound **31** ^{13}C-NMR

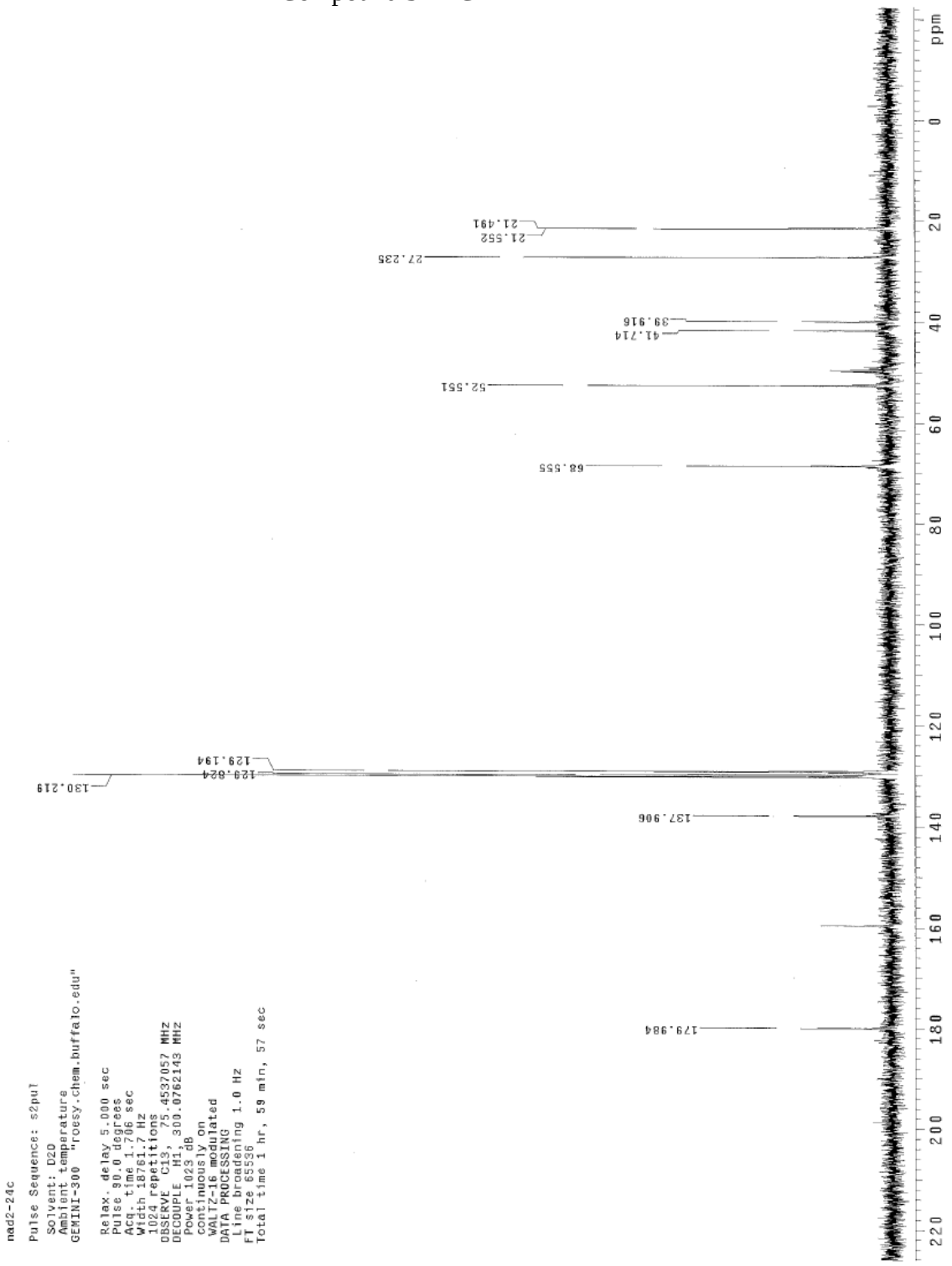

Compound **35** ^{1}H-NMR

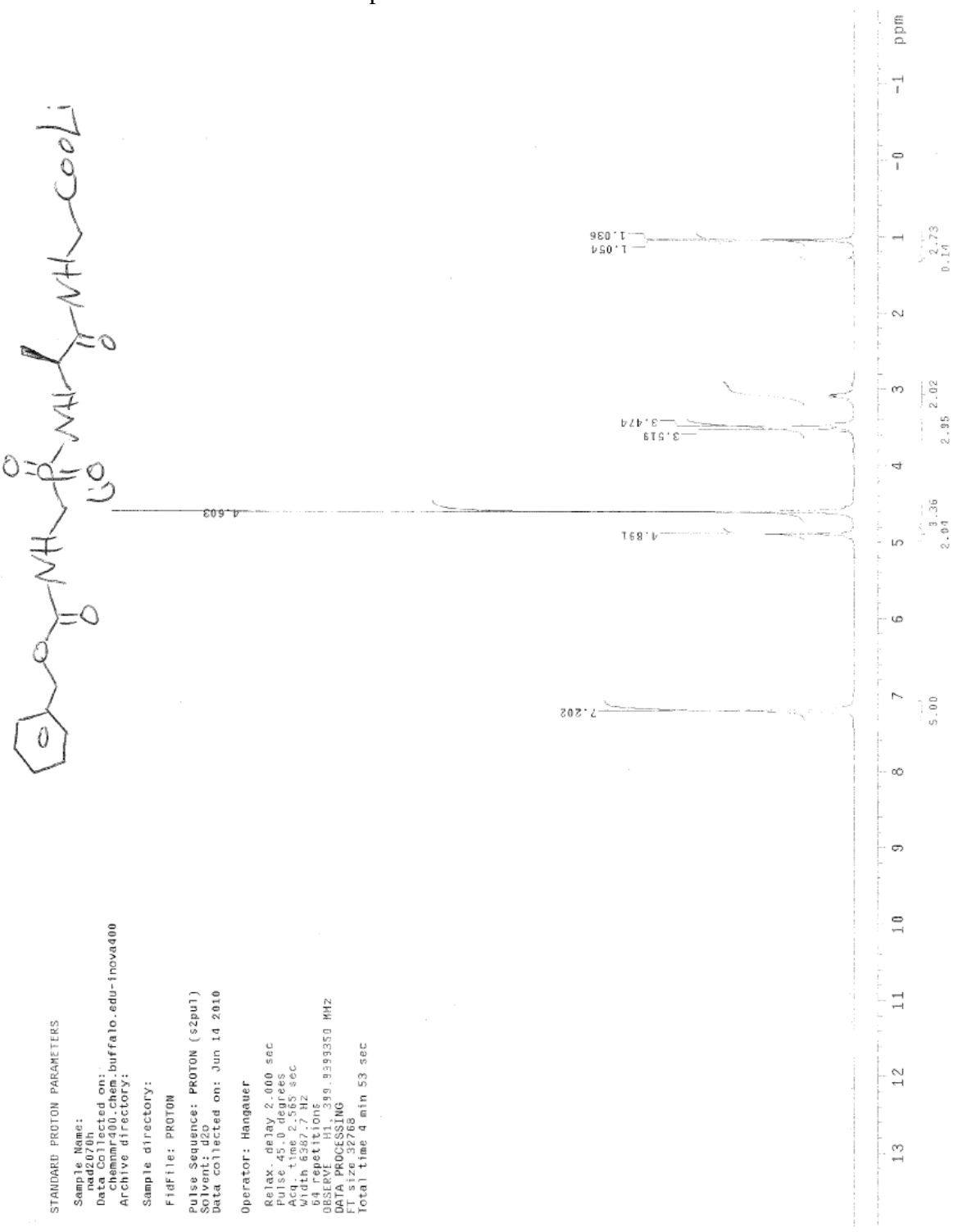

Compound **35** ^{31}P-NMR

Compound **38** ^{1}H-NMR

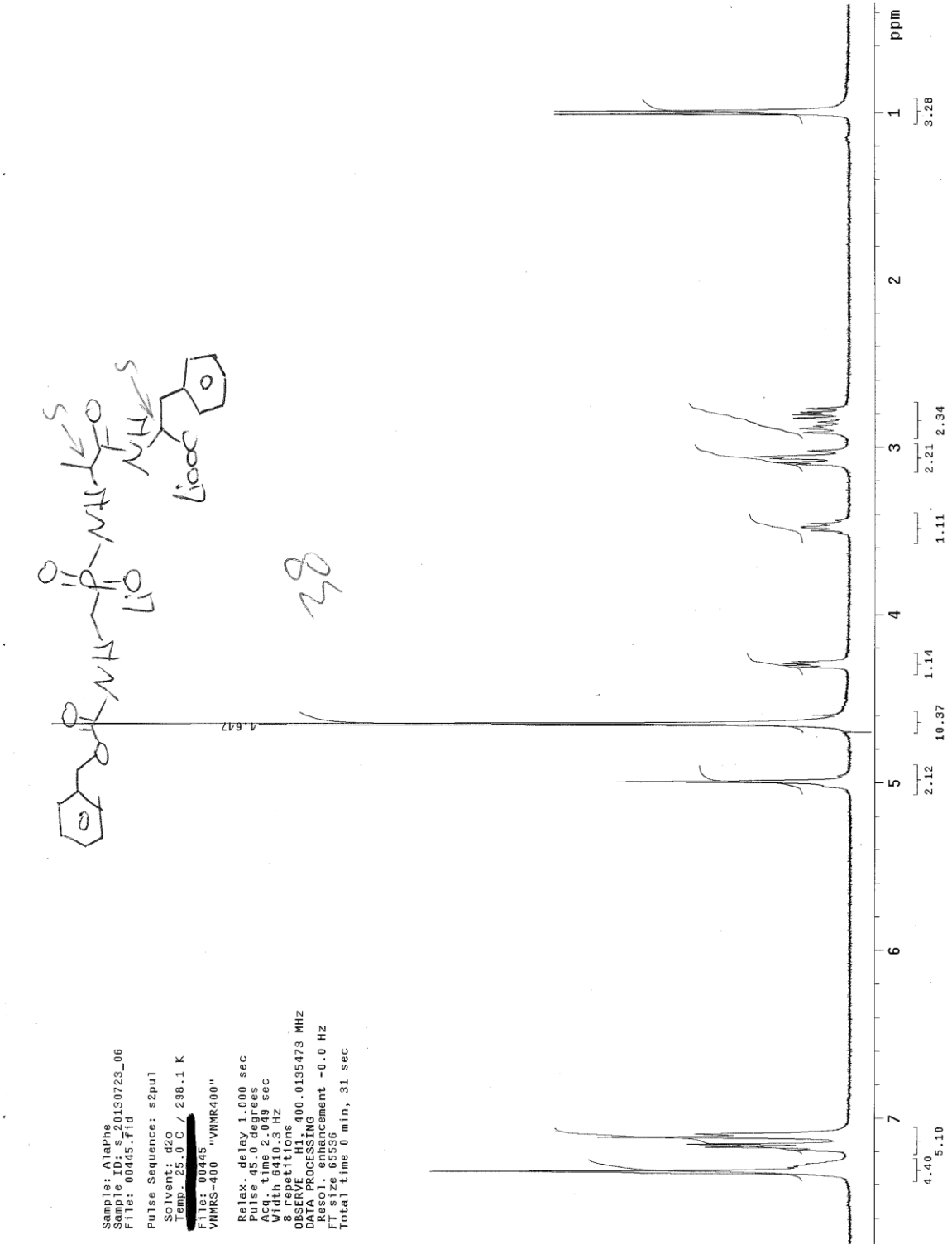

Compound **38** ^{31}P-NMR

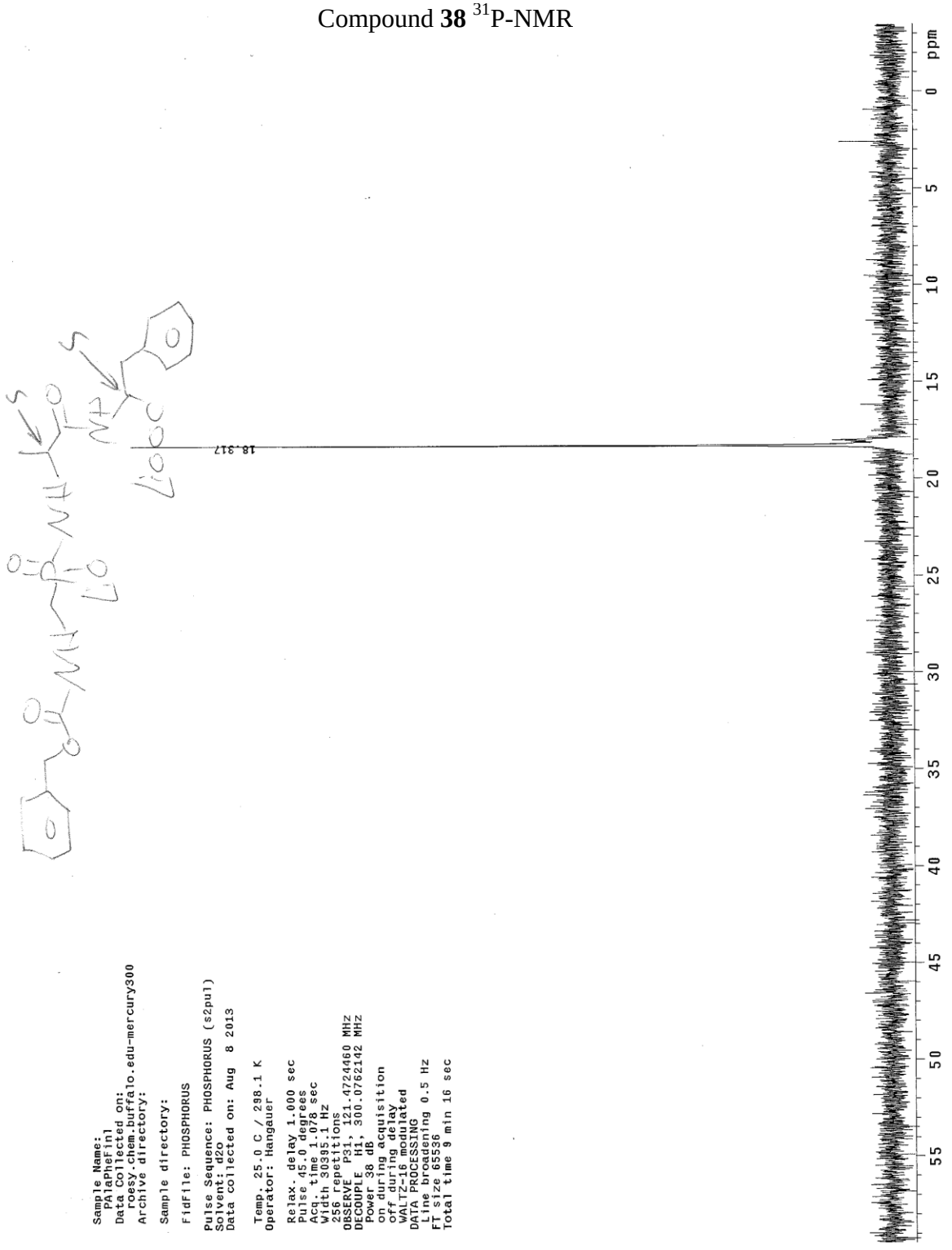

Compound **38** ^{13}C-NMR